



**SS. CYRIL AND METHODIUS
UNIVERSITY
FACULTY OF CIVIL ENGINEERING
SKOPJE, REPUBLIC OF NORTH
MACEDONIA**



Bujar Azem Jashari

**EXPERIMENTAL AND ANALYTICAL INVESTIGATION OF GLUED
SOLID TIMBER (GST) BEAMS**

Doctoral thesis

Skopje, 2025



**SS. CYRIL AND METHODIUS
UNIVERSITY
FACULTY OF CIVIL ENGINEERING
SKOPJE, REPUBLIC OF NORTH
MACEDONIA**



Bujar Azem Jashari

**EXPERIMENTAL AND ANALYTICAL INVESTIGATION OF GLUED
SOLID TIMBER (GST) BEAMS**

Doctoral thesis

Skopje, 2025

Doctoral student:

BUJAR AZEM JASHARI

Topic:

**EXPERIMENTAL AND ANALYTICAL INVESTIGATION OF GLUED
SOLID TIMBER (GST) BEAMS**

Mentor:

Prof. Dr. Kiril Gramatikov

Mentor's Institute

Civil Engineering - Department of Construction

Defense Panel:

Chairman's Institute

Prof. Dr. Elena Dumova

Ph.D. NAME AND SURNAME,

Member's Institute

Scientific area:

Timber Construction

Date of defense:

(If the date is not specified, it is added manually)

xx.xx.2025

CONTENT

LIST OF FIGURES.....	8
LIST OF TABLES.....	12
EQUATIONS	13
ABBREVIATIONS.....	14
ABSTRACT	15
АНЦТРАКТ	16
SUMMARY.....	17
РЕЗИМЕ.....	18
ACKNOWLEDGEMENTS.....	19
1. INTRODUCTION.....	21
1.1. GENERAL BACKGROUND.....	21
1.2. OBJECTIVES AND SCOPE	21
1.3. THESIS OUTLINE	22
2. LITERATURE REVIEW	23
2.1. TIMBER AS BUILDING MATERIAL.....	23
2.1.1. Wood processing as a construction material	23
2.1.2. Types of wood and their use in construction.....	24
2.2. ENGINEERED WOOD PRODUCTS	25
2.3. LAMINATED TIMBER.....	27
2.3.1. The history of Glued Laminated Timber.....	27
2.3.2. Glued Laminated Timber (GLT).....	28
2.3.3. Glued Solid Timber (GST).....	32
2.4. PRODUCTION PROCESS AND ADHESIVES	34
2.4.1. Finger-joint of Glued Laminated Timber.....	35
2.4.2. Adhesives.....	36
2.5. MECHANICAL PROPERTIES.....	39
2.6. LONG TERM BEHAVIOR – CREEP	39
2.7. FAILURE MODES.....	40
2.8. SHEAR FAILURE.....	43

2.9.	ADHESIVE FAILURE	44
2.10.	LINEAR ELASTIC BEHAVIOR	44
2.11.	NON - LINEAR SECTION BEHAVIOR.....	45
3.	FABRICATION OF GLUED SOLID TIMBER (GST) BEAMS FOR EXPERIMENTAL INVESTIGATION.....	46
3.1.	DESCRIPTION OF THE SELECTION OF WOOD MATERIAL.....	46
3.2.	DETERMINATION OF MOISTURE CONTENT OF TEST PIECES	47
3.2.1.	Defining dimensions of the samples	48
3.2.2.	Cutting slices.....	48
3.2.3.	Measuring and scaling the test samples	49
3.2.4.	Drying the samples in oven.....	50
3.2.5.	Determination of density of test samples.....	51
3.3.	PRODUCTION AND ITS STAGES	53
3.3.1.	Processing of lamellas in machines	53
3.3.2.	Bonding process.....	55
3.3.3.	The press time application	56
4.	EXPERIMENTAL INVESTIGATION OF GLUED SOLID TIMBER (GST) BEAMS.....	59
4.1.	TESTING PROGRAM (TABLE TEST SERIES)	59
4.2.	TEST SET – UP AND INSTRUMENTATION (DATA ACQUISITION).....	61
4.2.1.	Structural Support and Loading System	62
4.2.2.	Hydraulic Loading System	63
4.2.3.	Instrumentation and Measurement Devices.....	63
4.3.	MATERIAL MECHANICAL CHARACTERISTICS IN COMPRESSION	67
4.3.1.	Compression Strength Parallel to the Grain (Serie E)	68
4.3.2.	Compression Strength Perpendicular to the Grain (Serie F).....	75
4.4.	FOUR POINT BENDING TESTING	78
4.4.1.	Local and Global Modulus of Elasticity in Bending (Serie A)	79
4.4.2.	Shear Field Test Method (Serie B).....	89
4.4.3.	Bending Strength Parallel to the Grain (Serie C).....	98
4.4.4.	Long - Term Behaviour (Serie D).....	102
5.	NUMERICAL MODELING	107
5.1.	CONSTITUTIVE MODEL.....	107

5.2.	GEOMETRY AND BOUNDARY CONDITIONS AND MESH DISCRETIZATION	109
5.3.	COMPARISON AND DISCUSSION: FOUR-POINT BENDING TEST (SERIE A)	112
5.3.1.	AI2 Comparison and discussion	121
5.3.2.	AI3 Comparison and discussion	128
5.4.	LONG TERM BEHAVIOR UNDER SUSTAINED LOAD (SERIE D)	135
6.	CONCLUSION.....	139
	REFERENCES.....	141

LIST OF FIGURES

Figure 1. Engineered Wood Products	25
Figure 2. Fibre size and beam types for timber products	26
Figure 3. Glued Laminated Timber Product.....	28
Figure 4. Standard shapes of glulam and range of spans	29
Figure 5. Application of Glued Laminated Timber at Prishtina Mall.....	30
Figure 6. Relation of European Standards for structural timber products prepared by CEN/TC 124	31
Figure 7. Examples for glued solid timber made of two and five laminations.....	33
Figure 8. Cross section dimensions of full-scale glued solid timber beam for experimental and analytical investigation.	34
Figure 9. Production process of Glued Laminated Timber	34
Figure 10. Orientation of finger-joints	36
Figure 11. Polyurethane one-component adhesive used for bonding.....	38
Figure 12. Strain and stress distribution at tensile failure, occurring before the onset of compressive plasticity	42
Figure 13. Strain and stress distribution at tensile failure with the compression zone reaching plasticity	43
Figure 14. Selection of material based in Structural Timber Design to Eurocode 5	46
Figure 15. a & b view of the raw material deposited before transportation	47
Figure 16. Cutting samples for determination of moisture content and density	47
Figure 17. Extraction and preparation of samples from the lamellae for material testing according to EN 13183-1 ..	48
Figure 18. Cutting the test pieces according to EN 13183-1 on the designated sections	48
Figure 19. View of the cut and marked samples prepared for testing	49
Figure 20. Scaling of test samples for weight measurement	49
Figure 21. Measuring samples with caliper in three directions	50
Figure 22. Adjustment of temperature in oven $103 \pm 2^{\circ}\text{C}$	50
Figure 23. Placing the samples in the oven	51
Figure 24. Initial stage of lamella preparation	54
Figure 25. Selection and acquisition of the required lamellas.....	54
Figure 26. Graphic showing industrial Assembly time and curing time application for the beams	55
Figure 27. a) and b) Laying of glue with a thickness of more than 0.1 mm with the density of adhesive at around 1,16 g/cm ³	56
Figure 28. a & b Tightening lamellas by mechanical clamps and vices.....	57
Figure 29. Thirty-six head beams in different model dimensions	57
Figure 30. GST beams produced from the author	58
Figure 31. Label notification.....	61
Figure 32. Compression strength parallel to the grain welded metal;.....	62
Figure 33. LVDT placement for shear field testing.....	62
Figure 34. a) Hydraulic jack b) ZRMK machine press	63
Figure 35. a) Measuring of Moisture Content b) Measuring Relative Humidity	63

Figure 36. a) Straing gauges and special glue b) Strain gauges connection c) Strain gauges setting.....	64
Figure 37. LVDT used to measure relative and absolute displacement depending on the testing module	64
Figure 38. Load Cell, load applied through hydraulic jack	65
Figure 39. Dial gauge.....	65
Figure 40. a) Cables and equipment b) Strain gauges connection.....	66
Figure 41. Catman Data Acquisition Software.....	66
Figure 42. a) Cables and data logger b) HBM data logger.....	67
Figure 43. a) and b) Real-time data monitoring and storage.....	67
Figure 44. The example of application of load for the determination of compression strength parallel to the grain ...	68
Figure 45. Experimental test of compression force parallel to the grain beam EI1	69
Figure 46. Experimental test of compression force parallel to the grain – beam EI2	69
Figure 47. Load–displacement curve of experimental specimen E_Test 01 and calculation of the elastic modulus ...	72
Figure 48. Load–displacement curve of experimental specimen E_Test 05 and calculation of the elastic modulus ...	72
Figure 49. Crack of timber under compression parallel to the grain (beam EI1)	73
Figure 50. a) Beam EI2 b) Beam EI2.....	74
Figure 51. a) beam EI3 b) beam EI1;EI2 and EI3.....	74
Figure 52. Determination of compression strength perpendicular to the grains.....	75
Figure 53. Press machine for determination of compression strength perpendicular to the grains	75
Figure 54. The view of cross section of experimental test sample.....	76
Figure 55. Beam FI1 a) front view b) side view	77
Figure 56. Beam FI2 a) front view b) side view	77
Figure 57. Beam FI3 a) front view b) side view	78
Figure 58. Samples from Serie F.....	78
Figure 59. Four point bending test (408:2010+A1:2012)	79
Figure 60. Beam (AI1) the setup for the local and global modulus of elasticity in bending.	80
Figure 61. Beam (AI2) the setup for determining the local and global modulus of elasticity in bending.	81
Figure 62. Beam (AI3) setup for determining the local and global modulus of elasticity in bending.....	82
Figure 63. Local Modulus of Elasticity in Bending – AI1	83
Figure 64. Relative deflection on beam AI2.....	83
Figure 65. Relative deflection on beam AI3.....	84
Figure 66. Determination of Global Modulus of Elasticity-AI1	85
Figure 67. Determination of Global Modulus of Elasticity-AI2	86
Figure 68. Determination of Global Modulus of Elasticity-AI3	86
Figure 69. Front of the beam AI1 – defect and the crack description	88
Figure 70. Front of the beam AI2.....	88
Figure 71. Bottom view of the beam AI2.....	88
Figure 72. Experimental investigation of shear field test according to EN 408_2010+A1	89

Figure 73. Beam (BI1) setup for Shear Field Test Method	90
Figure 74. Beam (BI2) setup for Shear Field Test Method	91
Figure 75. Beam (BI3) setup for Shear Field Test Method	92
Figure 76. Force–deflection response from the Shear Field Test for beam BI1	94
Figure 77. Force–deflection response from the Shear Field Test for beam BI2	95
Figure 78. Force–deflection response from the Shear Field Test for beam BI3	95
Figure 79. Experimental investigation of shear field test.....	96
Figure 80. Shear-field experimental test accessories	96
Figure 81. Shear-Field Test Methods beams (BI1, BI2, BI3).....	97
Figure 82. Experimental test for bending strength parallel to the grain	98
Figure 83. Experimental test for bending strength parallel to the grain	99
Figure 84. Beam CI1 Front view.....	99
Figure 85. Beam CI1 – Back view	100
Figure 86. Beam CI2 – Bottom view	100
Figure 87. Beam CI3 – Bottom view	101
Figure 88. Determination of long-term behavior of beam DI1 and DI2	102
Figure 89. Long-term effect and creep coefficient under sustained load for DI1 and DI2.....	102
Figure 90. Visual simulation	103
Figure 91. Equipment for temperature and relative humidity monitoring.....	103
Figure 92. Weighing each of the steel billets	104
Figure 93. Constitutive law behavior for timber used in numerical modeling: Brittle behavior in tension	107
Figure 94. Constitutive law behavior for timber used in numerical modeling: Elastic–perfectly plastic behavior in compression	108
Figure 95. Position of the accessories where the load is supported and applied	109
Figure 96. Geometry and boundary conditions of the numerical model	110
Figure 97. Arrangement of load application and support conditions in the numerical model.....	110
Figure 98. Finite element mesh of the GST beam with steel plates at supports and loading points.....	111
Figure 99. Load – displacement comparison Experiment vs Numerical for beam AI1.....	112
Figure 100. Strain gage comparison in compression and tension for beam AI1	113
Figure 101. Position of strain gauges: Illustration of the placement of strain gauges along the beam, showing both the tension and compression zones, for beam AI1	113
Figure 102. Typical deformed shape of the beam from numerical analysis.....	114
Figure 103. Stress evolution across the beam cross-section under increasing load for beam AI1	115
Figure 104. Bending Tension of Mean SG6 SG7, SG8 for beam AI1	117
Figure 105. Bending Tension of Mean SG5 and, SG9 for beam AI1	117
Figure 106. Bending Compression Test of Mean SG5 and, SG9 for beam AI1	118
Figure 107. Bending Compression of Mean SG5 and, SG9 for beam AI1	119
Figure 108. Bending Compression/Tension Strains for beam AI1	120

Figure 109. Load – displacement comparison Experiment vs Numerical for beam AI2.....	121
Figure 110. Strain gage comparison in compression and tension for beam AI2	122
Figure 111. Position of strain gauges: Illustration of the placement of strain gauges along the beam, showing both the tension and compression zones, for beam AI2	122
Figure 112. Stress evolution across the beam cross-section under increasing load for beam AI2	123
Figure 113. Bending Tension of Mean SG6 SG7, SG8 for beam AI2.....	124
Figure 114. Bending Tension of Mean SG5 and, SG9	125
Figure 115. Bending Compression Test of Mean SG1, SG2 and SG9	126
Figure 116. Bending Compression of Mean SG4 and, SG10.....	126
Figure 117. Experimental results bending compression/tension strains AI2.....	127
Figure 118. Comparison of experimental and numerical results for beam AI3	128
Figure 119. Bending Tension Test of Mean SG6, SG7 and SG8 for beam AI3.....	129
Figure 114. Bending Tension of Mean SG5	130
Figure 121. Bending Compression Test of Mean SG2	131
Figure 122. Bending compression test of mean of SG4.....	131
Figure 123. Experimental results bending compression/tension strains AI3	132
Figure 124. Comparison of experimental vs numerical results for beam A1, A2, A3	134
Figure 125. Mid-span deflection depending on hours (DI1)	135
Figure 126. Mid-span deflection depending on hours (DI2)	136
Figure 127. Comparison of experimental results between DI1 and DI2, including approximated function	136
Figure 128. Creep trend and the elastic modulus of DI1 and DI2 under sustained load	137

LIST OF TABLES

Table 1. Characteristic strength and stiffness properties for T-classes in N/mm ² and densities in kg/m ³ for boards or planks for GLT / Source: Class of boards from table 1, Standard EN14080	52
Table 2. Recording and calculation of data, averaging dimension measurements (longitudinal, radial and tangential) and weights	52
Table 3. Table test series	59
Table 4. Experimental Results for Serie E (Compression Parallel to the Grain)	71
Table 5. Highlighted results from the experimental test compression strength perpendicular to the grains	76
Table 6. Highlighted results for the Elastic Modulus (Stiffness).....	85
Table 7. Highlighted experimental results for Global Modulus of Elasticity	87
Table 8. Highlighted experimental results for bending strength parallel to the grain.....	99
Table 9. The data were recorded as presented in the following table report (Beam DI1):	105
Table 10. The data were recorded as presented in the following table report (Beam DI2):	106
Table 11. Data obtained from Modulus of Elasticity.....	111

EQUATIONS

Equation 1.....	51
Equation 2.....	51
Equation 3.....	70
Equation 4.....	70
Equation 5.....	71
Equation 6.....	76
Equation 7.....	84
Equation 8.....	87
Equation 9.....	93
Equation 10.....	93
Equation 11.....	93
Equation 12.....	99

ABBREVIATIONS

<i>GST</i>	<i>Glued Solid Timber</i>
<i>GLT</i>	<i>Glued Laminated Timber</i>
<i>IGST</i>	<i>Interlocking Glued Solid Timber</i>
<i>FEM</i>	<i>Finite Element Method</i>
<i>PSL</i>	<i>Parallel Strand Lumber</i>
<i>CLT</i>	<i>Cross Laminated Timber</i>
<i>X-Lam</i>	<i>Cross Laminated Timber</i>
<i>LSL</i>	<i>Laminated Strand Lumber</i>
<i>LVL</i>	<i>Laminated Veneer Lumber</i>
<i>CFRPs</i>	<i>Carbon Fiber – Reinforced Plastic</i>
<i>FRP</i>	<i>Fiber – Reinforced Plastic</i>
<i>MDFs</i>	<i>Medium Density Fiber Boards</i>
<i>OSBs</i>	<i>Oriented Strand Boards</i>
<i>UF</i>	<i>Urea – Formaldehyde</i>
<i>MUF</i>	<i>Melamine Urea – Formaldehyde</i>
<i>PUR</i>	<i>Polyurethane</i>
<i>RPM</i>	<i>Revolutions Per Minute</i>
<i>OT</i>	<i>Operation Time</i>
<i>LVDTs</i>	<i>Linear Variable Differential Transducers</i>
<i>HBM</i>	<i>Hottinger Brüel & Kjær</i>
<i>SG</i>	<i>Strain Gauge</i>
<i>RH</i>	<i>Relative Humidity</i>
<i>EN</i>	<i>European Norm</i>
<i>3D</i>	<i>3 Dimensional</i>
<i>PCAB</i>	<i>Picea Abies</i>
<i>EWPs</i>	<i>Engineered Wood Products</i>
<i>Dm</i>	<i>Deflection meter</i>

ABSTRACT

Timber, as a sustainable and versatile building material, continues to play a key role in modern construction, while reducing reliance on large, old-growth timbers and other heavy materials. While numerous studies have focused on glued laminated timber beams (GLT), this research explores the potential of an innovative engineered product Glued Solid Timber (GST) beams as a durable, long-lasting alternative with broad application.

This study presents a first series of experimental and analytical investigations conducted within the framework of Eurocode 5. The data generated may benefit both industry and society, with relevance to fields such as architectural and civil engineering construction.

Three GST beams were tested under bending, shear-field, and other load conditions, each fabricated according to applicable standards. The beams had a cross-section of 170 mm × 138 mm, composed of three lamellae (trio) with a thickness of lamella of 46 mm, and standard defined length.

The experimental results validated theoretical models and provided practical insight into the structural behavior of GST beams under various loading scenarios.

Alongside the experiments, numerical simulations were carried out using the Finite Element Method (FEM) to model the performance of GST beams under short and long-term loading. The numerical models incorporated experimentally derived material properties and used appropriate constitutive laws to simulate timber behavior in tension and compression.

A strong correlation was achieved between experimental and numerical results both globally through load displacement curves and locally through strain gauge validation. The simulations successfully captured the transition from elastic to plastic behavior, as well as time dependent deformations due to sustained loading, including stiffness loss from creep. These findings affirm the reliability of FEM for predicting GST beam performance.

GST beams present a compelling mix of structural performance, sustainability, versatility, and visual appeal. Their advantages over traditional solid timber and other materials make them a valuable option for modern construction aiming to balance performance, environmental responsibility, innovative design, and cost efficiency.

Keywords: *Glued solid timber, Innovative, Sustainability, Environmental, Numerical, Cost-efficiency, Innovative.*

АПСТРАКТ

Дрвото, како одржлив и разновиден градежен материјал, и понатаму игра клучна улога во современото градежништво, намалувајќи ја зависноста од големи, старорастечки дрвја и други тешки материјали. Додека бројни студии се фокусираа на гредите од лепено ламелирано дрво (GLT), ова истражување ја разгледува можноста на еден иновативен инженерски производ – греди од лепено масивно дрво (GST), кои претставуваат издржлива и долготрајна алтернатива со широка примена.

Оваа студија претставува прва серија на експериментални и аналитички истражувања спроведени во рамките на Еврокод 5. Генерираните податоци можат да бидат корисни како за индустријата, така и за општеството, со примена во области како архитектонското и градежното инженерство.

Три GST-греди беа тестирани при свиткување, сечење и други оптоварувања, при што секоја беше изработена согласно важечките стандарди. Гредите имаа напречен пресек од 170 mm × 138 mm, составени од три ламели (трио) со дебелина на ламелата од 46 mm, а должината беше определена според стандардот.

Експерименталните резултати ги потврдија теоретските модели и понудија практичен увид во конструктивното однесување на GST-гредите под различни услови на оптоварување.

Покрај експериментите, беа спроведени и нумерички симулации со Метод на Крајни Елементи (FEM) за моделирање на однесувањето на GST-гредите при краткотрајни и долготрајни оптоварувања. Нумеричките модели вклучуваа материјални својства добиени од експерименталните податоци и користеа соодветни конститутивни закони за симулација на однесувањето на дрвото при затегнување и притисок.

Постигната е силна корелација помеѓу експерименталните и нумеричките резултати – и глобално преку кривите на товар–деформација, и локално преку верификација со деформациски сензори. Симулациите успешно ја прикажаа транзицијата од еластично во пластично однесување, како и временски зависните деформации поради долготрајно оптоварување, вклучувајќи ја и загубата на крутост поради ползење (сгеер). Овие наоди ја потврдуваат доверливоста на FEM при предвидување на однесувањето на GST-гредите.

GST-гредите претставуваат привлечна комбинација на структурни перформанси, одржливост, разновидност и визуелна естетика. Нивните предности во однос на традиционалните масивни дрвени греди и други материјали ги прават вредна опција за современи градежни проекти кои тежнеат кон рамнотежа меѓу перформанси, еколошка одговорност, иновативен дизајн и економичност.

Клучни зборови: залепено цврсто дрво, иновативно, одржливост, еколошка, нумеричка, економичност, иновативно.

SUMMARY

This study explores the structural performance of Glued Solid Timber (GST) beams through an integrated approach combining experimental testing and Finite Element Modeling (FEM). The beams were fabricated under strict quality control following EN standards, with precise lamella preparation and adhesive bonding. The experimental program included short-term tests such as four-point bending and compression (parallel and perpendicular to grain), as well as long-term sustained loading tests to assess creep behavior.

In the bending tests (Serie A), all specimens showed consistent structural behavior characterized by three distinct phases: elastic, plastic, and failure. This classification was supported by both global load–displacement curves and local strain gauge measurements. Failure consistently initiated in the mid-span tension zone, providing a clear indication of the beam’s load-bearing progression. These findings allowed for the generalization of a three-phase response typical of GST beams under four-point bending.

Numerical analysis using 3D FEM models in DIANA software was performed in parallel, incorporating material parameters derived from experimental data. Timber was modeled as a homogenous material with brittle tension and elastic perfectly plastic compression behavior. The simulations closely reproduced the experimental results, including accurate predictions of deflection, strain distribution, stress evolution, and the movement of the neutral axis during loading. This validated the model’s capacity to capture both linear and nonlinear behavior.

In the long-term tests (Serie D), sustained loads caused notable stiffness loss in the early loading stages, followed by a gradual stabilization. The model successfully replicated the creep trend and time dependent deflection, aligning closely with experimental measurements. This emphasizes the importance of accounting for creep effects in the long-term structural analysis of timber elements.

Overall, the study confirms that FEM is an effective and reliable tool for simulating the behavior of GST beams under both short-term and long-term loading. The combined experimental and numerical approach offers valuable insights for the future design and application of engineered timber in structural systems.

РЕЗИМЕ

Оваа студија го истражува конструктивното однесување на гредите од лепено масивно дрво (GST) преку интегриран пристап кој комбинира експериментално тестирање и моделирање со Метод на Крајни Елементи (FEM). Гредите беа изработени под строг квалитетен надзор согласно EN стандардите, со прецизна подготовка на ламелите и нанесување на лепак. Експерименталната програма вклучуваше краткотрајни тестови како што се четириточково виткање и притисок (паралелно и нормално на влакната), како и долготрајни тестови под постојано оптоварување за проценка на ползењето (creep).

Во тестовите за виткање (Серија А), сите примероци покажаа конзистентно конструктивно однесување, карактеризирано со три јасно разграничени фази: еластична, пластична и фаза на откажување. Оваа класификација беше потврдена преку глобалните криви на товар–деформација и мерењата од локалните деформациски сензори. Откажувањето постојано започнуваше во зоната на затегнување на средишниот распон, што претставуваше јасен показател за носивоста на гредата. Овие наоди овозможува генерализација на трифазен одговор, типичен за GST-гредите под четириточково виткање.

Паралелно со експериментите, беше извршена и нумеричка анализа со употреба на 3D FEM модели во DIANA софтвер, при што беа вградени материјални параметри добиени од експерименталните податоци. Дрвото беше моделирано како хомоген материјал, со кршливо однесување на затегнување и еластично–совршено пластично однесување на притисок. Симулациите верно ги репродуцираа експерименталните резултати, со точни предвидувања за деформација, распределба на напрегања, еволуција на напрегањата и поместување на неутралната оска при оптоварување. Ова го потврди капацитетот на моделот да ја долови и линеарната и нелинеарната фаза на однесување.

Во долготрајните тестови (Серија D), континуираното оптоварување предизвика значително намалување на крутоста во почетната фаза, проследено со постепена стабилизација. Моделот успешно ја репродуцираше тренд линијата на ползење и временски зависната деформација, при што резултатите покажаа висока усогласеност со експерименталните мерења. Ова ја потенцира важноста од вклучување на ефектите од ползење во долгорочните структурални анализи на дрвени елементи.

Во целина, студијата потврдува дека FEM е ефикасна и сигурна алатка за симулирање на однесувањето на GST-гредите и при краткотрајни и при долготрајни оптоварувања. Комбинираниот експериментален и нумерички пристап нуди вредни сознанија за идниот дизајн и примена на инженерски дрвени конструкции.

ACKNOWLEDGEMENTS

This dissertation entitled "Experimental and Analytical Investigation of Glued Solid Timber Beams", would not have been possible without the support and dedication of many important people in my life, therefore, I would like to express my deep gratitude to all those who have supported me along this journey.

First, I would like to express my heartfelt gratitude to my mentor, Prof. Dr. Kiril Gramatkov, for his professional guidance, valuable advice and dedication throughout my research work for years. A special thanks also goes to my co-mentor, Prof. Dr. Toni Arangelovski, for his unstinting help and support.

I wholeheartedly thank my parents, Azem and Fahrije Jashari, for the unconditional love and tireless support they have given me at all stages of my studies. Without their sacrifices, this achievement would not have been possible.

I also thank my wife, Saranda Omura Jashari, for her patience, understanding, and constant encouragement. Her presence and support have been my strength in the most challenging days.

Any words of thanks are small compared to the gratitude I feel for each of the working group composed of colleagues, teachers, industry representatives and other stakeholders that I cannot include here.

Thank you!

Herein, I provide my personal statement for originality of the stated doctoral dissertation that I duly provide a reference of the quoted sources and that this paper is not used in any other university study for acquiring other knowledge

Handwritten signature of the doctoral student
(on the electronic version signature and the abbreviation p.s)

(on the electronic version of the doctoral dissertation)

I declare that the electronic version of the doctoral dissertation is identical to the printed doctoral dissertation.

Signature of the author, p.s.

1. INTRODUCTION

1.1. General Background

Timber has long been recognized as a sustainable and versatile construction material. In recent years, its use has gained prominence in modern architectural and civil engineering projects due to its environmental benefits, aesthetic appeal, and structural performance (Masoumi, Haghghi and Mohammadi, 2024). As global efforts to reduce the reliance on traditional materials such as steel and concrete intensify, engineered wooden products have emerged as a promising solution. Among these products, Glued Solid Timber (GST) beams stand out for their strength, durability, and adaptability in various construction applications (Shehada, 2024).

The research and development of GST beams are essential, especially in regions like the Western Balkans, where timber construction is increasingly popular but relies heavily on imports from countries like Germany, Austria, etc. By utilizing local resources, such as Spruce (*Picea Abies* PCAB), and adhering to European standards, the potential for producing high-performance structural timber elements locally can be explored and optimized.

1.2. Objectives and Scope

This dissertation aims to evaluate the structural performance of Glued Solid Timber (GST) beams through comprehensive experimental and analytical investigations. The primary objectives of this research include:

- **Experimental Analysis:** Conducting a first series of tests, including a variety of test series, on GST beams to determine their local and global modulus of elasticity, shear-field test, etc.
- **Analytical Validation:** Comparing experimental results with theoretical models to validate the mechanical properties of GST beams.
- **Material Performance Evaluation:** Assessing the suitability of Spruce (*Picea Abies*) as a raw material for GST beam production, focusing on strength, stiffness, and load-bearing capacity.

The scope of this research encompasses the production and testing of three-layer GST beams manufactured with structural adhesive in accordance with EN standards. The investigation covers

short-term and long-term behaviors, addressing critical aspects of mechanical performance and compliance with EN 408:2010+A1 and EN 14080:2013 standards.

1.3. Thesis Outline

- **Chapter 1: Introduction:** Provides the background, objectives, and scope of the research, and outlines the overall structure of the dissertation.
- **Chapter 2: Literature Review:** Discusses the properties and applications of timber as a building material, focusing on engineered timber products such as Glued Laminated Timber (GLT) and Glued Solid Timber (GST). The chapter also covers the production processes, including adhesives and other essential components based on the literature review.
- **Chapter 3: Design Models:** Explores different failure modes and presents analytical models for linear section behavior and finite element models (FEM) for non-linear section behavior.
- **Chapter 4: Fabrication of Glued Solid Timber (GST) Beams for Experimental Investigation:** Details the selection and preparation of wood materials, determination of moisture content and density, and production stages, including lamella processing, bonding, and press application.
- **Chapter 5: Experimental Investigation of Glued Solid Timber (GST) Beams:** Outlines the testing program, test setup, and instrumentation. It covers material mechanical characteristics in compression and the results from four-point bending tests, shear field tests, and long-term behavior assessments.
- **Chapter 6: Numerical Modeling:** Describes the constitutive model, boundary conditions, and mesh discretization. The chapter presents results from numerical simulations of four-point bending tests and long-term behavior under sustained loads, with comparative discussions.
- **Chapter 7: Conclusions:** Summarizes the key findings and evaluates the success of the research objectives.

2. LITERATURE REVIEW

2.1. Timber as Building Material

Timber is one of the most valuable materials in construction that has been used since ancient times. Its anatomical structure makes it not only aesthetic, but also a material that allows it to be easy to work with and achieve high structural durability.

In these early decades of the 21st century, timber is enjoying a renaissance as a mainstream structural material (Dickson and Parker, 2014).

Timber has been utilized as a building material for centuries due to its excellent strength-to-weight ratio, aesthetic appeal, and sustainability. Compared to steel and concrete, timber exhibits a significantly lower carbon footprint, making it a key material in sustainable construction practices (Dziurka *et al.*, 2022).

Timber structures offer good insulation properties, easy processing, and environmental benefits such as being a CO₂ reservoir, contributing to climate protection (Jamnitzky and Deák, 2019). Timber's anisotropic and hygroscopic nature necessitates careful selection and treatment, especially considering biological degradation and environmental variations (He *et al.*, 2022).

Modern advancements in timber processing and preservation techniques have greatly improved its durability, expanding its application in various structural systems, from residential to commercial and industrial buildings, as well as in infrastructure projects like bridges and towers.

2.1.1. Wood processing as a construction material

To use wood in building constructions, it must go through a technological processing process that includes several necessary steps to be undertaken. Initially, the wood cut from the forest must go through a first stage (primary wood processing) before the mechanical process, namely the drying stage, to avoid its dimensional deformation in different environmental conditions (Chauhan, 2025). Then, the wood must be processed to be ready for use, including sawing, dividing into different elements based on standards and treating in special cases to make it stronger and more durable. These techniques improve the quality and durability of the material for a longer life-span.

2.1.2. Types of wood and their use in construction

Different types of wood are used in construction, each with different characteristics that adapt to applications according to needs. There are species of wood from the coniferous (gymnosperm) and broadleaf (angiosperm) families that have different anisotropic properties, which serve to build large structures as vertical and horizontal supports (Wengert and Denig, 1995). One of the important aspects of using wood is choosing the right type for each assortment of the building, to ensure aesthetics, durability, functionality and structural safety.

To ensure the use of high-quality wood, it is important to comply with the standards that oversee its use in construction.

The European Standard EN 14080-2013 covers glued laminated products made from one of the following species:

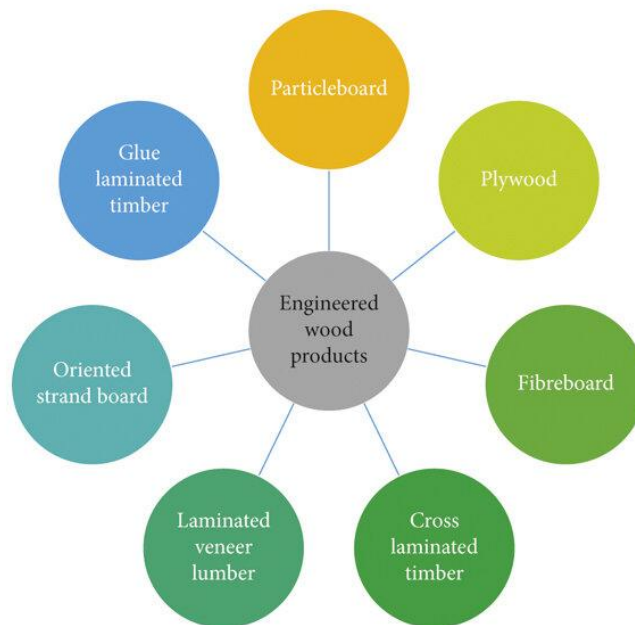
Spruce (*Picea abies*, PCAB), Fir (*Abies alba*, ABAL), Scots pine redwood (*Pinus sylvestris*, PNSY), Douglas fir (*Pseudotsuga menziesii*, PSMN), Western Hemlock (*Tsuga heterophylla*, TSHT), Corsican pine and Austrian black pine (*Pinus nigra*, PNNL), European larch (*Larix decidua*, LADC), Siberian larch (*Larix sibirica*, LASI), Dahurian larch (*Larix gmelinii* (Rupr.) Kuzen.), Maritime pine (*Pinus pinaster*, PNPN), Poplar (Applicable clones: *Populus x euramericana* cv “Robusta”, ”Dorskamp”, “I214” and “I4551”, POAL), Radiata-Pine (*Pinus radiata*, PNRD), Sitka-spruce (*Picea sitchensis*, PCST), Southern Yellow pine (*Pinus palustris*, PNPL), Western Red Cedar (*Thuja plicata*, THPL), Yellow Cedar (*Chamaecyparis nootkatensis*, CHNT). Whereas for the research within the framework of this dissertation, the selected wood species is Spruce (*Picea abies*, PCAB), of high quality, Class I (Šuhajdová *et al.*, 2023), inspected firstly and then selected mainly as radial wood (primarily) without natural defects, such as knots, twists, bending, etc. Quality control includes inspecting the wood for damage and assessing its strength and durability. The wood is chosen as treated (dried) to prevent damage from insects and various possible defects.

Engineered materials used in construction, such as Glulam (glued laminated timber) and Glued Solid Timber (glued solid timber) are more advanced alternatives to natural wood and offer significant benefits in structural construction. These engineered materials are created using modern technology with the aim of improving the overall properties of wood (Azzi *et al.*, 2025).

2.2. Engineered Wood Products

Engineered wood products (EWP) are manufactured wood materials that offer enhanced structural properties and innovative performance compared to traditional solid timber. These products are created by bonding or assembling multiple layers or strands of wood together using adhesives, heat, and pressure.

Engineered wood products are designed to optimize the use of timber resources and overcome some of the limitations of solid timber, making them a versatile and sustainable alternative in construction. EWP offer several advantages over traditional solid timber, including improved strength-to-weight ratio, reduced waste, enhanced dimensional stability, and the ability to achieve larger spans and heights. These products contribute to sustainable construction practices by utilizing timber resources more efficiently and reducing environmental impact. Wood-based composite materials can be made up of various wood elements, including fibers, particles, flakes, veneers, or laminates (Stark and Cai, 2021).



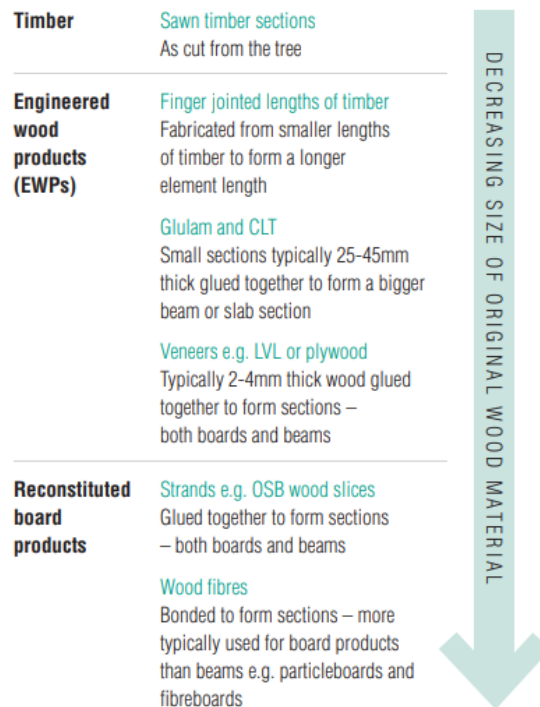
Source author: Creator: Zhang Haohao

Figure 1. Engineered Wood Products

Recently, there have been significant developments in the range of EWPs for structural applications with materials such as laminated veneer lumber (LVL), parallel strand lumber (PSL), laminated strand lumber (LSL), prefabricated I-beams, metal web joists and ‘massive’ or cross-

laminated timber (CLT) becoming more widely available. These EWPs are typically manufactured by adhesively laminating together smaller softwood sections or laminates (e.g. glulam and CLT) or veneers or strands of timber (e.g. LVL, LSL and PSL)(Stark and Cai, 2021).

Nowadays, has been a notable rise in research focused on glulam beams that are reinforced with synthetic fibers, including carbon, aramid, and glass fibers. Furthermore, investigated how reinforcing wood with carbon/epoxy fiber-reinforced plastics (CFRPs) impacts its performance (Plevris and Triantafillou, 1992). While (Plevris and Triantafillou, 1992) studied the creep behavior of wood reinforced with FRP and created an analytical method to forecast time-dependent deformations of timber beams reinforced with CFRP laminates of varying thicknesses. (Triantafillou and Deskovic, 1992)] examined the impact of pre-stressed CFRP reinforcement attached to European beech wood. Extensive research has been conducted to explore the structural behavior of glulam beams and solid timber beams that are reinforced with FRP sheets or bars (Dagher *et al.*, 1996); (Hernandez, 1997);(Romani and Blass, 2000) (Romani and Blaß, 2001); (Gentile, Svecova and Rizkalla, 2002);(Fiorelli and Dias, 2003).



Source: *Engineered wood products and an introduction to timber structural systems Timber Engineering Bulletin*

Figure 2. Fibre size and beam types for timber products

The varying performance of EWPs is influenced by the size of wood component used in the product. At one end of the spectrum smaller sections of timber are laminated and finger jointed to form sections of glulam, whilst at the other end, reconstituted board products such as oriented strand boards (OSBs) and medium density fibre boards (MDFs) use small wood strands or fibres bonded together (Engineered wood products and an introduction to timber structural systems – Timber Engineering Bulletin).

2.3. Laminated Timber

Laminated timber, referred to as engineered wood, is a structural material produced by bonding multiple layers of wood to improve strength, stability, and longevity.

It is frequently utilized in building projects for beams, columns, and panels because of its enhanced load-bearing ability in comparison to solid wood.

Glued wood species have a number of advantages, such as the possibility of creating complex structural shapes, the functioning of products in changing climatic conditions (high humidity, high and low temperature), resistance to loads, the use of low-grade raw materials, and improved aesthetic appearance associated with the possibility of applying valuable wood species (Shevchuk K,A, 2021).

2.3.1. The history of Glued Laminated Timber

Laminated timber, also known as Glulam, has a rich history tied to attempts to enhance the structural properties of natural wood. As far back as the 1800s, builders and engineers started to experiment with bonding wooden layers together to form larger and more robust components. Nonetheless, it was in the early 20th century that significant advancements were made in glulam manufacturing, driven by innovations in synthetic adhesives and wood processing methods.

Otto Hetzer (1846-1911), born in Weimar in Germany, was the first to demonstrate that beams and arches can be laminated together industrially into units with such great composite sections that they could be used in advanced structures for wide spans. Hetzer, who was a qualified carpenter, was also the owner of a sawmill and a gifted structural engineer. Hetzer started a company, Otto Hetzer Holzpflege und Holzbearbeitungs AG, within which he developed new timber components and applied for patents for various types of joined beams (Bautchtechnik, 2006, V83). In 1906 Hetzer got the patent for the invention that laminates boards to curved members. In the patent

application it can be seen that Hetzer handled most of the technical aspects, which are still relevant for the production and use of glulam.

The inherent constraints of wood regarding size and form have been overcome. While mechanical methods could have achieved this earlier, the introduction of glulam allowed wood to start competing with materials such as steel and reinforced concrete in structures that bear loads over large spans. In recent times, various modifications within standards have been reached to enhance the properties of glulam using different hybrid components and having a design with a varying cross sectional dimensions.

2.3.2. Glued Laminated Timber (GLT)

Glued laminated timber (glulam) is an engineered wood product created by laminating multiple layers of dimensioned timber using high-strength adhesives. Glued laminated structural timber is a product member composed by at least two essentially parallel laminations which may comprise of one or two boards side by side having finished thicknesses from 6 mm up to 45 mm (EN 14080:2013).



Source: Regstab timberlab

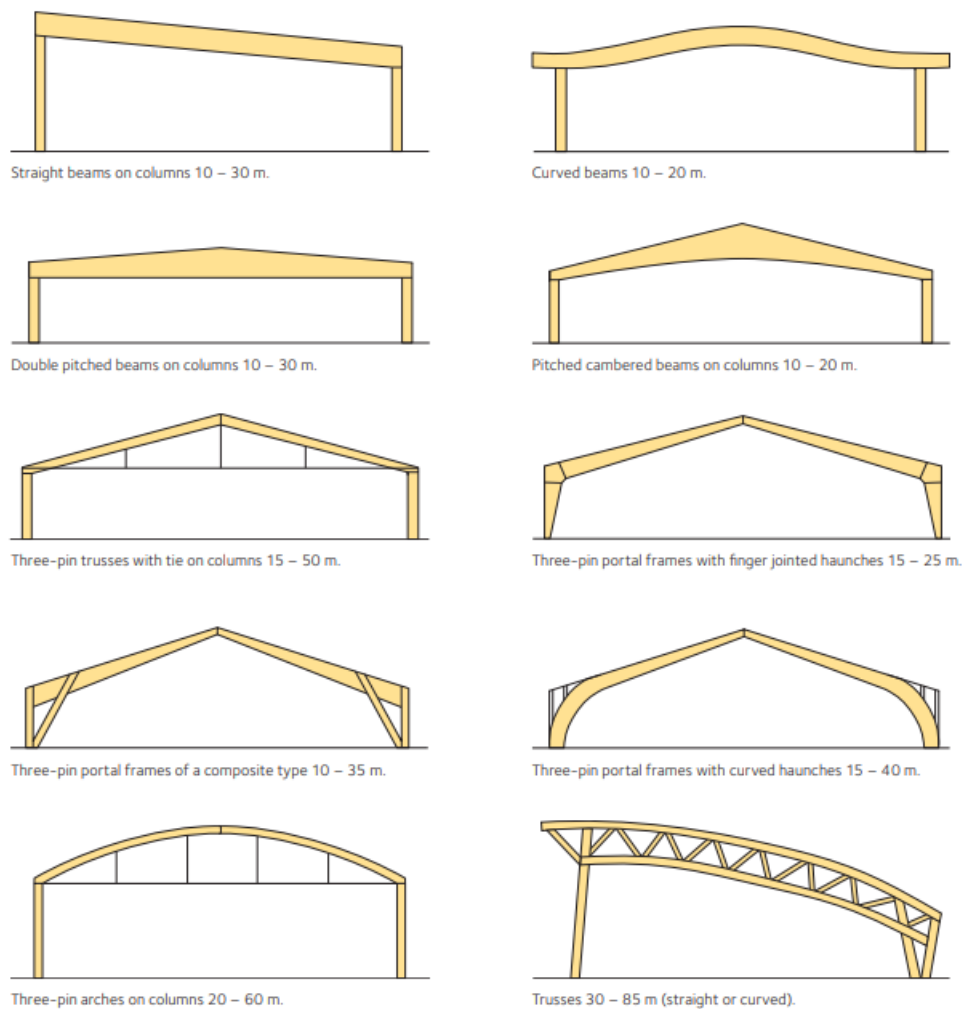
Figure 3. Glued Laminated Timber Product

Glulam is extensively used for its superior mechanical properties, design flexibility, and aesthetic appeal (EN14080:2013.) outlines the European requirements for glulam products, addressing mechanical resistance, bonding strength, and durability against biological attack (CEN, 2013). (Šuhajdová *et al.*, 2023) noted the mechanical comparability of hybrid hardwood glulam beams to traditional homogeneous beams, suggesting potential weight savings. Reinforcement techniques, such as using CFRP sheets, significantly improve glulam beams' structural

performance, allowing broader structural applications (He *et al.*, 2022; de Vito Junior William Martins, 2023).

Arguments for laminating by gluing together boards were to make the load bearing structure's formation independent of the dimensions of the growing trees and the possibility of manufacturing different shapes and suitable composite sections (The glulam handbook, volume I; edition 1:2024).

Glulam also offers architectural versatility, enabling the creation of large, curved, or complex structures, previously difficult to achieve with traditional timber products.



Source: *The glulam handbook, volume I; edition 1:2024*

Figure 4. Standard shapes of glulam and range of spans

This versatility has led to a significant increase in the use of glulam in large-span structures such as sports arenas, exhibition halls, airport terminals and shopping centers where both aesthetic and structural requirements are demanding.



Figure 5. Application of Glued Laminated Timber at Prishtina Mall

The European Standard (EN 14080) has set the performance requirements of the following glued laminated products:

- Glued laminated timber (glulam);
- Glued solid timber;
- Glulam with large finger joints;
- Block glued glulam.

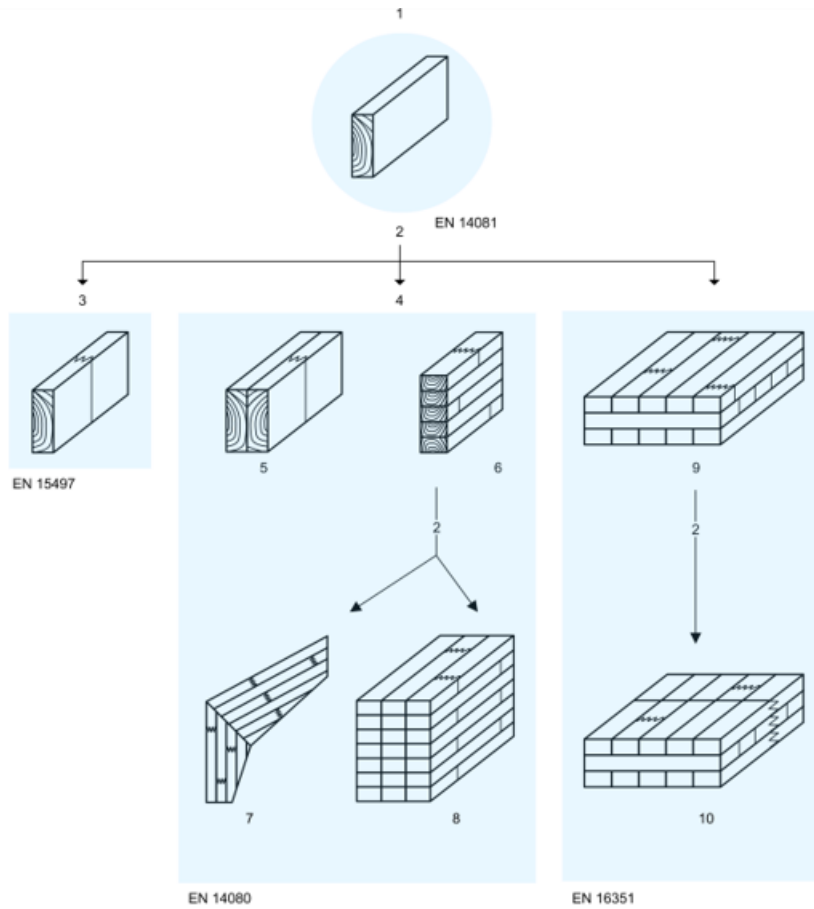


Figure 6. Relation of European Standards for structural timber products prepared by CEN/TC 124

Key 1

1. Boards;
2. Is a component for;
3. Structural finger jointed timber;
4. Glued laminated products;
5. Glued solid timber;
6. Glued laminated timber (glulam);
7. Glulam with large finger joints;
8. Block glued glulam;
9. Cross laminated timber (X-Lam);
10. Cross laminated timber (X-Lam) with large finger joints.

Based on the literature review for engineering products related to wood structures, namely laminated connections and consultations with professionals, it was noted that there is a need to further research a product such as Glued Solid Timber (GST) beam, product number 5 according to EN 14081 (fig. 6), aiming at experimental and analytical investigation across multiple test modules. Through the literature review, successful production of beams was made, which then began to be experimented at the University of St. Cyril and Methodius, respectively the Faculty of Civil Engineering in Skopje, North Macedonia.

2.3.3. Glued Solid Timber (GST)

Glued solid timber (GST) refers to timber elements bonded in various configurations forming larger structural sections, often using interlocking joints rather than thin laminations as in glulam. A notable system is the Interlocking Glued Solid Timber (IGST), which employs overlapping patterns and diagonal cuts, offering mechanical properties comparable to solid timber without traditional finger joints (Patlakas Michele Christovasilis, Ioannis Nocetti, Michela Pizzo, Benedetto, 2019).

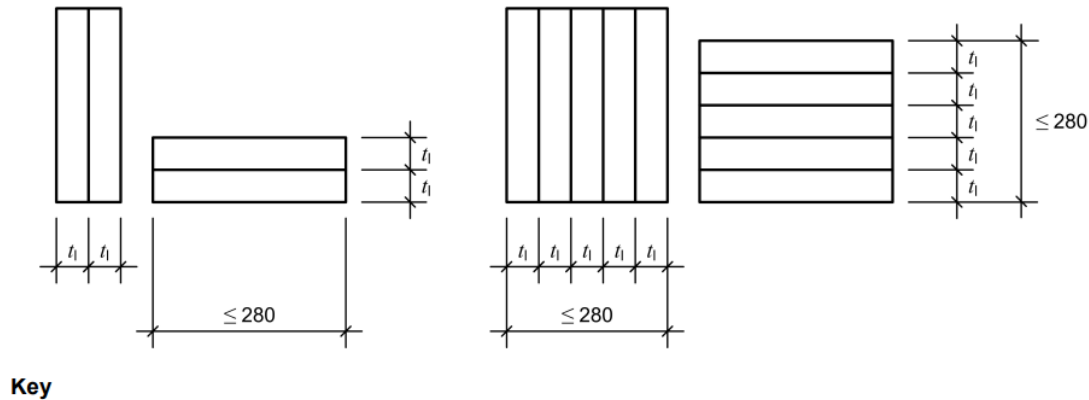
GST provides greater flexibility in production, reduced manufacturing time, and can be an effective alternative or complement to traditional glulam and CLT structures. The innovative joint designs in GST contribute to enhanced structural integrity and facilitate rapid construction, meeting contemporary building demands for efficiency and sustainability.

The structural efficiency and rapid assembly provided by this product have broadened its application in multi-story residential and commercial buildings, demonstrating substantial potential for future growth in the timber construction sector.

Structural timber member with overall cross-sectional sizes not exceeding 280 mm comprising two to five essentially parallel laminations bonded having the same strength class or manufacturer

specific strength class and a finished lamination thickness greater than 45 mm up to 85 mm (EN 14080).

EN 14080:2013 (E)



Source: EN14080:2013 (E)

Figure 7. Examples for glued solid timber made of two and five laminations

The decision to take this product into consideration and initiate the testing idea was based on several key reasons:

According to the latest research, the selected material offers a number of advantages over traditional construction materials, including lower environmental impact, higher energy efficiency, and the promotion of local economic development;

In the Western Balkans region, there is a lack of literature and previous studies addressing the use of this type of product and similar materials in construction;

There is considerable potential for the use of spruce wood (*Picea abies* – PCAB), thanks to its favourable physical, mechanical, and ecological characteristics, which make it a sustainable alternative for modern construction.

In this particular study, all Eurocode 5 data were taken as a basis, in addition, the cross-section of the tested product is 170mm x 138mm, with three lamellas glued together. In the current research of the full-scale models, thickness of lamella is 46mm, height 170mm (max. allowed 280mm).

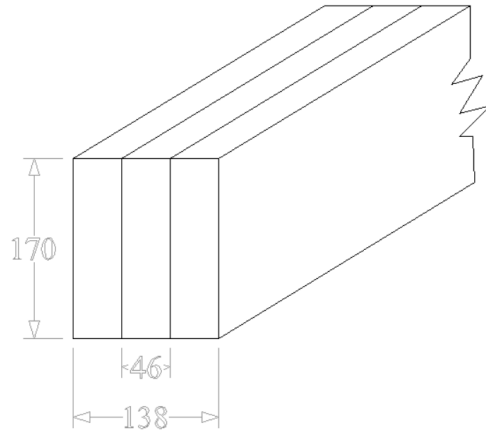
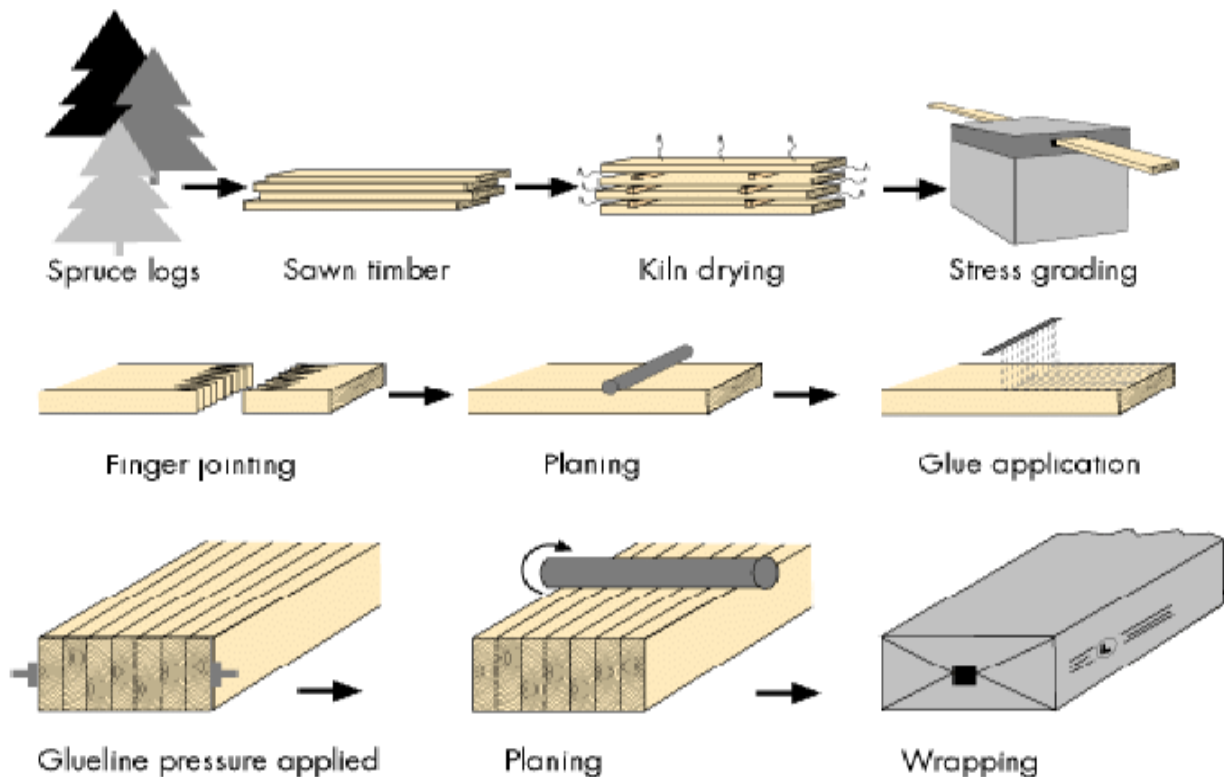


Figure 8. Cross section dimensions of full-scale glued solid timber beam for experimental and analytical investigation.

2.4. Production Process and Adhesives

The production processes for GLT and GST are heavily dependent on adhesive systems, which greatly influence the mechanical properties, durability, and environmental impact.



Source: Glulam Manufacturing (Courtesy Moelven Töreboda AB)

Figure 9. Production process of Glued Laminated Timber

The manufacture of glulam timber must follow recognized national standards to justify the specified engineering design values (Moody and Liu, 1999).

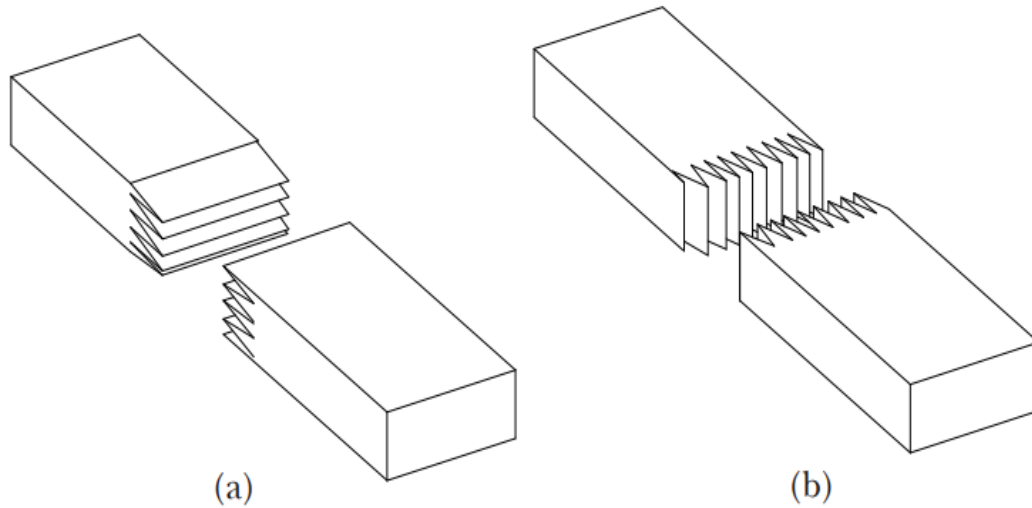
In the technological workflow, the wood is first delivered from forests in accordance with the required class. It is then delivered to primary wood processing as raw material, where the cutting of the elements based on specifications begins. After cutting and preparing the boards to meet specifications, they are stacked for the drying phase, which is a mandatory process. Once the drying is complete, the boards are squared on all four sides through planner machines and then finger-jointed as necessary to facilitate extension. After extending the boards to the required length, they are shaped to the final dimensions. Following this, an adhesive layer is applied to all elements. Pressing occurs to enhance adhesion strength. After the pressing stage, the final shape is adjusted once more, followed by packaging and preparation for shipment. With this technological process complete, the laminated beams are ready for their intended use.

2.4.1. Finger-joint of Glued Laminated Timber

The orientation of finger-joints, the orientation of the laminates would also depend on its end use. (Technology bulletin no. 63, 2016, an overview of manufacturing process of glued-laminated timber). Since the timber is not long enough naturally for use in wooden structures, there is the possibility of using finger-joints, which is an extent connection that can today be easily performed through technological processes.

There are two types of laminated beams, namely horizontally laminated beam (Figure 10a) and vertically laminated beam (Figure 10b). Horizontally laminated glulams are the common configuration used in most construction. Vertically laminated glulams are meant for components that need to be curved when looking from plan view such as the timber rafters used in a round tent-like roof, etc.

As for the study for this dissertation, the finger-joint connection was not applied, since the length required by the standard for the full-scale beam was sufficient (the longest 3570mm, and the shortest 185mm).



Source: *An overview of manufacturing process of glued-laminated timber how ss, sik hs & anwar umk*

Figure 10. Orientation of finger-joints

2.4.2. Adhesives

Common adhesives include resorcinol-phenol-formaldehyde (RPF), melamine-urea-formaldehyde (MUF), and polyurethane-based adhesives, each offering different strengths and environmental suitability (Dziurka *et al.*, 2022). EN 14080:2013 specifies rigorous tests for bonding strength and durability under varying environmental conditions (CEN, 2013). Advances in adhesives and production technology, including the integration of steel or CFRP reinforcements, significantly enhance the performance and reliability of timber beams, enabling their use in complex structural engineering applications (Mei Nan Li, Ling Zuo, Hongliang Zhao, Yan, 2021; Harrach Muayad Movahedi Rad, Majid, 2022). Additionally, proper quality control, including visual and machine strength grading as per EN 14081-1:2016+A1:2019, ensures the structural integrity and consistency of engineered timber products (CEN, 2019).

For the production of laminated timber, only adhesives are used, which have found high strength and durability under long-term loading. The formal requirements are given in the European standard EN 14080 and under the standard EN 301, which classifies two types of adhesives as type I and type II adhesives. Instead of the requirements in EN 301, the requirements for one-component polyurethane adhesives based on EN 15425 must be met (Gross H, 2013).

Type I adhesives are designed to endure complete outdoor exposure and temperatures exceeding 50°C. Type II adhesives are suitable for use in heated and ventilated structures as well as sheltered

exteriors. They can handle brief exposure to the elements but are not suited for extended weather exposure or temperatures above 50°C. (Kuklik P, 2008).

The adhesive releases very small amounts of substances that affect the environment, in addition the percentage of adhesive in the laminate is negligible, approximately 1% by weight. The manufacturer must test and verify the formaldehyde emission in class E1 or E2 according to the European standard (EN 14080, 2013). Current types of structural wood adhesives can also be found as follows:

Resorcinol formaldehyde (RF) and Phenol-resorcinol formaldehyde (PRF) adhesives

RF and PRF are type I adhesives according to EN 301. They are used in laminated beams, in bonding structural joints, in I-beams, in box beams, etc., both indoors and outdoors.

Phenol-formaldehyde (PF) adhesives

Hot-setting PF cannot be classified according to EN 301. Phenol-formaldehyde (PF) adhesives, cold-setting, cold-setting PFs are classified according to EN 301, but the current types are likely to be eliminated by the "acid damage test" given in EN 302-3.

Urea-formaldehyde (UF) adhesives

Urea-formaldehyde (UF) adhesives Only special cold-setting UFs are suitable for structural purposes. In a fire they will tend to delaminate. UFs for structural purposes are classified according to EN 301 as type II adhesives.

Melamine urea formaldehyde (MUF) adhesives

Cold sets are classified according to EN 301. However, they are less resistant than resorcinols and are not suitable for marine purposes. However, MUFs are often preferred for economic reasons and because of their lighter color.

Casein Adhesives

Casein adhesives are probably the oldest type of structural adhesive have been used a lot in the past but have been used for the industrial production of Glulam since before 1920. Casein does not meet the requirements of EN 301.

Two-component polyurethane adhesives

These adhesives offer strong bonding and lasting performance; however, practical usage indicates that they may not withstand all weather conditions. (Kuklík P, 2008).

Innovations in adhesive technology have further reduced environmental impacts, promoting the broader adoption of engineered timber in eco-friendly construction (Maithani and Mishra, 2024). Continuous research and development efforts focus on improving adhesive formulations to meet stricter environmental standards, enhance mechanical performance, and provide greater durability under harsh conditions.

For the production of Glued Solid Timber (GST) beams, respectively the study taken as a basis in this dissertation by the author, one-component polyurethane adhesive was used (fig. 11), which implies that EN15425 was respected.



Figure 11. Polyurethane one-component adhesive used for bonding

2.5. Mechanical Properties

Glulam and Glued Solid Timber exhibit exceptional mechanical properties due to their engineered nature. Glulam beams typically have higher strength and stiffness compared to solid timber of equivalent dimensions due to their layered composition.

The controlled fabrication processes, including finger jointing and precise lamination, enhance load-bearing capacities and structural reliability. Hetzer's patent (1906) (Rug, 2006) fundamentally changed timber engineering by introducing laminated timber elements with improved load-bearing capacities, making possible large structural spans and complex geometries (Rug, 2006). These properties allow glulam beams to be widely used in various structural applications such as large-span roofs, bridges, and multi-story buildings (Derix, 2016). Additionally, glulam's anisotropic properties are minimized by cross-layering techniques, improving dimensional stability and consistency in mechanical performance across different environmental conditions.

Modern research and testing continue to refine understanding of timber's mechanical behavior, including investigations into the effects of load duration, moisture content, and temperature on structural performance, enabling engineers to design safer and more efficient timber structures.

2.6. Long Term Behavior – Creep

Timber and engineered timber products like GLT and GST exhibit creep under sustained load, which is a critical consideration for long-term structural performance.

Creep behavior in timber results from the viscoelastic nature of wood, leading to gradual deformation under continuous stress. This deformation can be significant in long-span structures and heavily loaded beams. It is very important to accounting for creep in the design and analysis of timber structures to ensure long-term serviceability and structural integrity (Dziurka *et al.*, 2022) evaluated the long-term effects of periodic loading on glulam beams and confirmed that proper design and load limits could mitigate adverse effects on structural performance over time. Understanding and predicting creep behavior is essential for ensuring the durability and reliability of engineered timber structures over their expected service life.

Advances in modeling techniques and empirical studies continue to refine the prediction and mitigation strategies for creep in timber engineering. Models such as Burger's and Schapery's are commonly used to predict this behavior, though their accuracy varies.

Understanding and predicting creep is essential for ensuring serviceability, especially in long-span beams where deflection limits often govern design more than strength criteria (Creep in Timber Structures. Edited by P. Morlier – Rilem Report 8)

Current research for the dissertation efforts are increasingly focused on long-term monitoring and real-time data collection to enhance the precision of creep models, which will further improve the lifespan and reliability of timber structures in diverse applications.

2.7. Failure modes

Identifying different failure modes is essential for achieving accurate and reliable results in both modeling and experimental analysis of structural behavior. A clear understanding of how and why a material or structural element may fail under various conditions allows for the development of predictive models that more closely reflect real-world performance.

Structures have to adopt, and transfer external loads to the ground and also to deal with the corresponding internal loads (normal force, shear force and moment)(Franke, Franke and Harte, 2015).

The mechanical strength of wood depends on whether load is compressive or tensile and on loading direction in relation to fiber direction (Livas, Ekevad and Öhman, 2022).

In this study, failure modes were systematically classified based on key parameters, including inherent material properties such as strength and stiffness, as well as the nature of the applied loading configurations. These identified modes of failure were then incorporated into the computational model to ensure a more representative simulation of actual behavior.

Nevertheless, it is important to acknowledge that the model does not capture all factors that may influence failure. Specifically, the presence of natural defects and other imperfections within the wood such as checks, grain deviations, or local density variations can significantly alter the stress distribution and initiate premature failure. These aspects, while critical in practice, were excluded from the current modeling scope due to their stochastic nature and the complexity involved in their quantification.

In practical design scenarios, however, the influence of such strength reducing characteristics should not be overlooked. Appropriate correction or safety factors must be applied to account for this inherent variability in material quality and to ensure a robust and conservative design.

Tensile failure is one of the most prevalent and critical failure modes observed in timber structures, primarily due to the inherently brittle behavior of wood under tensile loading. Unlike materials that exhibit ductile characteristics, timber lacks the ability to undergo significant plastic deformation when subjected to tensile forces. Tension stress has to be considered parallel to the grain and perpendicular to the grain directions (Franke, Franke and Harte, 2015). As a result, this failure mode often manifests suddenly and without warning, typically through the formation of cracks along the fiber direction. These cracks can rapidly propagate and lead to catastrophic failure of the cross-section.

The tensile limit state of timber is considered to be reached when the maximum tensile stress within the member equals its tensile strength. Structurally, failure is assumed to occur when the tensile stress in the outermost fiber of the tension zone exceeds this limit. Depending on the stress distribution across the section, two global tensile failure modes can be identified, each influenced by the state of stress in the compression zone.

a) Failure in the Tensile Zone with a Linear-Elastic Cross Section

This type of failure occurs when the outermost tensile fiber reaches its tensile strength while the entire cross section, including the compression zone, remains in the linear-elastic range. It is typical in unreinforced or minimally reinforced timber beams, particularly when the tensile strength is significantly lower than the compressive strength. The failure is abrupt and brittle, as no significant redistribution of stress occurs prior to fracture. Strain and stress distribution at the onset of tensile failure without compressive plastification. The tensile failure occurs when the tensile stress in the outermost fiber reaches the tensile strength ($\sigma_t = f_t$), while the compression zone remains within the linear-elastic range ($\epsilon_c < \epsilon_{c,el}$) (Figure 12). This typically results in a brittle failure mode.

b) Failure in the Tensile Zone with a Linear-Elastic-Ideal-Plastic Cross Section

In this mode, the tensile strength of the outermost fiber is reached only after some degree of plastification has occurred in the compression zone. However, the compressive zone has not yet reached its ultimate strain capacity. This scenario is commonly observed in beams with light reinforcement, either solely in the tension zone or symmetrically in both tension and compression zones. Although some degree of ductility is introduced at the global level due to partial plastification, the failure remains locally brittle, as tensile fibers still fracture without plastic deformation. In this failure mode, the tensile stress in the outermost fiber reaches the tensile strength limit ($\sigma_t = f_t$), signifying failure. Unlike the purely elastic failure mode, the compressive zone has exceeded its elastic limit (ϵ_c, el) but has not yet reached its ultimate plastic strain (ϵ_c, pl), indicating a linear-elastic–ideal-plastic response on the compression side (Fig. 13). This behavior introduces some global ductility in the member, though the failure remains locally brittle due to fiber rupture in tension. It should be noted that, in this case, the position of the neutral axis shifts when compressive plasticity occurs, compared to its location under purely linear-elastic behavior.

Understanding these tensile failure modes is essential for accurately assessing the structural performance of timber elements and for informing effective reinforcement strategies. While some ductility may be achieved through appropriate reinforcement, the brittle nature of tensile failure in timber highlights the importance of careful design, especially in tension-dominated regions.

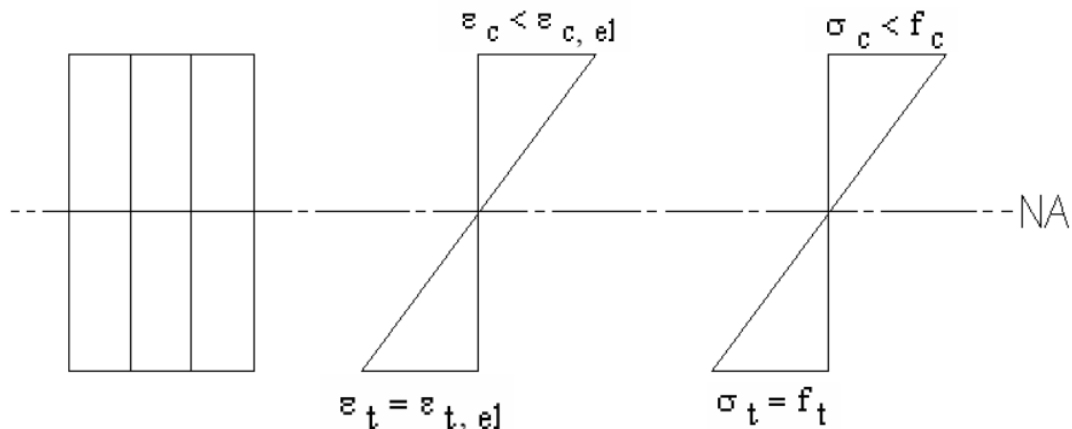


Figure 12. Strain and stress distribution at tensile failure, occurring before the onset of compressive plasticity

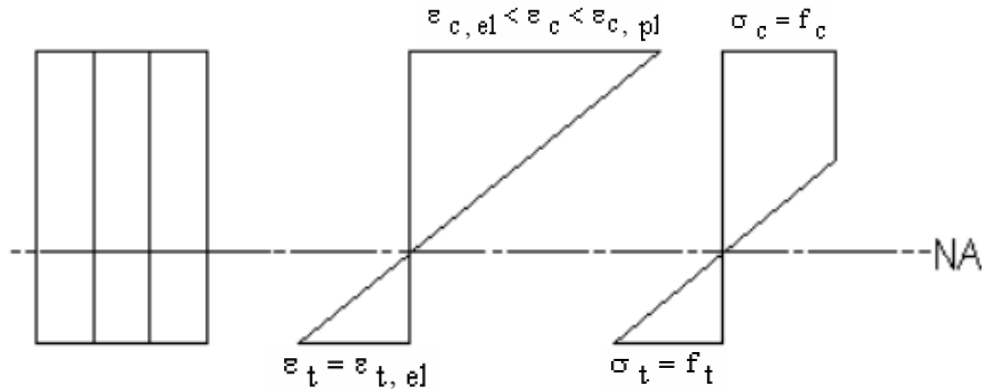


Figure 13. Strain and stress distribution at tensile failure with the compression zone reaching plasticity

Failure under longitudinal compression stress occurs mainly in timber trusses, beams or columns (Franke, Franke and Harte, 2015).

This failure mode is not commonly observed in unreinforced timber sections. However, its likelihood increases when reinforcement is added on the tension side of the beam. The ultimate compressive state is reached when the maximum compressive strain in the section attains the material's ultimate compressive strain.

Compressive failure preceding tensile rupture typically occurs in beams that are heavily reinforced in the tension zone. In such cases, plastic deformation develops in the compression zone, resulting in a more ductile structural response and allowing the beam to absorb greater energy before failure.

2.8. Shear failure

Shear failure is a significant and commonly observed failure mode in both unreinforced and reinforced timber elements. In most cases, bending stress and deflection limits govern the design of the members (Franke, Franke and Harte, 2015). It typically occurs along planes parallel to the grain, where wood exhibits its weakest resistance to stress. In reinforced timber beams, where the tensile and compressive capacities are enhanced through reinforcement, the critical failure mode often shifts to shear. This happens when the shear stress within the cross-section exceeds the timber's inherent shear strength.

Shear failure is generally brittle and abrupt, characterized by crack propagation along the fiber direction, often originating near supports or at points of high transverse loading. In unreinforced timber, shear strength is often significantly lower than axial strengths, making it a limiting factor in design. The failure typically manifests as a diagonal shear crack or longitudinal splitting, depending on the loading and support conditions.

2.9. Adhesive failure

The quality of the glue line plays a fundamental role in the mechanical resistance of beams (Faria *et al.*, 2024).

Adhesive failure in glued laminated timber (glulam) compromises structural performance by disrupting the bond between lamellae. It can occur at the glue line (adhesive failure) or within the wood near the bond (cohesive failure), often due to poor surface preparation, inadequate pressure during gluing, or environmental factors like moisture and temperature. This type of failure may lead to delamination or cracking along the glue lines, especially under shear or tension perpendicular to the grain. Ensuring proper adhesive application and using durable adhesives such as PRF or PUR are essential to prevent such failures and maintain long-term structural integrity.

2.10. Linear elastic behavior

Linear elastic behavior in structural materials, including timber, can be effectively observed using strain gauges. These devices measure strain at specific locations on the surface of a material under load, allowing for precise monitoring of deformation. In the linear elastic range, stress and strain maintain a proportional relationship, as described by Hooke's Law. By plotting the measured strain values against the applied stress, a linear trend indicates that the material is behaving elastically and has not yet experienced permanent deformation. This method is particularly useful in experimental testing, where strain data can confirm theoretical assumptions about elastic limits, stiffness, and material uniformity. Additionally, strain gauges can be strategically placed to detect local stress concentrations, identify the location of neutral axes, and assess the onset of nonlinearity, helping to evaluate both global and localized structural response.

2.11. Non - linear section behavior

While linear elastic analysis provides valuable insights into the initial response of timber structures, it becomes insufficient once the material exhibits nonlinear behavior.

Nonlinearities in timber arise due to factors such as plastic deformation, cracking, crushing in the compression zone, tension softening, and the presence of defects like knots or grain deviations. In such cases, the stress-strain relationship is no longer proportional, and localized phenomena such as stress redistribution, damage accumulation, and material anisotropy become significant. To accurately capture these complex responses, especially beyond the elastic range, advanced numerical tools like the Finite Element Method (FEM) are essential.

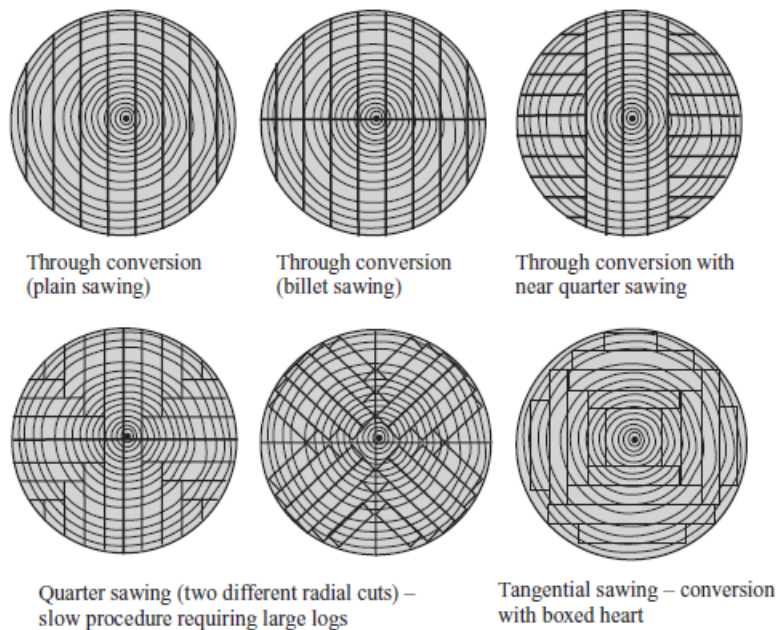
FEM enables the modeling of both material nonlinearities, providing detailed insights into the progression of failure mechanisms under various loading conditions. It allows for the simulation of strain localization, crack initiation and propagation, and plasticity in both tension and compression zones.

FEM can incorporate contact behavior, that is difficult to be evaluated experimentally or analytically. Therefore, to fully understand and predict the nonlinear response of timber structural elements, especially when approaching ultimate load conditions, the use of FEM becomes an indispensable tool of modern structural analysis and design.

3. FABRICATION OF GLUED SOLID TIMBER (GST) BEAMS FOR EXPERIMENTAL INVESTIGATION

3.1. Description of the selection of wood material

From the many investigations done for the timber in the local market of Kosovo, with the aim of finding wood from the first class, there were found two companies offering us material according to our request standard. The wood specie selected as wood type is defined Spruce wood family (Picea Abies PCAB). The lamellas were selected with initial thickness of 50mm, width of 200mm \pm 20mm and length of 4000mm. All were selected with extra care (checked and measured in thickness from stack) (Porteous and Kermani, 2008) .



Source: J. Porteous and B. Kermani, Structural Timber Design to Eurocode 5

Figure 14. Selection of material based in Structural Timber Design to Eurocode 5

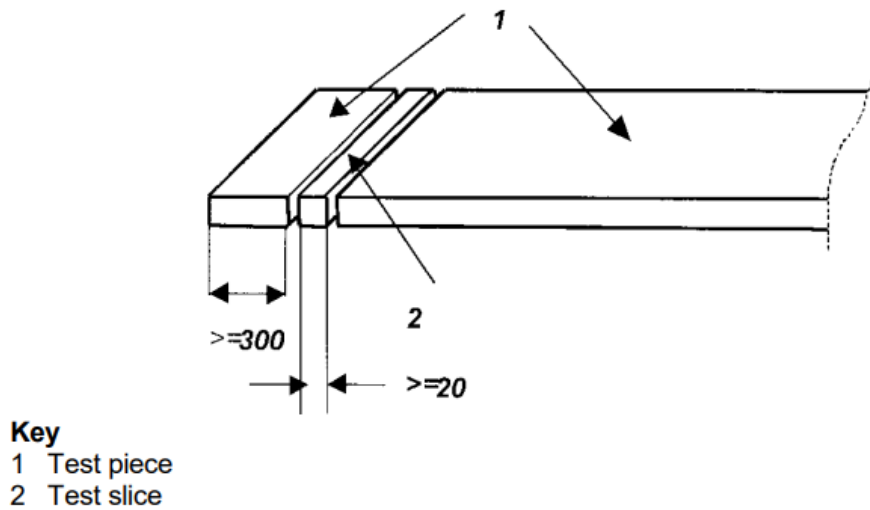
The class of these lamellas belongs to quality I (axial and central log boards, mainly radial), each lamella is individually measured in thickness due to the delicacy of twisting, bending, knots, resin and other possible defects.



Figure 15. a & b view of the raw material deposited before transportation

3.2. Determination of moisture content of test pieces

The moisture content of the test piece is determined in accordance with EN 13183-1 on the sections of the test pieces taken from 11 lamellas (boards) as described in standard.

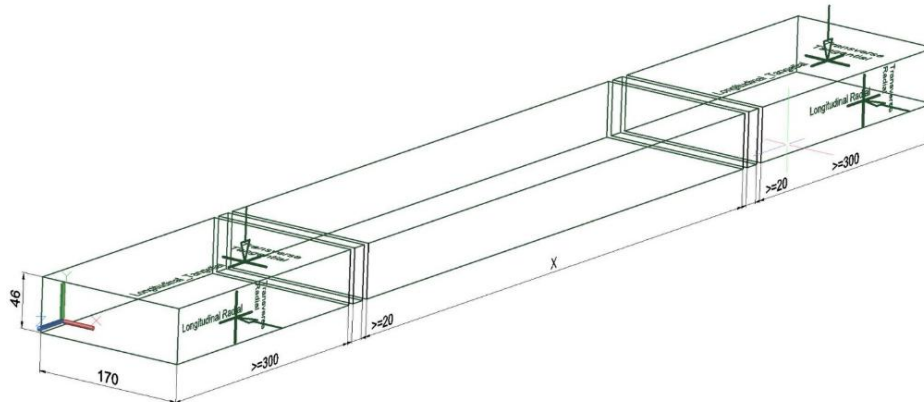


Source: Standard EN 13183-1

Figure 16. Cutting samples for determination of moisture content and density

3.2.1. Defining dimensions of the samples

The test slice was cut of full cross section and minimum 20 mm dimension in the direction of the grain, at a point by at 300 mm from either end of the test piece. The test slice was free from resin wood and features such as bark, knots and resin pockets.



Source: Author, dimensions referred to EN 13183-1

Figure 17. Extraction and preparation of samples from the lamellae for material testing according to EN 13183-1

3.2.2. Cutting slices

From each of the 11 test pieces, one test slice was cut, resulting in a total of 11 test slices. Each slice was extracted with its full cross-section preserved, measuring 170 mm in width and 20 mm in thickness, oriented in the direction parallel to the grain.

This preparation ensured that the material properties could be evaluated under conditions representative of the original lamella configuration.



Figure 18. Cutting the test pieces according to EN 13183-1 on the designated sections



Figure 19. View of the cut and marked samples prepared for testing

3.2.3. Measuring and scaling the test samples

Each test slice was marked and measured in longitudinal, radial and tangential directions (8 measurements were done per each piece with Nonius Caliper) and each piece has been scaled (accurate equip. to 0,01 g).

Balance accurate scale was accurate to 0,01 g, because of the mass of the test slice were less than 100g in an oven dry state. Equipment for drying wood, ensuring free internal circulation of air and capable of maintaining a temperature of $(103 \pm 2) ^\circ\text{C}$.



Figure 20. Scaling of test samples for weight measurement



Figure 21. Measuring samples with caliper in three directions

3.2.4. Drying the samples in oven

First time each of the slices were scaled as a weight grain before drying in gram (Fig. 20);

Second time the slices were scaled after 5 hours dried in the special experimental oven;

Third time again three hours more were dried, until the difference between samples was not higher than 0.1gram.



Figure 22. Adjustment of temperature in oven $103 \pm 2^{\circ}\text{C}$



Figure 23. Placing the samples in the oven

Calculation of the moisture content is done using the formula (Simpson, 1971; Rosli *et al.*, 2023):

$$\omega = \frac{m_1 - m_0}{m_0} \times 100 \dots (1)$$

Where:

- m_1 – is the mass of the test slice before drying, in grams;
- m_0 – is the mass of the oven dry test slice, in grams;
- ω - is the moisture content, in percent.

The average of the weight of cut slices (samples) was 70.25gr. and the average after 8 hours drying in the oven was 61.78gr. According to the formula written above, the moisture content is equal to 13.70%.

3.2.5. Determination of density of test samples

The density of wood is determined based on the ISO 13061-4:2014 standard.

Samples with proper dimensions (fig. 21) were measured before the drying process and were calculated using the formula (Simpson, 1971):

$$\rho_w = \frac{m_w}{a_w b_w l_w} = \frac{m_w}{V_w} [\text{kg/m}^3] \dots (2)$$

Where:

- m_w - mass in kilograms (or grams) of the test piece at moisture content W,
- a_w , b_w and l_w - are the dimensions, in meters (or centimeters), of the test piece at moisture content W,
- V_w – is the volume in m³ (or cm³) of the test piece at moisture content W.

Measuring Weight/Volume through the formula, the density of the test pieces is 438.33 kg/m^3 T30 (C50) characteristic strength, according to Class of boards (table 1) EN 14080.

Table 1. Characteristic strength and stiffness properties for T-classes in N/mm^2 and densities in kg/m^3 for boards or planks for GLT / Source: Class of boards from table 1, Standard EN14080

T - class of boards	ft,0,l,k	Et,0,l,mean	ρ ,k
T8 (C14)	8	7 000	290
T9	9	7 500	300
T10 (C16)	10	8 000	310
T11 (C18)	11	9 000	320
T12 (C20)	12	9 500	330
T13 (C22)	13	10 000	340
T14 (C24)	14	11 000	350
T14,5	14,5	11 000	350
T15	15	11 500	360
T16 (C27)	16	11 500	370
T18 (C30)	18	12 000	380
T21 (C35)	21	13 000	390
T22	22	13 000	390
T24 (C40)	24	13 500	400
T26	26	14 000	410
T27 (C45)	27	15 000	410
T28	28	15 000	420
T30 (C50)	30	15 500	430

^a The C-Classes according to EN 338:2009 meet at least the required values of the respective T-classes.

Table 2. Recording and calculation of data, averaging dimension measurements (longitudinal, radial and tangential) and weights

Sample	Longitudinal					Tangential			Radial			Weight green	Weight after 5 hours	Final	
	1	2	3	4	Average	1	2	Average	1	2	Average				
1	19.9	19.96	19.91	20.02	19.95	50.1	50.94	50.52	162.4	162.6	162.50	74.4	62.5	62.4	
2	19.92	19.95	19.94	20.02	19.96	50.07	50.82	50.45	158.4	156.85	157.63	73.2	60.9	60	
3	19.98	20.02	19.8	19.96	19.94	51.01	49.71	50.36	160.45	160.9	160.68	67.9	61.9	61.9	
4	19.88	19.82	20.01	19.89	19.90	45.71	45.97	45.84	165.55	163.35	164.45	67.6	61.6	61.6	
5	19.85	20.01	20.07	20.03	19.99	45.68	45.89	45.79	164.55	162.5	163.53	68	61.3	61.3	
6	19.93	19.83	20.04	20.07	19.97	49.86	49.11	49.49	161.25	160.1	160.68	66.3	56.1	56.1	
7	20.29	19.94	19.97	20.01	20.05	50.49	50.52	50.51	159.65	160.6	160.13	70.6	58	58	
8	19.92	19.92	19.94	19.94	19.93	49.63	48.43	49.03	166.15	165.55	165.85	68.7	62.4	62.4	
9	20.18	20.07	20.95	20.11	20.33	49.44	48.19	48.82	165.7	165.95	165.83	68.4	62.3	62.2	
10	19.92	20	19.96	19.99	19.97	50.46	50.75	50.61	165.8	165.15	165.48	74.2	67.3	67.2	
11	20.19	20.07	20.94	20	20.30	50.14	49.39	49.77	162.95	162.75	162.85	73.5	66.6	66.5	
												Average:70.25		Average: 61.78	

3.3. Production and its stages

3.3.1. Processing of lamellas in machines

After the delivery of the wooden material to the workshop, the lamellas were allowed to rest for a period of three days to achieve moisture equilibrium with the ambient conditions of the work environment. This acclimatization step is essential to minimize dimensional changes and internal stress during subsequent processing. Once the material reached a stable moisture balance, the lamellas were cut to the desired length according to the specifications of the target plan.

A series of preparation steps were then carried out to shape and refine the samples for further testing and assembly. The following machining operations were performed:

- Longitudinal and perpendicular cutting: Carried out using a circular saw machine to dimension the lamellas accurately in both length and width.
- Planning (edge and face): A planer machine was used to smooth and straighten one edge and one face of each lamella, providing reference surfaces for further processing.
- Thickness planing: The thickness planer machine was used to achieve uniform thickness across all lamellas, ensuring consistent cross-sectional dimensions.
- Sanding: Final surface preparation was done using a sanding machine to remove any surface irregularities, improve surface quality, and prepare the lamellas for bonding or testing.

These operations were performed with care to preserve the integrity of the material and ensure high precision in sample preparation.



Figure 24. Initial stage of lamella preparation



Figure 25. Selection and acquisition of the required lamellas

The lamellas were passed through the planer machine one by one, on one face and on one edge. From 50mm the dimensions decreased to 46mm. The feed rate speed was around 3-6m/min.

The next stage in the processing sequence involved the use of a thickness planer machine to achieve uniform thickness across all lamellas.

This machine was equipped with an automatic feed system, operating at a consistent feed rate of 7 meters per minute, which ensured efficient and continuous material flow during planing. The cutter head rotated at a speed of 4500 revolutions per minute (rpm), providing a smooth and accurate finish.

A high-quality four-edge cutting tool was used to guarantee precision and surface quality, contributing to consistent dimensions and improved bonding performance in later stages of fabrication.

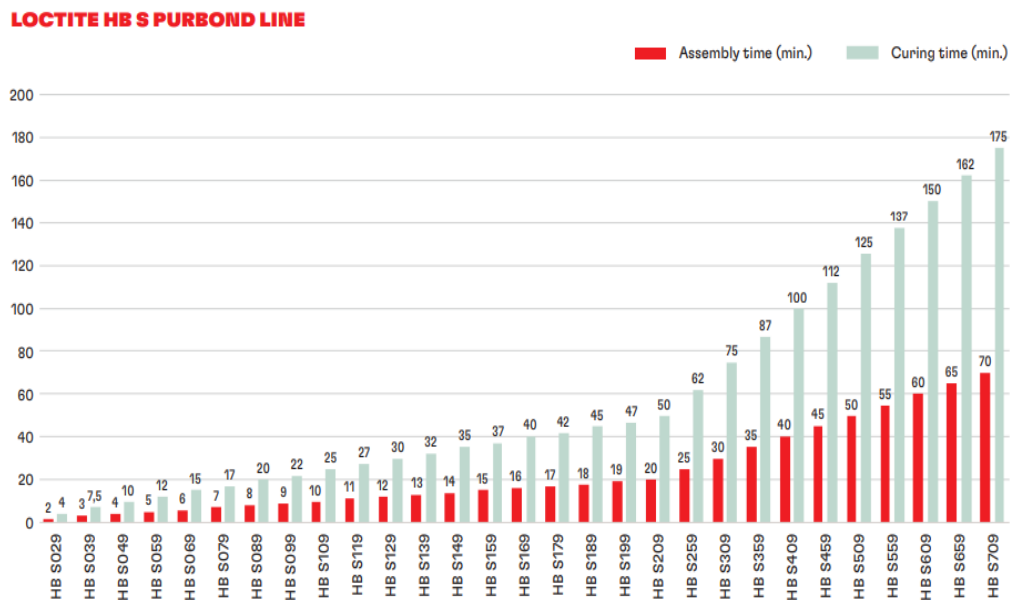
3.3.2. Bonding process

The type of adhesive that is used for gluing the lamellas is for moisture curing one-component polyurethane adhesive, normative reference is made to EN 15425.

Having a variety of 4 different grades of Henkel Loctite HB S-adhesives available in bottles, I've chosen the type HB S709 (75 min OT /175 min PT):

- HB S049 (4 min open time / 10 min press time)
- HB S109 (10 min OT / 25min PT)
- HB S309 (30 min OT / 75 min PT)
- HB S709 (75 min OT /175 min PT)

During our bonding process is used type HB S709 is chosen because due to manual application and thought slower adhesive suits better to our needs.



Source: Henkel adhesive technical data sheet

Figure 26. Graphic showing industrial Assembly time and curing time application for the beams



Figure 27. a) and b) Laying of glue with a thickness of more than 0.1 mm with the density of adhesive at around $1,16 \text{ g/cm}^3$

3.3.3. The press time application

According to the Technical Data Sheet, the glue line thickness should be around 0,1 mm. This is to be expected, as the density of the adhesive is $1,16 \text{ g/cm}^3$. But we made the pouring by manual application (spatula), and as foreseen the glue line thickness increased, which resulted in a longer press time to at least keep the timber lamellas double the press time (around 5 hours).

Industrial adhesive application systems apply $125\text{-}150 \text{ g/m}^2$. By manual application of the adhesive with a spatula was better to be applied from $150\text{-}200 \text{ g/m}^2$ (recommended from the producer). While for the pressure is taken in consideration the size of lamella starting from 0.6 N/mm^2 and not exceeding 1.0 N/mm^2 .

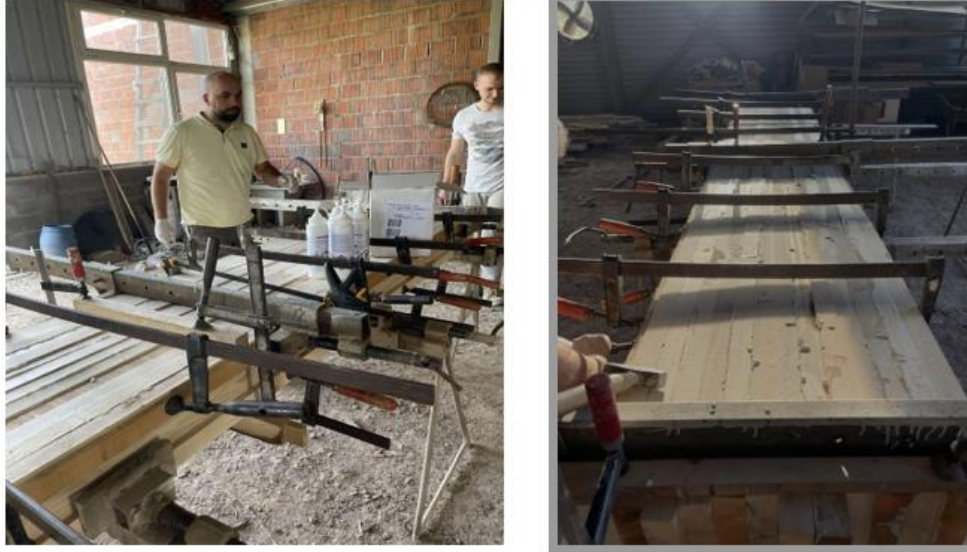


Figure 28. a & b Tightening lamellas by mechanical clamps and vices

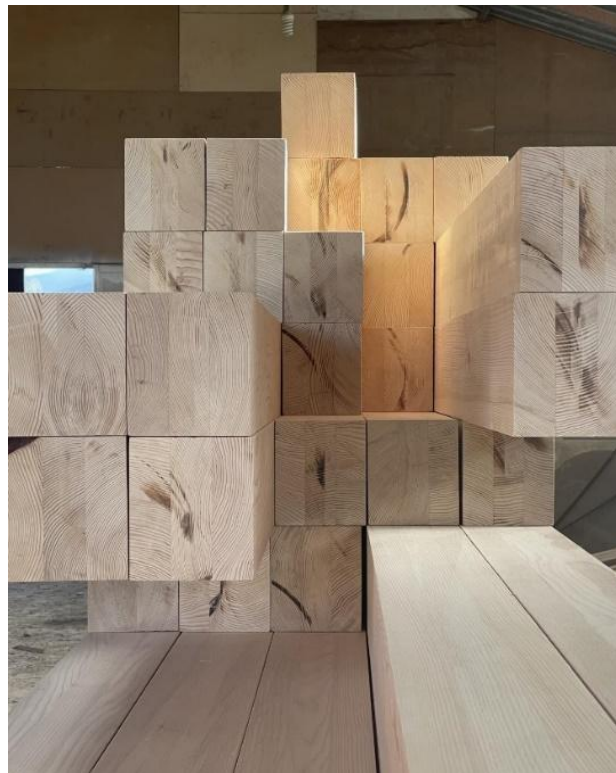


Figure 29. Thirty-six head beams in different model dimensions



Figure 30. GST beams produced from the author

4. EXPERIMENTAL INVESTIGATION OF GLUED SOLID TIMBER (GST) BEAMS

4.1. Testing program (table test series)

The first part of the research, namely, cutting samples according to the standard, researching the moisture content in wood through the experimental oven, measuring and scaling the samples and finding the density of wood was carried out at the Faculty of Architecture, Design and Wood Technology, University of Applied Sciences in Ferizaj, Kosovo. While the main part of the investigation of beams, with emphasis on testing beams according to modules, was carried out at the Laboratory of the Faculty of Civil Engineering at Ss. Cyril and Methodius University in Skopje, North Macedonia. The focus of the experiments was to evaluate the behavior of Glued Solid Timber (GST) beams using standardized test methods. The experiments were designed to assess both short-term and long-term performance. The tests followed the EN 408:2010 +A1 standard and were conducted on Spruce timber (*Picea Abies*).

All test models are full-scale and prepared in accurate dimensions in the cross section 138mm x 170 mm (EN 14080-2013), while the length of the beams is determined by referring to the procedures of the standard EN 408:2010+A1.

Table 3. Table test series

Standard	EN 408:2010 +A1			
Material	Spruce (<i>Picea Abies</i>)			
Product	Glued Solid Timber (GST) Beams			
Series	Modulus	Beam I	Beam II	Beam III
Series A	Local and Global Modulus of Elasticity on Bending	138mm x 170 mm x 3570 mm	138mm x 170 mm x 3570 mm	138mm x 170 mm x 3570 mm
Series B	Shear Field Test Method	138mm x 170 mm x 3570 mm	138mm x 170 mm x 3570 mm	138mm x 170 mm x 3570 mm
Series C	Bending Strength Parallel to the Grain	138mm x 170 mm x 3570 mm	138mm x 170 mm x 3570 mm	138mm x 170 mm x 3570 mm
Series D	Determination on Long-Term Effect and Creep Coefficient	138mm x 170 mm x 3570 mm	138mm x 170 mm x 3570 mm	-
Series E	Determination of Compression Strength Parallel to Grain	138mm x 170 mm x 828 mm	138mm x 170 mm x 828 mm	138mm x 170 mm x 828 mm
Series F	Determination of Compression Strength Perpendicular to Grain	138mm x 170 x 185 mm	138mm x 170 x 185 mm	138mm x 170 x 185 mm

Experimental Series and their Purpose

The tests were divided into six main series, each evaluating different properties of the beams.

1. Series A – Elasticity in Bending

- This test measured the local and global modulus of elasticity in bending.
- Beams tested: 138mm × 170mm × 3570mm.

2. Series B – Shear Strength

- Used the Shear Field Test Method to assess shear properties.
- Beams tested: 138mm × 170mm × 3570mm.

3. Series C – Bending Strength Parallel to Grain

- Evaluated how well the beams withstand bending stress along the grain direction.
- Beams tested: 138mm × 170mm × 3570mm.

4. Series D – Long-Term Effects and Creep

- Investigated the long-term deformation (creep) of the beams under sustained load.
- Beams tested: 138mm × 170mm × 3570mm.

5. Series E – Compression Strength Parallel to Grain

- Measured how well the timber resists compression along the grain.
- Beams tested: 138mm × 170mm × 828mm.

6. Series F – Compression Strength Perpendicular to Grain

- Focused on compression resistance perpendicular to the grain.
- Beams tested: 138mm × 170mm × 185mm.

4.2. Test set – up and instrumentation (Data Acquisition)

To ensure accurate and reliable measurements, a controlled experimental setup was used for testing glued solid timber (GST) beams under different loading conditions. The setup included loading frames, displacement sensors, strain gauges, and a data acquisition system to continuously monitor responses.

Each test was conducted under controlled laboratory conditions using a mechanical testing system that applied the required loads. The test configuration followed the EN 408:2010 +A1 standard, with customized supports and accessories to suit each test type.

Data from all testing phases were systematically recorded and stored in structured data sheets to ensure traceability and reproducibility of results. Each testing phase was clearly marked by updating the notification labels attached to the samples, as illustrated in the figure below (fig. 31).

This labeling system allowed for clear identification of test stages and helped minimize confusion during the preparation, testing, and documentation process. Data from all testing phases has been saved as data sheets, while each phase has been accompanied by a change in the notification label as in the figure below (fig. 31).

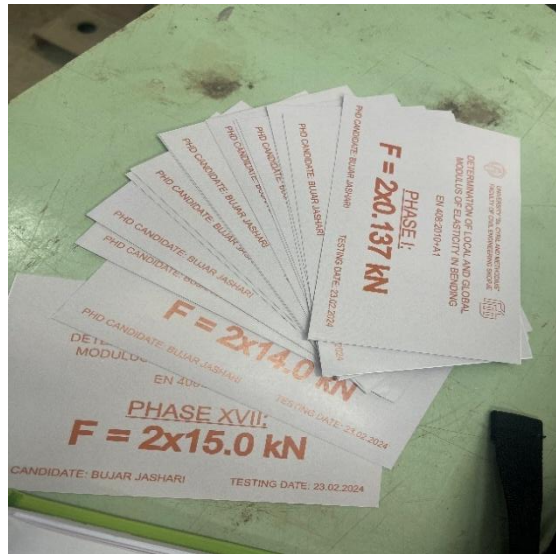


Figure 31. Label notification

4.2.1. Structural Support and Loading System

The beams were tested using specialized metal supports, which were welded and adapted to fit the specific requirements of the test standard. Also, were used capable of accommodating different test setups, including bending, shear, compression and other tests.



Figure 32. Compression strength parallel to the grain welded metal;



Figure 33. LVDT placement for shear field testing

4.2.2. Hydraulic Loading System

Hydraulic jacks were used to apply controlled loads, varying based on the test module. A ZRMK press was specifically used for compression strength tests perpendicular to the grain.

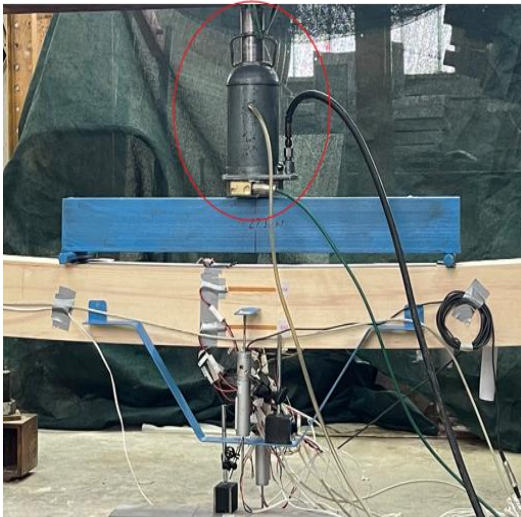


Figure 34. a) Hydraulic jack



b) ZRMK machine press

4.2.3. Instrumentation and Measurement Devices

a. Moisture and Environmental Conditions

The wood moisture content and relative humidity of the environment were measured before and during the tests to assess their impact on mechanical behavior.



Figure 35. a) Measuring of Moisture Content



b) Measuring Relative Humidity

b. Strain and Deformation Measurement

Strain gauges (Kyowa) were used to measure strain on the timber surface. They belong to type: KC-120-120-A1-11. Measuring Instruments Lab PL-120-11. These gauges were attached using the special adhesive of Cyanoacrylate CN-E to ensure accurate and stable readings.



Figure 36. a) Strain gauges and special glue b) Strain gauges connection c) Strain gauges setting

c. Displacement Measurement

Linear Variable Differential Transformers (Kyowa LVDT DT 100) were used to measure beam deflections and deformations in real time. Through displacement transducers is measured relative and absolute displacement from a steady point of structures by converting detected displacement to voltage.

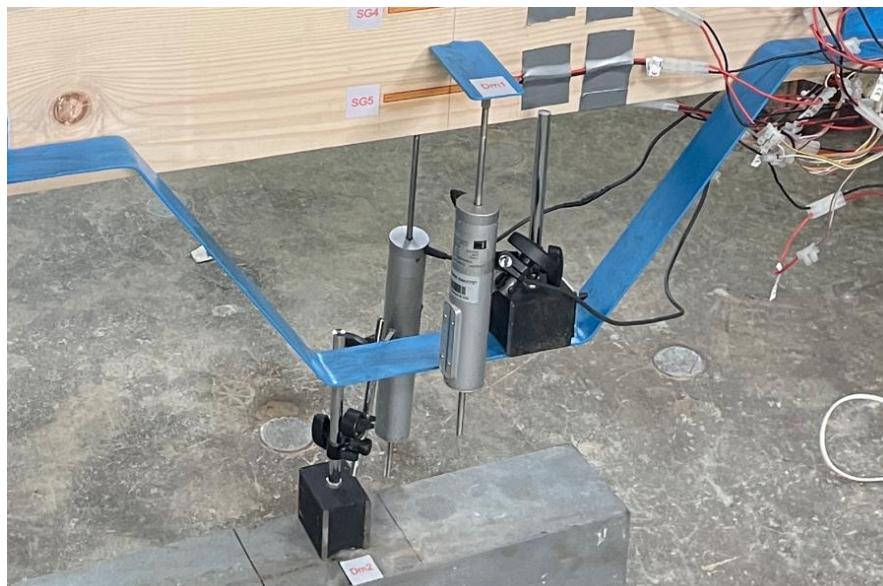


Figure 37. LVDT used to measure relative and absolute displacement depending on the testing module

d. Load and Force Measurement



Figure 38. Load Cell, load applied through hydraulic jack

Dial gauges were used to track local and global deflections in all experimental phases.



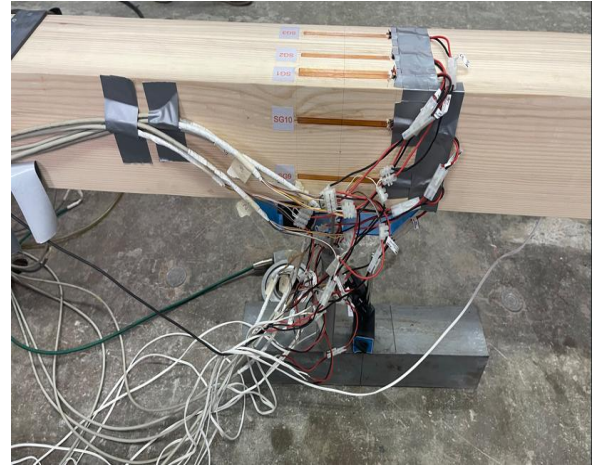
Figure 39. Dial gauge

e. Data Acquisition System

Data was collected using high-quality cables to ensure accurate signal transmission to the computer.



Figure 40. a) Cables and equipment



b) Strain gauges connection

To guarantee precise and ongoing monitoring of the experimental tests, Catman Easy Data Acquisition Software served as the main tool for collecting, visualizing, and analyzing data in real-time. This software was instrumental in consolidating data from different sensors and ensuring accurate measurements.



Figure 41. Catman Data Acquisition Software

HBM (Hottinger Brüel & Kjær) data acquisition device, specifically a data logger or signal amplifier is used in experimental testing setups for structural or mechanical measurements.

Through HBM is gained high-precision measurement from strain, force, pressure, and other displacement measurements.



Figure 42. a) Cables and data logger



b) HBM data logger



Figure 43. a) and



b) Real-time data monitoring and storage

4.3. Material mechanical characteristics in compression

Compression testing of timber is a fundamental method used to evaluate the material's ability to resist forces that tend to crush or shorten it. These tests are typically performed either parallel or perpendicular to the grain, as timber exhibits anisotropic behavior—its strength and deformation characteristics vary depending on the direction of loading relative to the grain.

Compression parallel to the grain reflects the load-bearing capacity of structural members such as columns and posts, while compression perpendicular to the grain is important for assessing bearing strength at connections or contact points. Standardized testing procedures, such as those outlined in EN 408, are used to determine key mechanical properties including compressive

strength, modulus of elasticity, and strain behavior. These properties are essential for the design and safety assessment of timber structures. The testing process involves placing a prepared specimen in a testing machine, applying load at a controlled rate, and recording force and deformation until failure occurs. Results from compression tests are also valuable for calibrating numerical models and verifying material assumptions in structural analysis.

4.3.1. Compression Strength Parallel to the Grain (Serie E)

The determination of compression strength parallel to the grain is made based on the EN 408:2010+A1:2012 standard.

The test was full cross section and had a length of six times the smaller cross-sectional dimension 828mm×138mm×170mm. The end grain surface was accurately prepared to ensure that they are plane and parallel to one another and perpendicular to the axis of the piece.



Figure 44. The example of application of load for the determination of compression strength parallel to the grain



Figure 45. Experimental test of compression force parallel to the grain beam EI1



Figure 46. Experimental test of compression force parallel to the grain – beam EI2

Through this equation is calculated the compression strength parallel to the grain of the wooden specimen, typically part of mechanical testing in structural timber design.

$$f_{c,0} = \frac{F_{c,0,max}}{bl} \dots (3)$$

Where:

- $f_{c,0}$ — Compression strength parallel to the grain (MPa or N/mm²)
- $F_{c,0,max}$ — Maximum compression force (N):
- b — Width of the specimen (mm):
- ℓ — Length or depth of the specimen under compression (mm): Typically refers to the dimension in line with the load application, aligned with the grain.

The formula essentially divides the maximum load the specimen can withstand by its cross-sectional area ($b \times \ell$). The result is a normalized stress value, which allows for comparison between different-sized specimens and standardizes the material's resistance.

While the other equation is used to calculate the modulus of elasticity $E_{c,0}$ from LVDT's for the specimen under compression parallel to the grain. It represents the stiffness of the material—how much it resists deformation when a compressive force is applied.

$$E_{c,0} = \frac{(F_{40} - F_{10})h_0}{(W_{40} - W_{10})bl} \dots (4)$$

Where:

- $E_{c,0}$ — Modulus of elasticity in compression parallel to the grain (MPa or N/mm²):
- F_{40}, F_{10} — Forces at 40% and 10% of the maximum load (N):
- h_0 — Initial height of the specimen (mm):
- w_{40}, w_{10} — Displacements (mm):
- b — Width of the specimen (mm) :
- ℓ — Length (or depth) of the specimen (mm).

Together $b \times \ell$ for the cross – sectional area

The table below presents the data obtained from the experimental compression tests (Serie E) performed parallel to the grain. These values of force and corresponding stress were then used as input for the numerical investigation. Test number 02, number 04 and number 06 are realized with LVDT for elastic regime in order to not damage the instruments.

Table 4. Experimental Results for Serie E (Compression Parallel to the Grain)

Designation	Force [kN]	Stress [N/mm ²]	Average strength (N/mm ²)
Serie E_Test 01	644	27.4	30.35
Serie E_Test 03	661	28.2	
Serie E_Test 05	762	32.5	
Serie E_Test 07	779	33.3	

Explanation:

The force values represent the peak compressive load applied to each specimen.

The stress is calculated by dividing the force by the cross-sectional area of the specimen, as per Equation:

$$f_{c,0} = \frac{F_{c,0,max}}{bl} \dots (5)$$

The average strength of the specimens tested in Serie E was **30.35 N/mm²**, which reflects the mean compressive strength parallel to the grain for use in numerical modeling and simulations.

Through the graph below (fig. 47) is shown the force–displacement response of the specimen in compression parallel to the grain.

The modulus of elasticity **E_c =8770MPa** is calculated from the linear portion of the curve between 10% and 40% of the maximum force, indicating the material's stiffness.

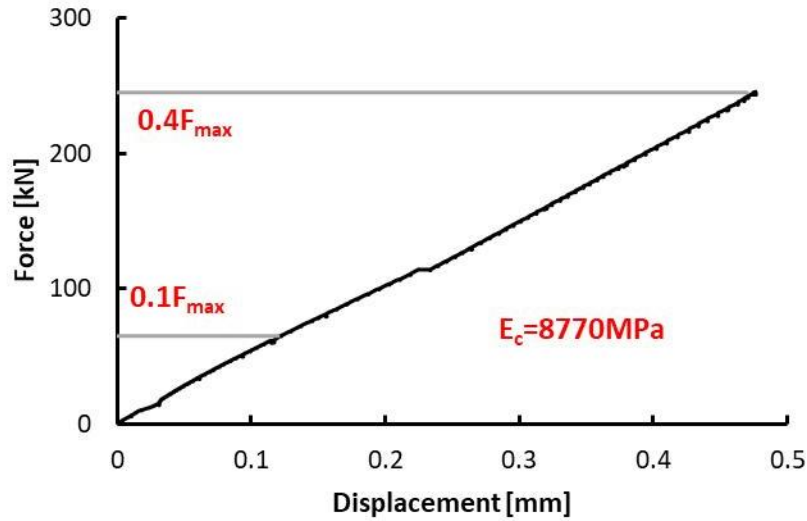


Figure 47. Load–displacement curve of experimental specimen E_Test 01 and calculation of the elastic modulus

Also, the other graph below (48) shows the force-displacement behavior of the specimen under compression parallel to the grain. The modulus of elasticity in this case is $E_c=11,935$ MPa, which is derived from linear F_{max} between 0.1 and 0.4 indicating a higher stiffness compared to the previous case.

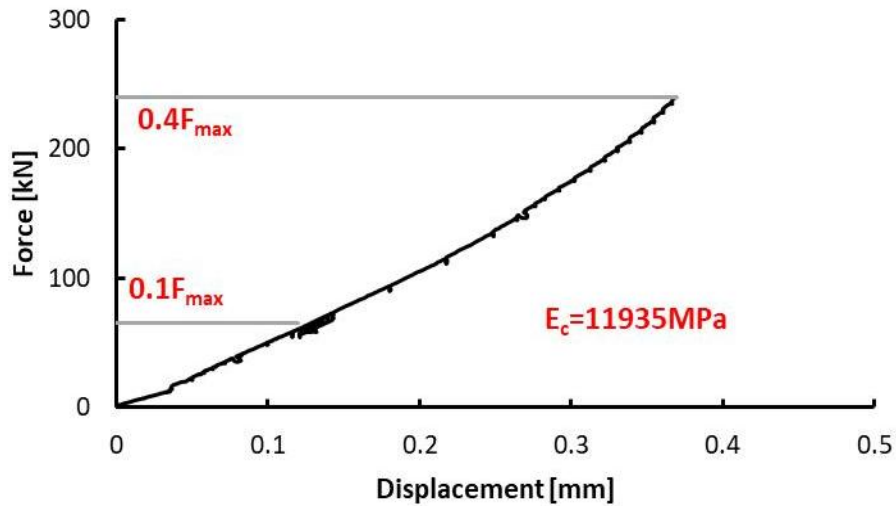


Figure 48. Load–displacement curve of experimental specimen E_Test 05 and calculation of the elastic modulus

The summary of the two cases presented in the graphs $E_c = 8770\text{MPa} + E_c = 11,935$ MPa gives us to understand that we have an average modulus of elasticity of E_c , **average= 10352 MPa**.

In the cross section, the upper end of the beam, a crack depth of approximately 30mm was observed, which was followed in the longitudinal direction of the beam, extending from the center of the lamella to the periphery of the beam with a length of 200mm.

In the other figure 49 of the same test model, 2 light crushes with a depth of 2-3mm and a length of 80 and 110 mm were also observed in the middle of the beam, the first outer lamella.

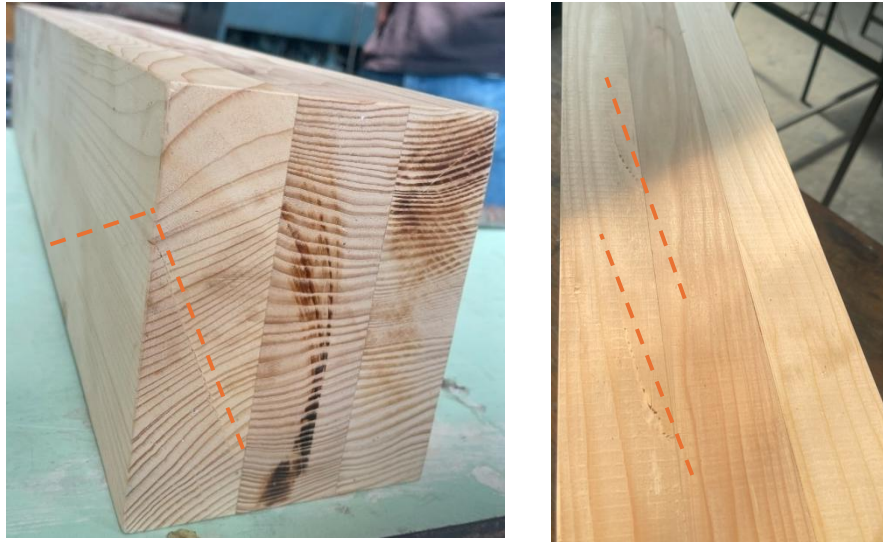


Figure 49. Crack of timber under compression parallel to the grain (beam EI1)

Light peripheral cracks were observed in beam EI2. One of these cracks started from the beam head 20mm down in the longitudinal direction. A second light crack also started 20mm down from the first crack, which has a length of approximately 200mm (fig. 50 a).

Meanwhile, on the right side of the beam EI2, a slight crack has also been observed from the head of the lower beam in the longitudinal direction, the length of which crack is 340mm (fig. 50 b).



Figure 50. a) Beam EI2



b) Beam EI2

Two light cracks were observed in beam EI3, which started from top to direction of bottom and the length is around 570mm, which is the longest crack from this test series (fig 51).

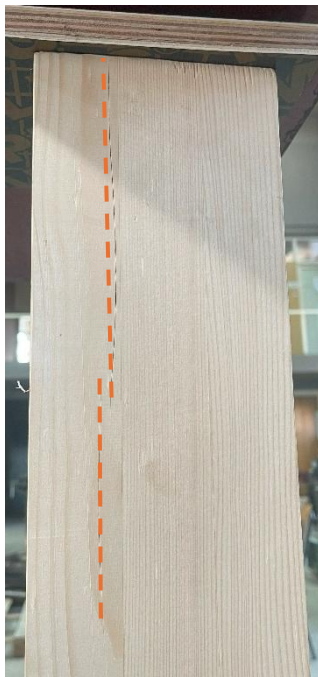


Figure 51. a) beam EI3



b) beam EI1;EI2 and EI3

4.3.2. Compression Strength Perpendicular to the Grain (Serie F)

The determination of compression strength perpendicular to the grain is made based on the EN 408:2010+A1:2012 standard.

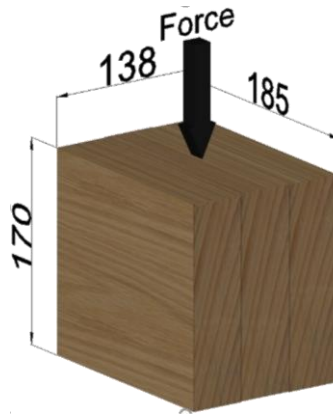


Figure 52. Determination of compression strength perpendicular to the grains

This experimental evaluation identifies the maximum resistance against forces applied perpendicular to the grain, yielding crucial information about the material's compressive properties along the fibers. Thus, through this experimental test is determined maximal resistance perpendicular to the grains.



Figure 53. Press machine for determination of compression strength perpendicular to the grains



Figure 54. The view of cross section of experimental test sample

The compressive strength $f_{c,90}$ is determined from the equation:

$$f_{c,90} = \frac{F_{c,90,max}}{bl} \dots (6)$$

Where:

- $f_{c,90}$ – is compressive strength perpendicular to the grain, in newtons per square millimetre:
- $F_{c,90,max}$ – is maximum compressive load perpendicular to the grain, in newtons:
- b – is width of cross section in mm:
- l – is span in bending, or length of test piece between the testing machine grips in compression and tension, in mm.

From the expression above is force is converted to the stress, data are highlighted on the table below (no 5):

Table 5. Highlighted results from the experimental test compression strength perpendicular to the grains

Designation	Force [kN]	Stress [N/mm ²]	Average strength (N/mm ²)
Serie FI1	135 kN	5.75	5.1
Serie FI2	106 kN	4.5	
Serie FI3	120 kN	5.1	

The table 5 highlights the experimental findings for Serie FI (three) samples subjected to compression testing. It outlines the peak force exerted and the associated stress from each test. The mean compressive strength was determined to be **5.1 N/mm²**, reflecting the material's standard resistance when under axial compression. These figures offer essential information for assessing structural efficiency or confirming numerical models.

Through the figure below (fig. 55. SampleFI1) we understand that the sample was damaged to a large extent during testing. It is observed that we have damage in the tangential, radial and longitudinal directions.



Figure 55. Beam FI1 a) front view



b) side view

In the second test of this series FI2, it was observed that we had deeper cracks and at the end of the test we also had partial breakage, and in the last lateral part of the right lamella a piece of wood was broken off. Through the lower figures (fig. 56 a & b) we notice the deformations, which are more pronounced compared to the first sample FI1.



Figure 56. Beam FI2 a) front view



b) side view

In the third sample FI3 there are more pronounced cracks in the middle lamella (fig. 57 beam FI3) but also in the peripheral lamellas. Greater damage is observed in the right lamella. Compared to the first two samples FI1 and FI2, less damage is observed.



Figure 57. Beam FI3 a) front view



b) side view



Figure 58. Samples from Serie F

4.4. Four Point Bending Testing

The four-point bending test is the method used in order to assess how the GST beams behave under bending loads. It is used especially for evaluation of the flexural strength and stiffness of beams depending on test series.

In this test setup, selected specimen (full-scale beam) acted as a simply supported beam, with two supports at the ends and two equally spaced loading points applied from above, typically symmetrically about the center of the span.

Through the configuration is aimed the constant bending moment zone between the two loading points, free from shear forces and determining the modulus of elasticity in bending and the maximum bending strength. Due to the uniform moment distribution in the central region, four-point bending is considered more reliable than three-point bending, especially when testing anisotropic or non-homogeneous material like wood in our case.

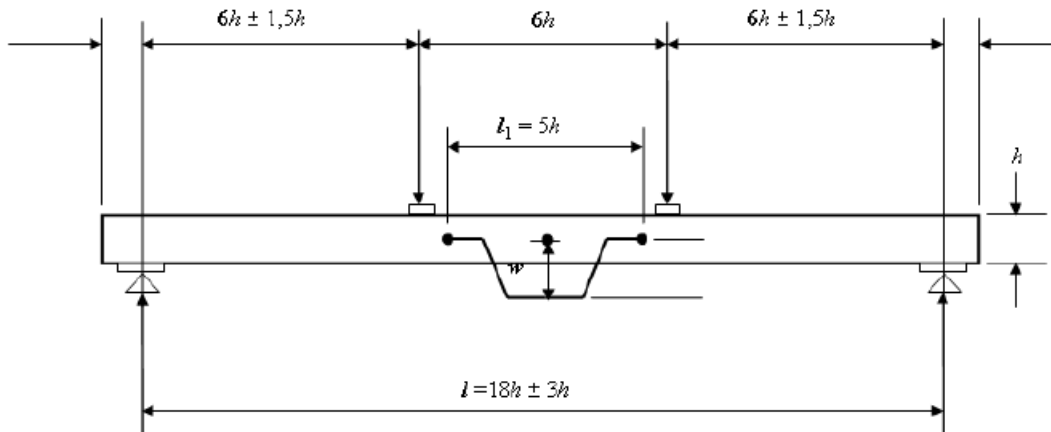


Figure 59. Four point bending test (408:2010+A1:2012)

In a simply supported beam, the supports permit horizontal movement and rotation while restricting vertical movement. This boundary condition offers an uncomplicated and realistic framework for assessing how structures behave when loads are applied.

Throughout the experiment, the force and displacement were consistently tracked, creating a force–displacement curve that allowed for the extraction of important mechanical characteristics. The results were crucial for confirming numerical simulations and for the design of structural elements intended for use under practical loading conditions.

4.4.1. Local and Global Modulus of Elasticity in Bending (Serie A)

Through this experimental test is measured the local and global modulus of elasticity in bending for six full-scale beams. Three were selected for local and three for global modulus of elasticity on bending. The test set-up is done based on EN408:2010+A1:2012.

Dimensions of each beam tested for this Serie are: 138mm × 170mm × 3570mm. Dimensions, positioning of instruments and others equipment for determination of local and global modulus of elasticity in bending are shown in the following. This serie (A) is the focus of the dissertation in which the flow work is oriented for modeling.

The diagram illustrates a setup for determining the local and global modulus of elasticity in bending.

Through figure 60 (AI1) is presented the simply supported beam, which is centrally loaded with force F_1 . Strain gauges (SG_1 to SG_{13}) are placed at key sections to measure local strain, while deflection meters (Dm_1 , Dm_2 , and mechanical Dm_3) record vertical displacements. This configuration allowed precise evaluation of both local and global elastic behavior under bending.

**DETERMINATION OF LOCAL AND GLOBAL MODULUS OF ELASTICITY IN BENDING
DISPOSITION OF MEASUREMENT EQUIPMENT - A I 1**

SCALE M=1:25

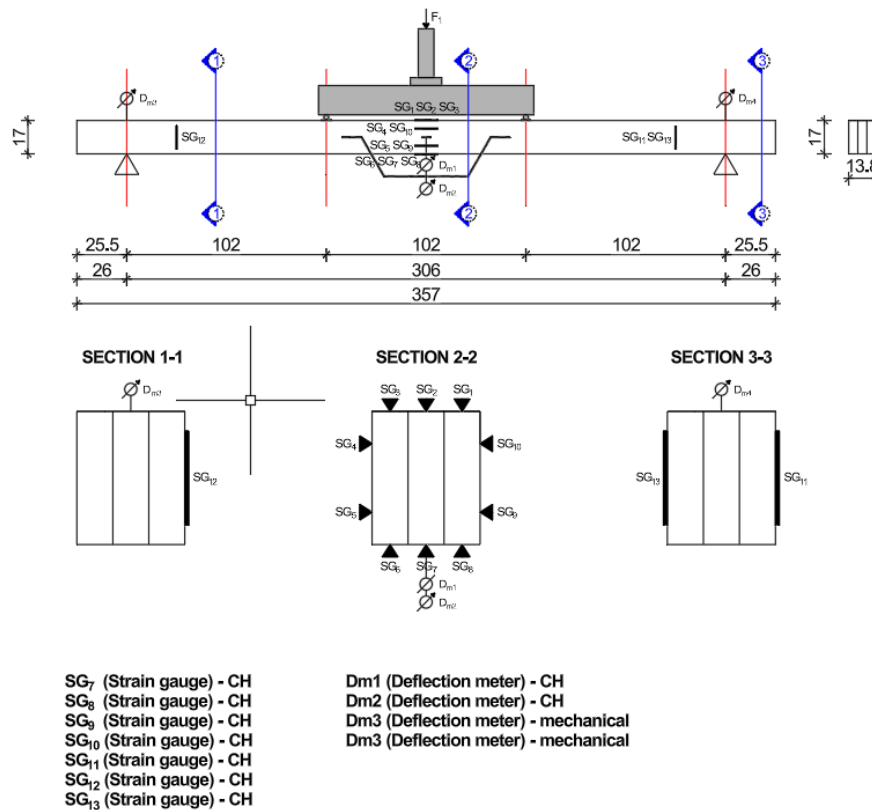


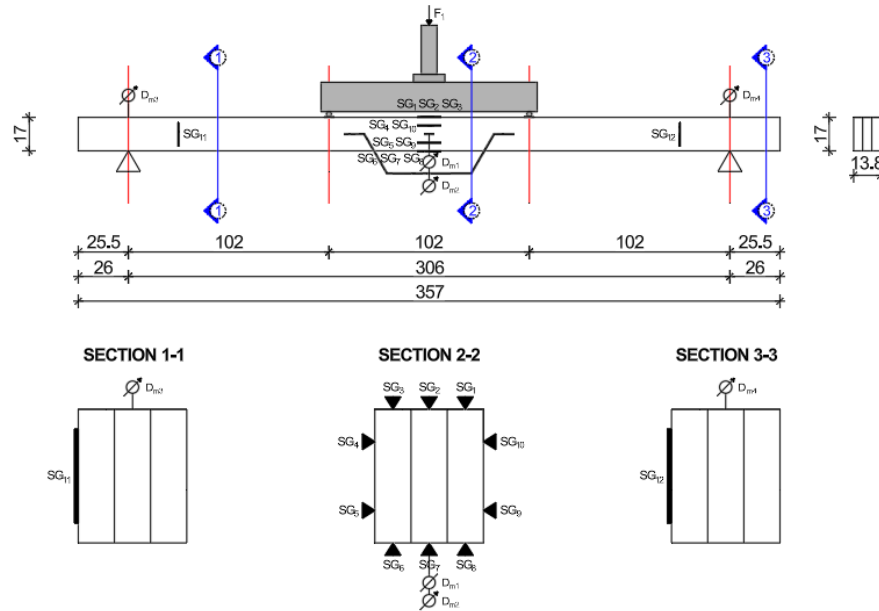
Figure 60. Beam (AI1) the setup for the local and global modulus of elasticity in bending.

Beam AI2 (fig. 61) is represented the setup for the local and global modulus of elasticity in bending Strain gauges (SG_1 to SG_{12}), which are not installed in the same way as the beam AI1 at three sections to capture strain data.

Deflection meters (Dm_1 , Dm_2 , and mechanical Dm_3 and Dm_4) measure vertical displacement.

The setup enabled precise evaluation of both local and global elastic behavior under bending conditions.

**DETERMINATION OF LOCAL AND GLOBAL MODULUS OF ELASTICITY IN BENDING
DISPOSITION OF MEASUREMENT EQUIPMENT - A I 2
SCALE M=1:25**



CHANNEL LIST:

F_1 (Force) - CH1 - Q2

SG₁ (Strain gauge) - CH1 - Q1
 SG₂ (Strain gauge) - CH2 - Q1
 SG₃ (Strain gauge) - CH3 - Q1
 SG₄ (Strain gauge) - CH4 - Q1
 SG₅ (Strain gauge) - CH5 - Q1
 SG₆ (Strain gauge) - CH6 - Q1

SG₇ (Strain gauge) - CH7 - Q1
 SG₈ (Strain gauge) - CH8 - Q1
 SG₉ (Strain gauge) - CH2 - Q2
 SG₁₀ (Strain gauge) - CH3 - Q2
 SG₁₁ (Strain gauge) - CH4 - Q2
 SG₁₂ (Strain gauge) - CH5 - Q2

Dm1 (Deflection meter) - CH6 - Q2
 Dm2 (Deflection meter) - CH7 - Q2
 Dm3 (Deflection meter) - mechanical
 Dm4 (Deflection meter) - CH8 - Q2 (mechanical)

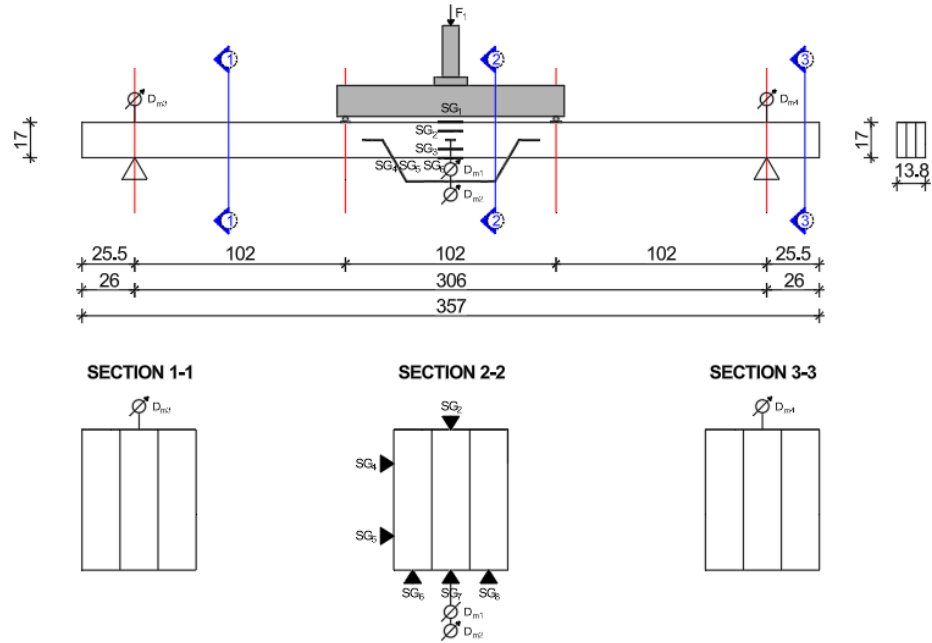
Q2 (172.21.108.2)
 Q1 (172.21.108.1)

Figure 61. Beam (AI2) the setup for determining the local and global modulus of elasticity in bending.

Compared to previous configurations, this version features fewer strain gauges (SG₁ to SG₆), all concentrated at the midspan (Section 2-2), allowing focused measurement of strain in the high-stress region.

Deflection meters (Dm₁, Dm₂, and mechanical Dm₃ and Dm₄) are placed to record vertical displacements. This streamlined layout emphasizes midspan behavior while still enabling accurate evaluation of both local and global elastic properties.

**DETERMINATION OF LOCAL AND GLOBAL MODULUS OF ELASTICITY IN BENDING
DISPOSITION OF MEASUREMENT EQUIPMENT - A I 3
SCALE M=1:25**



CHANNEL LIST:

F₁ (Force) - CH1 - Q2

SG₁ (Strain gauge) - CH1 - Q1
SG₂ (Strain gauge) - CH2 - Q1
SG₃ (Strain gauge) - CH3 - Q1
SG₄ (Strain gauge) - CH4 - Q1
SG₅ (Strain gauge) - CH5 - Q1
SG₆ (Strain gauge) - CH6 - Q1

Dm1 (Deflection meter) - CH2 - Q2
Dm2 (Deflection meter) - CH3 - Q2
Dm3 (Deflection meter) - CH4 - Q2 (mechanical)
Dm4 (Deflection meter) - CH5 - Q2 (mechanical)

Q2 (172.21.108.2)
Q1 (172.21.108.1)

Figure 62. Beam (AI3) setup for determining the local and global modulus of elasticity in bending

4.4.1.1. Local Modulus of Elasticity (Experimental results)

With blue color is shown elastic modulus that lies along in zone from 0.1-0.4 Fmax.

The linear correlation between load and displacement in the elastic region yielded a regression coefficient (R^2) of 0.99, indicating an excellent fit and high reliability in the calculation of the elastic modulus. This strong correlation suggests that the measured data closely follow a linear trend, confirming the consistency and accuracy of the test results within the elastic range.

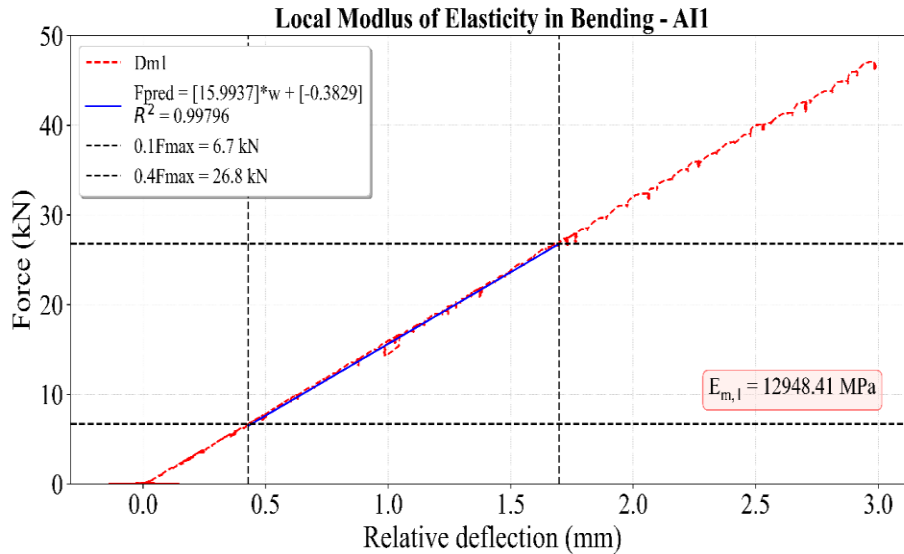


Figure 63. Local Modulus of Elasticity in Bending – AI1

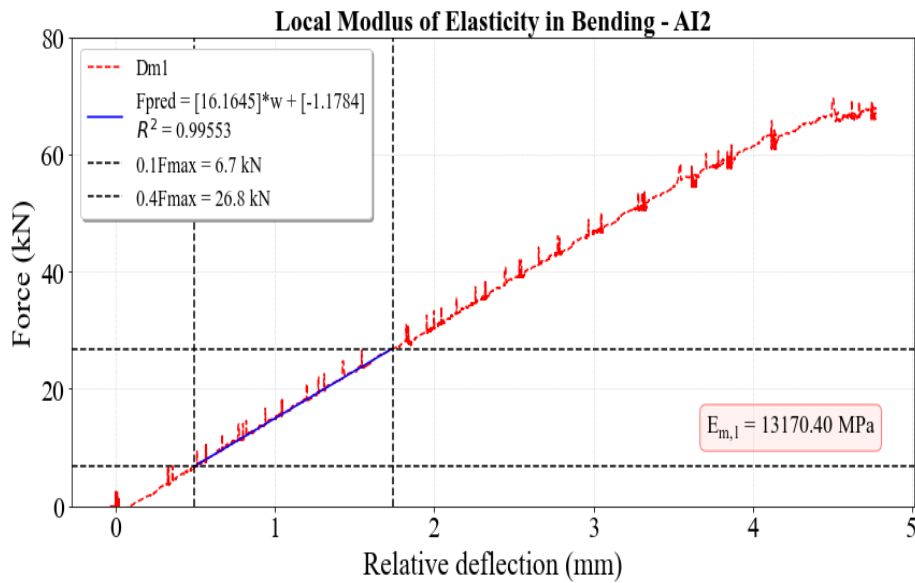


Figure 64. Relative deflection on beam AI2

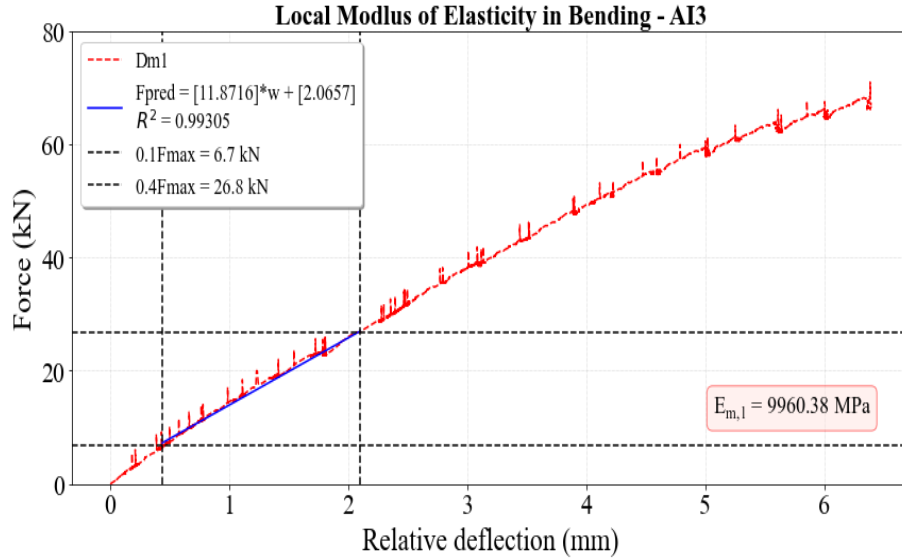


Figure 65. Relative deflection on beam AI3

Through the expression below is calculated Local Modulus of Elasticity in Bending:

$$E_{m,l} = \frac{al_1^2(F_2 - F_1)}{16I(w_2 - w_1)} \dots (7)$$

Where:

- $E_{m,l}$ - is the local modulus of elasticity:
- a - is distance between a loading position and the nearest support in a bending test, in millimetres:
- l - is span in bending in mm:
- I - is second moment of area, in millimetres to the fourth power:
- $F_2 - F_1$ - is an increment of load in newtons on the regression line with a correlation coefficient: and
- $w_2 - w_1$ is the increment of deformation in millimetres corresponding to $F_2 - F_1$.

Here, the results highlighted in the table show the Elastic Modulus (stiffness) obtained from three beam tests, which is represented from the graphs above AI1; AI2; AI3.

Table 6. Highlighted results for the Elastic Modulus (Stiffness)

Designation	Em,l [MPa]
Serie AI1	12948
Serie AI2	13170
Serie AI3	9960

4.4.1.2. Global Modulus of Elasticity (Experimental results)

From the same experimental test are obtained the results of Global Modulus of Elasticity. The results have been used as an input for numerical analysis.

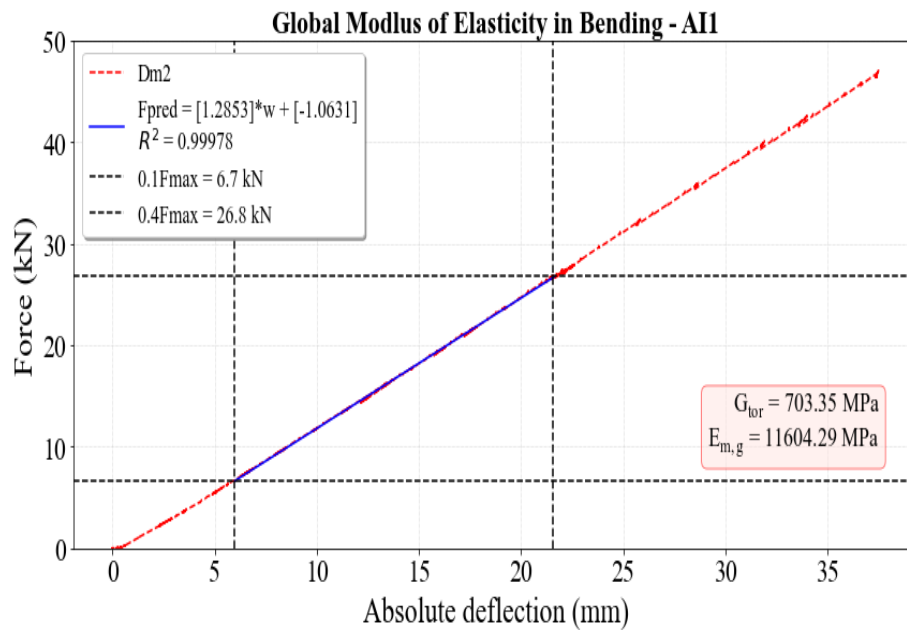


Figure 66. Determination of Global Modulus of Elasticity-AI1

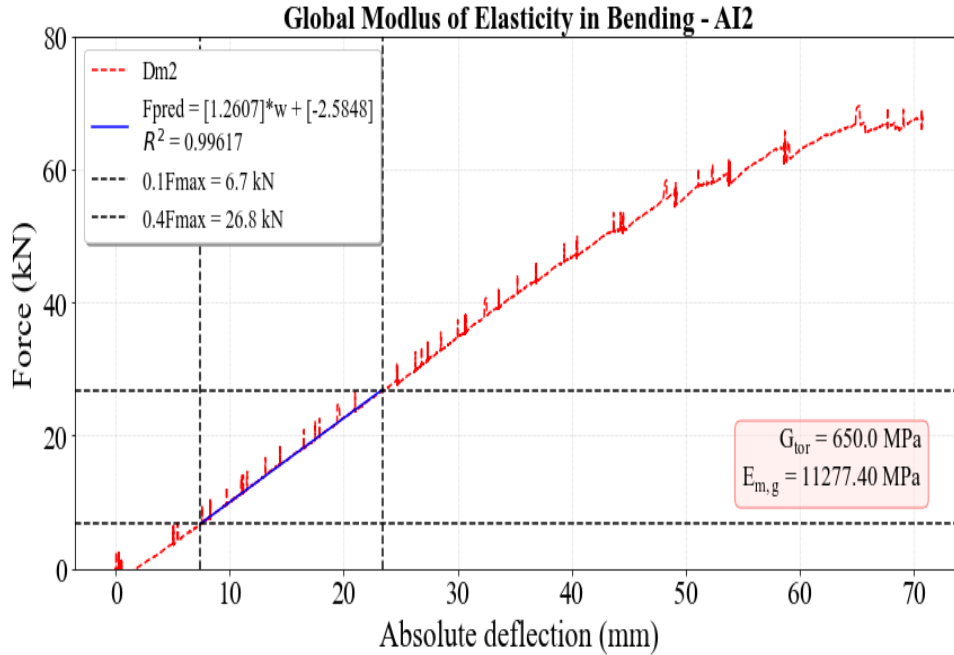


Figure 67. Determination of Global Modulus of Elasticity-AI2

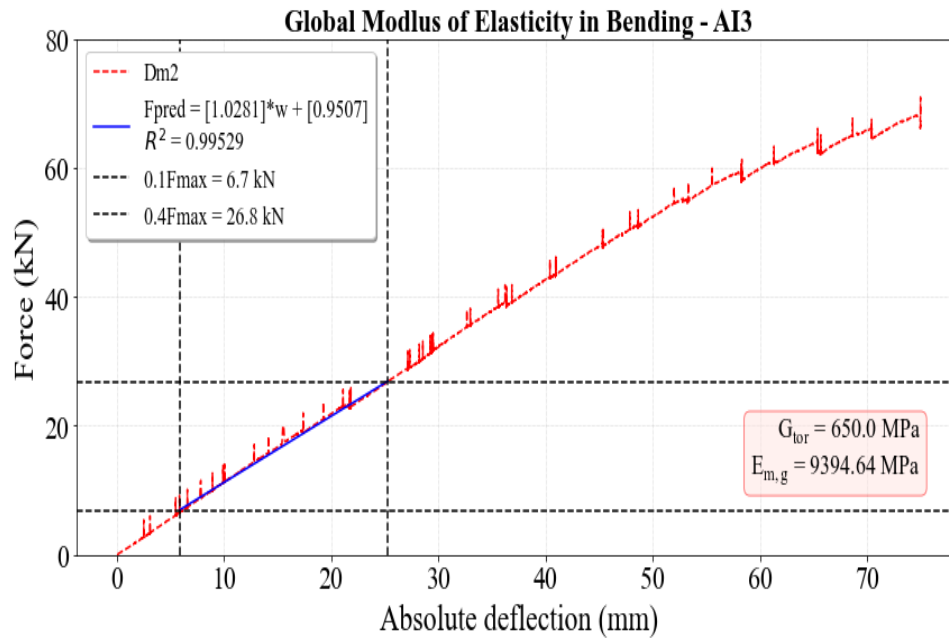


Figure 68. Determination of Global Modulus of Elasticity-AI3

From the same beam are obtained the results of Global Modulus of Elasticity. The results have been used as an input for numerical analysis.

Through the equation is calculated Global Modulus of Elasticity in Bending:

$$E_{m,g} = \frac{3al^2 - 4a^3}{2bh^3 \left(2 \frac{w_2 - w_1}{F_2 - F_1} - \frac{6a}{5Gbh} \right)} \dots (8)$$

Where:

- $E_{m,g}$ - is the global modulus of elasticity;
- a - is distance between a loading position and the nearest support in a bending test, in millimetres;
- l - is span in bending in mm;
- G - is shear modulus, in newtons per square millimetre;
- b - is width of cross section in a bending test in mm;
- h - is depth of cross section in a bending test or height;
- $w_2 - w_1$ - is the increment of deformation in millimetres corresponding to $F_2 - F_1$.

Table 7. Highlighted experimental results for Global Modulus of Elasticity

Designation	Em,g [MPa]
Serie AI1	11604
Serie AI2	11277
Serie AI3	9394

In the initial beam sample AI1 (viewed from the front), a significant crack was detected. In this sample crack initiation has started from the left end of the beam where it originated. Due to the knot found in the beam, in this case the concentration of force goes directly to the joint, which means that the elasticity is lower compared to the rest of the body, therefore the fracture begins in the middle of the beam. The fracture appears to be manageable and crack initiation and propagation happened from the left side of the beam where the length of the propagation was 1140mm on the inner side. This crack is also visible on the underside of the sample. Nonetheless, no signs of delamination were noted.



Figure 69. Front of the beam AI1 – defect and the crack description

From the second sample AI2, the cracking started approximately in the middle of the sample, continuing straight the right side over a length of 1725mm with a depth of 2mm to 35mm. The damage was greater at this stage comparing to the beam AI1.



Figure 70. Front of the beam AI2

On the bottom view of the beam, a triple crack is visible which extends over 1700 mm length, which goes along from the mid-span to the periphery



Figure 71. Bottom view of the beam AI2

A typical situation also occurred with beam number 3 (AI3) belonging to this test series, but which had deeper damage overall where the crack also is initiated from the mid-span.

4.4.2. Shear Field Test Method (Serie B)

In this case the test piece was symmetrically loaded in bending at two points over a span of 18 times the depth as shown from the picture, based on EN 408_2010+A1.

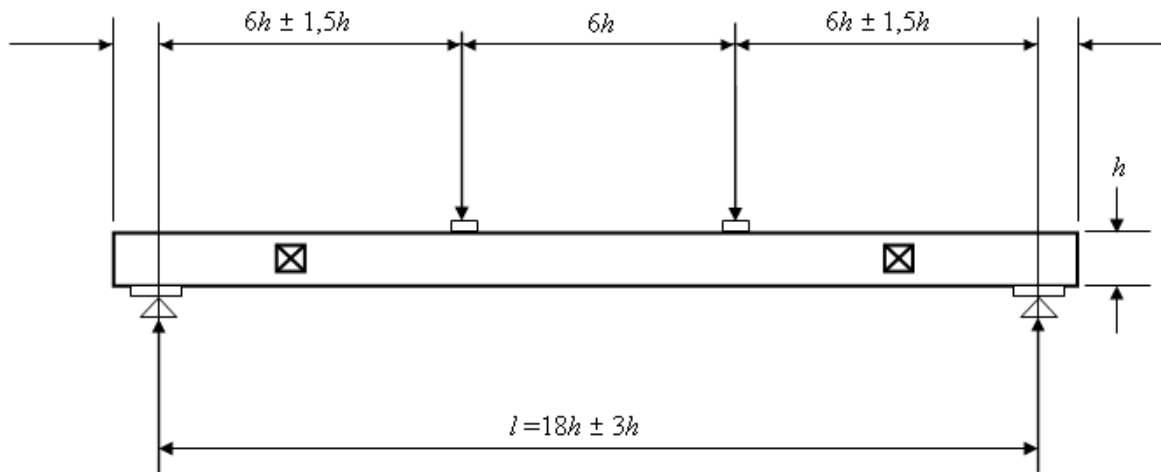


Figure 72. Experimental investigation of shear field test according to EN 408_2010+A1

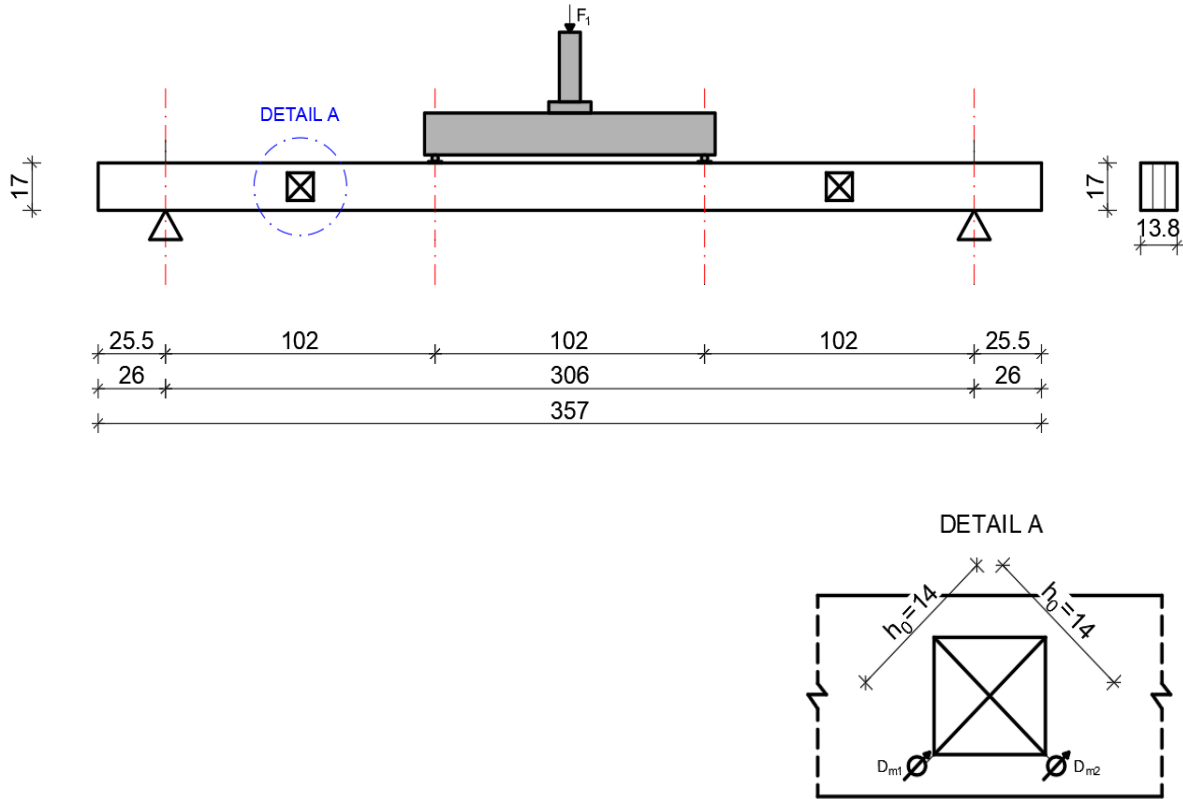
The beam model presented here has the same dimensions 138mm x 170mm x 3570mm, but the instrumentation setup and the types of instruments used are different from those in previous tests.

Through the view below (fig. 73) is presented a schematic diagram for setting up a shear field test to evaluate the mechanical behavior of a material or assembly under a centralized force. The drawing is to scale 1:25, indicating all dimensions are scaled down by a factor of 25.

This setup enabled the precise application of shear forces in order to make accurate measurement of deflections at key locations. Through this experimental test is investigated the performance and the behavior of beams and the results are also expressed on the graphs.

The test setup features a loading point (F_1) that is centrally located and symmetrically supported at both ends. To investigate deformations during the loading process, two deflection gauges (Dm_1 and Dm_2) are placed properly. These instruments are situated as illustrated in Detail A, at the corners of a square measuring 140 mm × 140 mm to accurately record local movements.

**SHEAR FIELD TEST METHOD
DISPOSITION OF MEASUREMENT EQUIPMENT - B I 1
SCALE M=1:25**



CHANNEL LIST:

F_1 (Force)

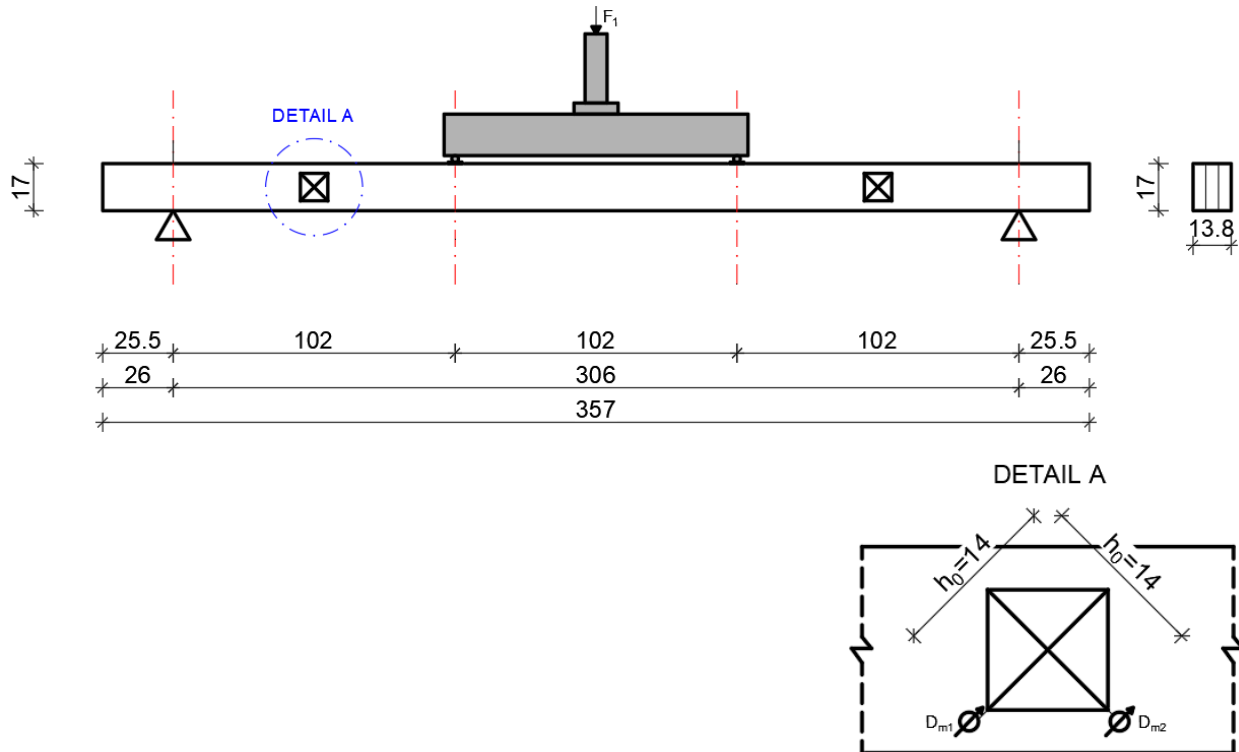
Dm1 (Deflection meter)

Dm2 (Deflection meter)

Figure 73. Beam (BI1) setup for Shear Field Test Method

The same procedure was also applied during the testing of the second beam (BI2), following the same methodological steps to ensure consistency in the experimental process. All accessories and measurement devices such as the force application system, support placement, and deflection meters were carefully reused and recalibrated to maintain the reliability of the setup. This attention to detail was essential to guarantee that the results recorded by the computer were accurate, comparable to those from the first beam (AI1) test, and suitable for further analysis (AI3) of structural performance under shear loading.

**SHEAR FIELD TEST METHOD
DISPOSITION OF MEASUREMENT EQUIPMENT - B I 2
SCALE M=1:25**



CHANNEL LIST:

F_1 (Force)

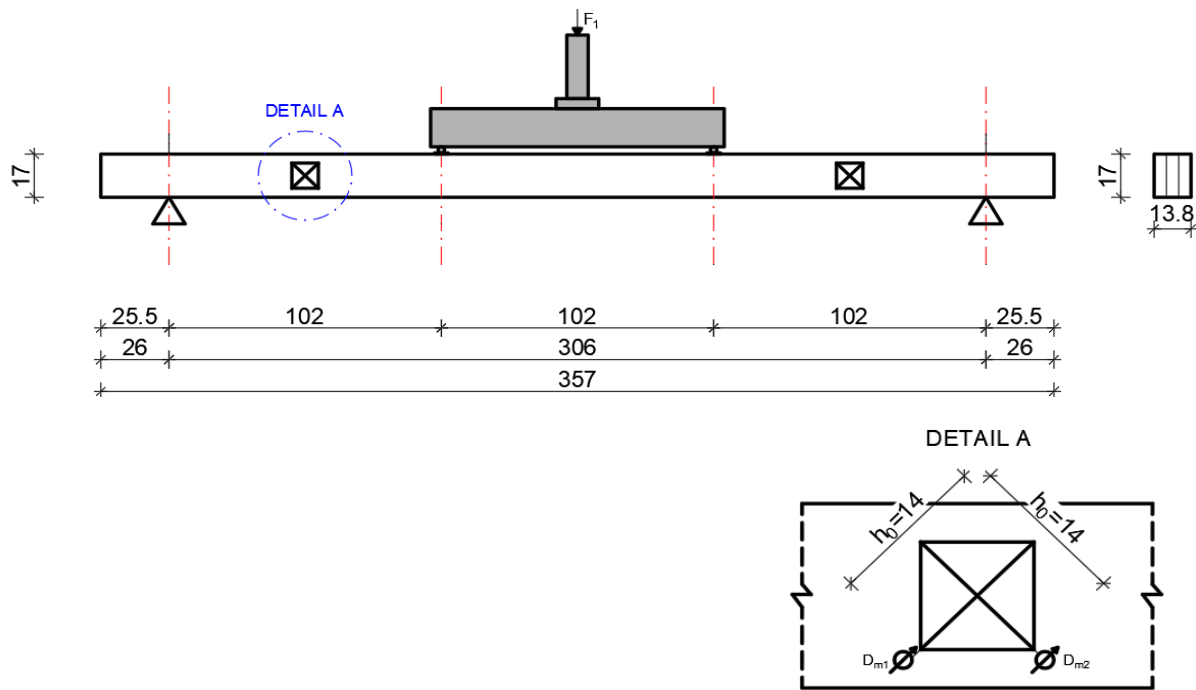
Dm1 (Deflection meter)

Dm2 (Deflection meter)

Figure 74. Beam (BI2) setup for Shear Field Test Method

Beam BI3 underwent testing using the identical configuration, guaranteeing accuracy and uniformity, while also ensuring dependable data gathering for comparison.

**SHEAR FIELD TEST METHOD
DISPOSITION OF MEASUREMENT EQUIPMENT - B I 3
SCALE M=1:25**



CHANNEL LIST:

F_1 (Force)

D_{m1} (Deflection meter)

D_{m2} (Deflection meter)

Figure 75. Beam (BI3) setup for Shear Field Test Method

Through the equations below were evaluated the mechanical properties of the adhesive bond in the tested beams, specifically its capacity to resist torsional deformations.

By analyzing the measured shear forces and corresponding displacements obtained during the experimental tests, the equations below allowed us to calculate the torsional shear modulus of the bonded interface. This parameter gave a crucial understanding how effectively the adhesive layer transfers shear stresses and contributes to the overall structural performance of the timber beam.

Through the equation below is calculated the shear modulus in a shear field test $G_{tor,s}$ of the bonded layer or shear zone:

$$G_{tor,s} = \alpha \frac{h_0 (V_{s,2} - V_{s,1})}{bh (w_2 - w_1)} \dots (9)$$

Where:

- h_0 – gauge length in mm;
- $V_{s,2} - V_{s,1}$ -shear force, in newtons;
- b – width of the cross section;
- h – height of the cross-section;
- $w_2 - w_1$ - the increment of deformation in millimeters;
- α – geometrical factor (defined in the following equation).

While for the geometric relationship between the adhesive layer and the full cross-section is used following equation:

$$\alpha = \frac{3}{2} - \frac{h_0^2}{4h^2} \dots (10)$$

Where:

- h_0 – the gauge length for shear deformation;
- h – height of the beam cross-section.

The correction factor α helped us to make sure that the calculated shear modulus is more accurate by adjusting for the shape of the cross-section.

Taking in consideration the formula below is calculated the average displacement at a given measuring location i , based on two sensors placed diagonally within the shear field.

$$w_i = \frac{(|w_{i,1}| + |w_{i,2}|)}{2}, \quad i = 1,2 \dots (11)$$

Where:

- $w_{i,1}, w_{i,2}$ – the mean deformation of both diagonals i on opposite side faces of the beam for a given shear load $V_{s,i}$, in millimeters.

4.4.2.1. Shear Field Test Method (Experimental results)

The graph below (fig. 76) shows the relationship between applied force (in kN) and measured deflection (in mm) during the Shear Field Test for beam BI1. Two deflection meters (Dm1 and Dm2) were used to capture localized deformations at opposite corners of the shear field zone, as indicated in the setup diagram.

The curves illustrate a nearly linear trend in both measurements, with Dm1 registering negative deflection and Dm2 positive, indicating opposite displacements due to shear distortion. The symmetrical but opposing behavior of the two curves confirms the presence of shear deformation in the central region of the beam. The smooth, continuous progression of the curves also suggests stable behavior during the loading process, without abrupt failures or sudden changes in stiffness within the observed load range.

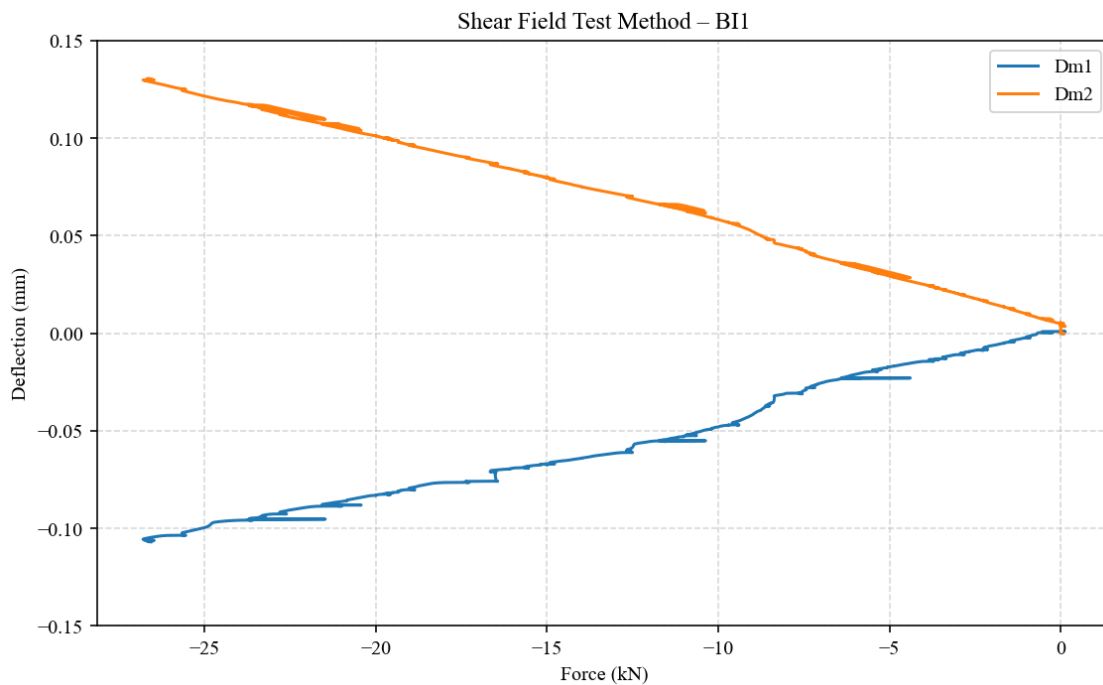


Figure 76. Force–deflection response from the Shear Field Test for beam BI1

The graph representing beam BI2 displays a steady and balanced shear response, with Dm1 and Dm2 demonstrating inverse yet almost linear deflections. This indicates a stable shear performance as the load increases, resembling the pattern seen in BI1.

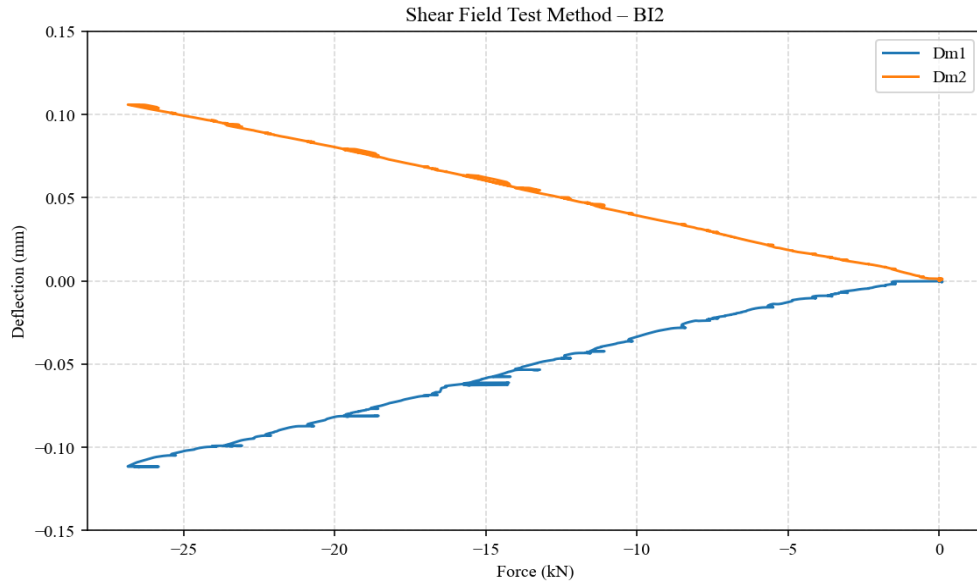


Figure 77. Force–deflection response from the Shear Field Test for beam BI2

The graph for beam BI3 illustrates the beam's response to the applied load. The two deflection meters, Dm1 and Dm2, documented opposing movements, clearly indicating shear deformation at the center of the beam. In comparison to BI1 and BI2, the curves for BI3 display a slightly greater curvature, which may imply some initial indications of material softening or heightened deformation as the load increased.

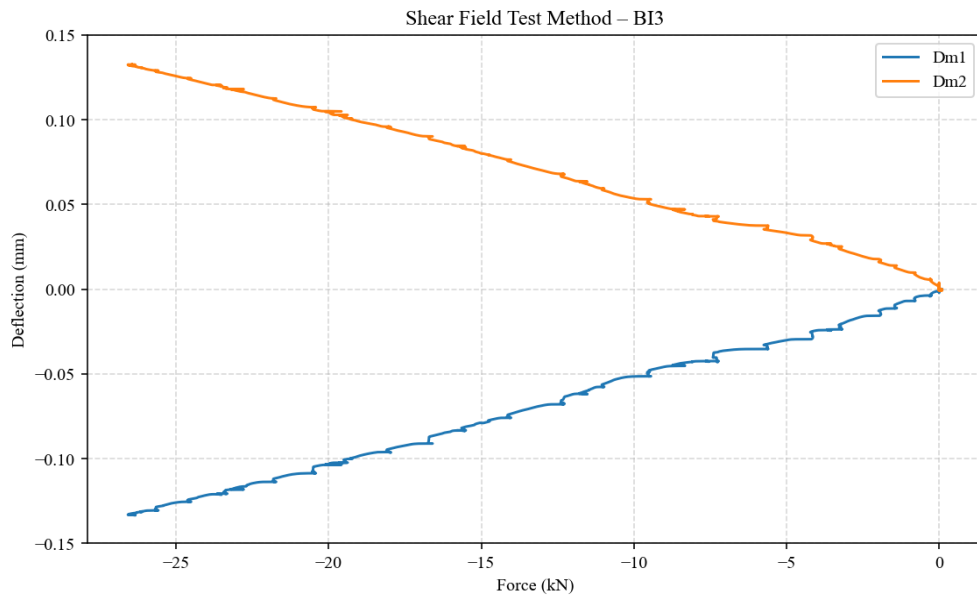


Figure 78. Force–deflection response from the Shear Field Test for beam BI3

The images below show the experimental arrangement utilized for evaluating beams BI1, BI2, and BI3 using the Shear Field Test approach.

Each beam was simply supported and subjected to a central load to create shear stress. Two deflection gauges were positioned diagonally within the shear field area to measure local displacements (Dm1 and Dm2), as shown in the related graphs.

The configuration was maintained consistently throughout all three tests to guarantee dependable and comparable outcomes.



Figure 79. Experimental investigation of shear field test



Figure 80. Shear-field experimental test accessories

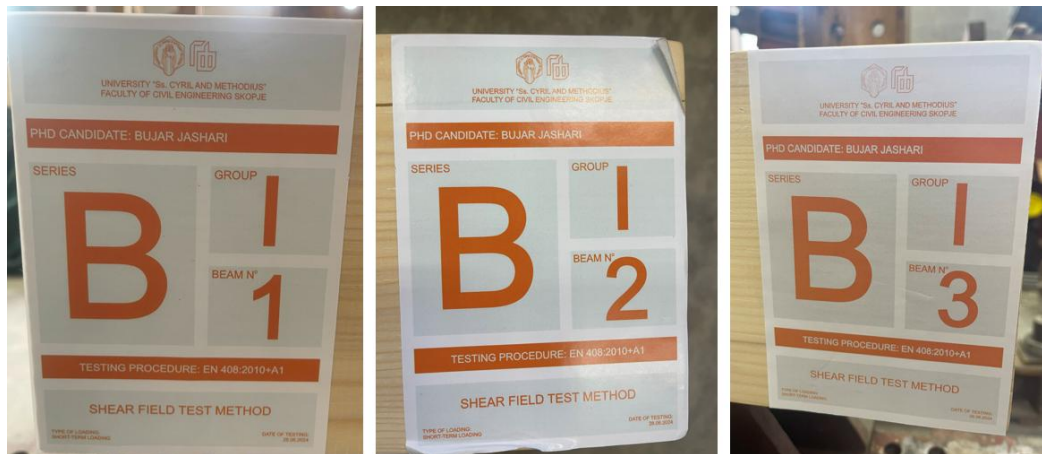


Figure 81. Shear-Field Test Methods beams (BI1, BI2, BI3)

Following the experimental evaluation of beams BI1, BI2, and BI3, all three exhibited comparable performance under load. The data collected from Dm1 and Dm2 indicated opposing yet consistent deformations, thereby affirming the distinct development of the shear field within the beams' central area.

In comparisons, beams BI1 and BI2 demonstrated a more linear and stable response, whereas BI3 exhibited a slightly more curved trend, implying a potential for greater deformation or a heightened impact of the material properties. However, the uniform testing setup and the repeatable behavior of the beams affirm the credibility of the testing method and the accuracy of the results obtained.

4.4.3. Bending Strength Parallel to the Grain (Serie C)

All three beams tested in Series C had identical dimensions. The maximum force applied during each test was recorded. The load was applied using a constant loading-head displacement rate, calibrated to ensure that the maximum load was reached within five minutes or 300 ± 120 seconds.



Figure 82. Experimental test for bending strength parallel to the grain

From the equation is calculated bending strength, which in average is 54.3 N/mm^2 .

$$f_m = \frac{3Fa}{bh^2} \dots (12)$$

Where:

- f_m – is the bending strength:
- F – is load in newtons:
- a - is distance between a loading position and the nearest support in a bending test, in millimetres:
- b – is width of cross section in a bending test in mm:
- h – is depth of cross section in a bending test or height



Figure 83. Experimental test for bending strength parallel to the grain

Table 8. Highlighted experimental results for bending strength parallel to the grain

Designation	Fmax. [kN]	Strength [N/mm ²]
Serie CI1	61.58	47.24
Serie CI2	82.0	62.9
Serie CI3	69.0	52.9

The Fmax average recorded across the three tested beams was 70.8 kN. This value reflects the peak load each specimen withstood before failure, indicating consistent material performance and serving as a basis for further analysis.

Regarding the experimental test of the C series beams, particularly for beam CI1 a crack was created approximately from the middle of the beam with a length of 1200 mm. The crack initiation started from the right side of the front-view, which was followed towards the center of the beam.



Figure 84. Beam CI1 Front view

The figure 78 shows the rear part of the beam, from which a fracture has also been created. In this part, the initiation of cracking from the center of the beam in the peripheral direction of the section has been observed.



Figure 85. Beam C11 – Back view

In beam C12, a continuous crack was observed at the end of the sample, which is shown in the figure below (fig. 79). This crack started from the middle of the beam at exactly 1375 mm length measured from the right side of the beam, while the depth of the crack was approximately 15 mm.



Figure 86. Beam C12 – Bottom view

In beam CI3, a larger fracture has been created, which has a length of over 1200mm, which started from the left side of the beam and gradually extends to the periphery (the part shown is the bottom of the beam), while the depth is approximately 30mm. Unlike beams CI1 and CI2, this sample has sustained greater damage.



Figure 87. Beam CI3 – Bottom view

4.4.4. Long - Term Behaviour (Serie D)

This series focused on investigating the long-term deflection behavior of beams under sustained loading conditions, specifically to evaluate creep development and determine the creep coefficient. The beams (2) tested had identical dimensions (138mm x 170 mm x 3570mm) and were subjected to a uniformly distributed load using full-steel billets (dimensions 140mm x 140mm x 500mm).



Figure 88. Determination of long-term behavior of beam DI1 and DI2



Figure 89. Long-term effect and creep coefficient under sustained load for DI1 and DI2

Two loading configurations were used: DI1 with a total mass of 613.8 kg and DI-2 with 608.35 kg.

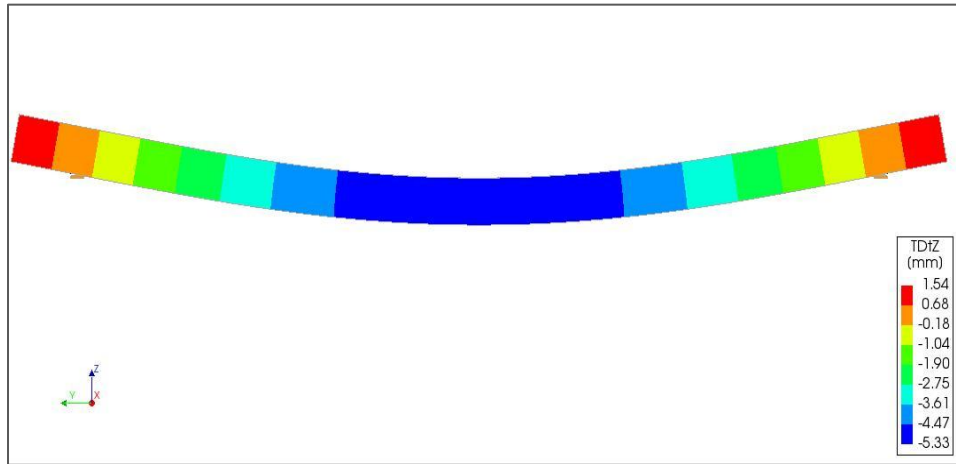


Figure 90. Visual simulation

The testing period lasted for 139 days (3336 hours), from July 10, 2024, to November 26, 2024, during which relative humidity (RH) and temperature (T) were kept constant to ensure consistent environmental conditions and minimize external influences on deformation behavior.

Throughout the testing period, the ambient relative humidity (RH) and temperature were continuously monitored to ensure stable conditions and minimize the influence of external factors on the mechanical behavior of the specimens.

The initial recorded values were approximately **23.6°C** for temperature and **64%** for relative humidity. These data were documented at each measurement phase and serve as a basis for evaluating the impact of environmental conditions on long-term deformation (creep) development.



Figure 91. Equipment for temperature and relative humidity monitoring

Each individual billet was carefully weighed on a scale to determine the total load applied to the beam.



Figure 92. Weighing each of the steel billets

Table 9. The data were recorded as presented in the following table report (Beam D11):

Long-term BEAM D11							
PHASE	DATE	HOUR	T[°C]	RH [%]	Dm1 [mm]	Dm2 [mm]	Weight kg
0	10.07.24	9:30	23.6	65	3.65	5.6	77.3+
1					4.35	5.76	79.4+
2					5.08	5.91	75.05+
3					5.55	6.04	76.45+
4					6.03	6.14	79.50+
5					6.75	6.27	76.85+
6					7.38	6.43	72.80+
7					7.78	6.52	76.45+
8					8.22	6.64	
G	11.07.24	10:00	23.7	64	8.39	6.64	
G	12.07.24	10:00	23.9	62	8.43	6.62	
G	13.07.24	10:30	24	60	8.46	6.62	
G	14.07.24	11:00	24.1	61	8.49	6.62	
G	15.07.24	10:15	24.2	62	8.53	6.62	
G	16.07.24	12:45	24.5	59	8.55	6.62	
G	17.07.24	8:45	24.5	54	8.52	6.57	
G	18.07.24	7:15	24.7	56	8.54	6.56	
G	19.07.24	15:05	25.2	64	8.62	6.58	
G	20.07.24	14:05	25.2	63	8.64	6.59	
G	21.07.24	10:35	25.1	62	8.64	6.59	
G	22.07.24	16:30	25.7	56	8.64	6.59	
G	29.07.24	9:50	24.6	52	8.67	6.47	
G	06.08.24	10:30	24.7	46	8.75	6.28	
G	12.08.24	10:50	25.3	50	8.83	6.27	
G	19.08.24	9:30	25.6	56	8.96	6.33	
G	26.08.24	8:20	25.2	50	8.96	6.36	
G	02.09.24	11:00	24.3	47	8.96	6.31	
G	09.09.24	9:40	24.5	57	9.06	6.35	
G	16.09.24	17:00	22.3	51	9.01	6.26	
G	23.09.24	16:30	22	51	9.02	6.3	
G	01.10.24	8:20	20.5	30	8.9	6.14	
G	07.10.24	15:00	20.3	55	9.09	6.34	
G	14.10.24	17:15	19.8	54	9.08	6.35	
G	21.10.24	19:15	18.6	52	9.06	6.32	
G	29.10.24	16:30	18.1	58	9.09	6.35	
G	04.11.24	8:20	20.5	50	9.06	6.32	
G	11.11.24	13:30	22.8	47	9	6.16	
G	19.11.24	19:10	22.1	40	9.04	6	
G	26.11.24	17:15	20.8	27	8.96	5.73	

Total weight (sustained distributed load = **613.8 kg**)

Table 10. The data were recorded as presented in the following table report (Beam DI2):

Long-term BEAM DI2							
PHASE	DATE	HOUR	T[°C]	RH[%]	Dm1[m]	Dm2[m]	Weight kg
0	10.07.24	9:30	23.6	65	4.47	4.17	
1					5.1	4.28	74.9+
2					5.75	4.39	77.05+
3					6.2	4.44	80.75+
4					6.65	4.54	73.2+
5					7.26	4.65	73.9+
6					7.91	7.79	74.9+
7					8.33	4.87	78.05+
8					8.74	4.98	75.6+
G	11.07.2	10:0	23.	64	8.89	4.98	Total weight (sustained distributed load = 608.35 kg)
G	12.07.2	10:0	23.	62	8.93	4.97	
G	13.07.2	10:3	24	60	8.97	4.97	
G	14.07.2	11:0	24.	61	9	4.97	
G	15.07.2	10:1	24.	62	9.02	4.97	
G	16.07.2	12:4	24.	59	9.09	4.97	
G	17.07.2	8:45	24.	54	9.05	4.98	
G	18.07.2	7:15	24.	56	9.06	4.92	
G	19.07.2	15:0	25.	64	9.12	4.93	
G	20.07.2	14:0	25.	63	9.14	4.93	
G	21.07.2	10:3	25.	62	9.14	4.93	
G	22.07.2	16:3	25.	56	9.16	4.93	
G	29.07.2	9:50	24.	52	9.24	4.82	
G	06.08.2	10:3	24.	46	9.38	4.57	
G	12.08.2	10:5	25.	50	9.47	4.57	
G	19.08.2	9:30	25.	56	9.58	4.64	
G	26.08.2	8:20	25.	50	9.6	4.68	
G	02.09.2	11:0	24.	47	9.64	4.68	
G	09.09.2	9:40	24.	57	9.69	4.67	
G	16.09.2	17:0	22.	51	9.72	4.58	
G	23.09.2	16:3	22	51	9.71	4.62	
G	01.10.2	8:20	20.	30	9.7	4.44	
G	07.10.2	15:0	20.	55	9.76	4.66	
G	14.10.2	17:1	19.	54	9.78	4.65	
G	21.10.2	19:1	18.	52	9.78	4.64	
G	29.10.2	16:3	18.	58	9.79	4.64	
G	04.11.2	8:20	20.	50	9.77	4.65	
G	11.11.2	13:3	22.	47	9.75	4.49	
G	19.11.2	19:1	22.	40	9.82	4.3	
G	26.11.2	17:1	20.	27	9.91	4	

5. NUMERICAL MODELING

5.1. Constitutive model

The numerical modeling process involved the definition of the constitutive relationships for the materials used. For the steel plates positioned at the beam supports and loading points, a linear elastic behavior was assumed. These components were characterized by a constant modulus of elasticity $E=210\text{GPa}$, reflecting the standard mechanical properties of structural steel and ensuring minimal deformation under applied loads.

The timber material, due to its inherently anisotropic and heterogeneous nature, required a simplified assumption for the purposes of numerical analysis. Hence, for the purposes of numerical analysis, a homogenized material model was adopted treating the Glued Solid Timber (GST) as an equivalent isotropic and homogeneous material with averaged mechanical properties derived from experimental results. This assumption simplifies the computational model while still capturing the global structural response with sufficient accuracy.

To reflect the different responses of wood under tension and compression, two distinct constitutive behaviors were defined:

In tension (Figure 93), the timber was modeled as a brittle material, failing upon reaching its ultimate tensile strength without significant post-peak deformation. This aligns with experimental observations where failure occurred suddenly and without plasticity.

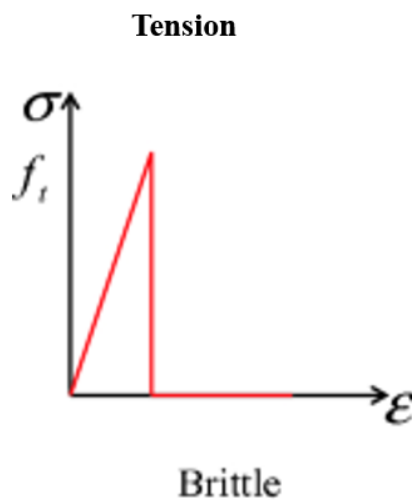


Figure 93. Constitutive law behavior for timber used in numerical modeling: Brittle behavior in tension

In compression (Figure 94), an elastic–perfectly plastic model was applied. This allowed the material to behave elastically up to the yield point, beyond which it exhibited a constant stress (plateau), effectively capturing the timber's ability to redistribute stresses post-yield before ultimate failure.

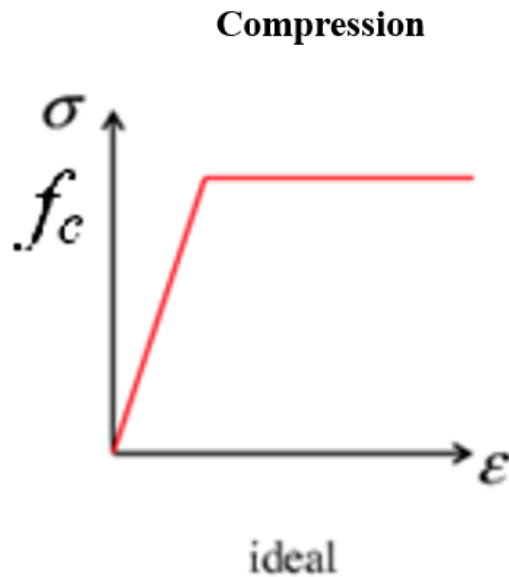


Figure 94. Constitutive law behavior for timber used in numerical modeling: Elastic–perfectly plastic behavior in compression

These material definitions were crucial in simulating both the pre-peak elastic response and the post-peak nonlinearities, enabling realistic representation of the load-deformation behavior observed during the four-point bending tests.

5.2. Geometry and Boundary Conditions and Mesh Discretization

In order to simulate the structural behavior of the Glued Solid Timber (GST) beams under various loading conditions, the DIANA Finite Element Method (FEM) software was utilized. This advanced computational tool provides robust capabilities for nonlinear analysis, allowing for detailed modeling of material behavior, load application, boundary conditions, and failure mechanisms.

The software enabled the implementation of custom constitutive laws for both timber and steel components, mesh generation with refined discretization at critical zones, and accurate tracking of stress-strain evolution throughout the loading process. By using FEM, the numerical simulations were able to closely replicate the experimental results, offering valuable insights into the mechanical response and failure modes of the tested beams.

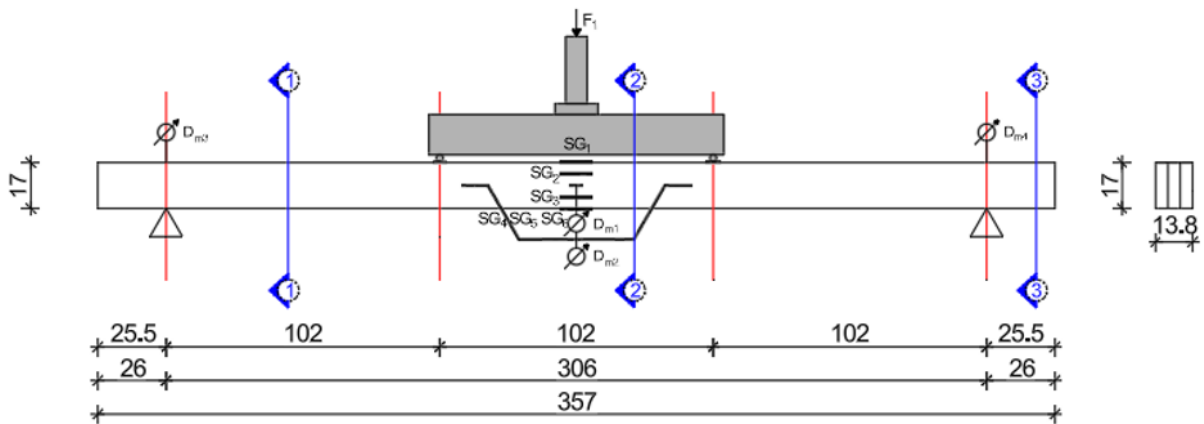


Figure 95. Position of the accessories where the load is supported and applied

The geometry and boundary conditions of the numerical model are presented here, with particular emphasis on the accurate representation of the support configurations and the locations of external load application. The beam was modeled at full scale, with dimensions identical to those of the experimentally tested specimens, ensuring consistency between the physical and numerical setups. The supports were assigned stiffness properties that realistically replicate the behavior of the steel plates used during the experimental testing, allowing for limited deformation while effectively restraining vertical displacement. The load was applied as an incremental vertical displacement at two loading points positioned symmetrically between the supports, accurately reproducing the conditions of the four-point bending test.

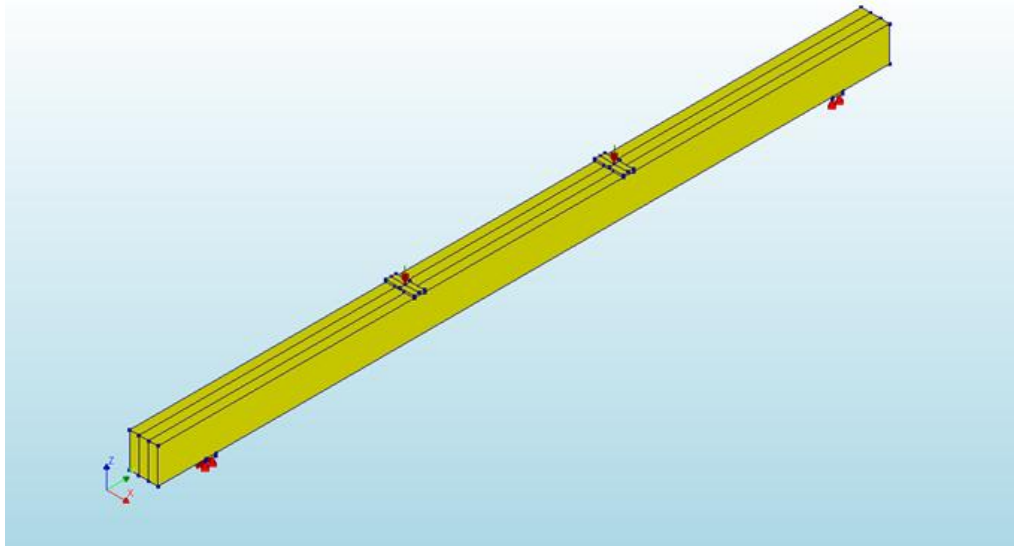


Figure 96. Geometry and boundary conditions of the numerical model

Since the bonding process during beam fabrication was carried out with high precision—using a structural polyurethane (PUR) one-component adhesive in accordance with EN 15425—it is assumed that a perfect bond exists between the lamellas in the numerical model.



Figure 97. Arrangement of load application and support conditions in the numerical model

An optimal mesh was generated using hexahedral elements with an approximate element size of ≈ 20 mm (optimal), ensuring a good balance between computational efficiency and result accuracy.

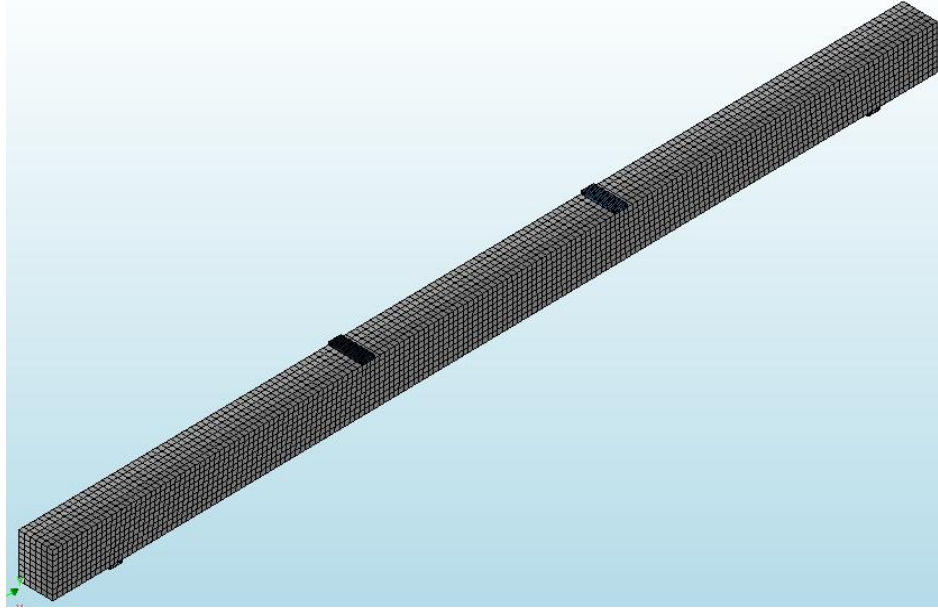


Figure 98. Finite element mesh of the GST beam with steel plates at supports and loading points.

In the following, the adopted parameters of the constitutive law used for the numerical modeling are presented. These include the material properties according to behavioral assumptions applied for the timber, which form the basis of the simulations.

The mechanical parameters, such as the modulus of elasticity were derived from the experimental results from series A, specifically from the global modulus of elasticity obtained through four-point bending tests.

Table 11. Data obtained from Modulus of Elasticity

Designation	Em,g [MPa]
Serie AI1	11604
Serie AI2	11277
Serie AI3	9394

The compressive strength value adopted for the numerical analysis, $f_c = 30.35$ N/mm², was uniformly applied across all simulations. This value represents the average compressive strength parallel to the grain, derived from Serie E and documented in Table 4 of the experimental campaign.

In contrast, the tensile strength values were adopted based on numerical trial-and-error calibrations to align the simulated failure points with those observed experimentally. As tensile failure in timber exhibits brittle behavior and is sensitive to local defects, the values were adjusted per test case. The resulting adopted values were:

Test AI1 – Not Applicable (N/A)

Test AI2 – $f_t=58 \text{ N/mm}^2$

Test AI3 – $f_t=60 \text{ N/mm}^2$

These adjustments allowed the numerical model to closely replicate the failure behavior and load capacity observed in the corresponding mechanical tests.

5.3. Comparison and Discussion: Four-Point Bending Test (Serie A)

The numerical and experimental results are compared to evaluate the accuracy and predictive capability of the developed finite element model. By examining both global and local responses such as load displacement behavior and strain distribution—the consistency between simulated and tested beam performance is assessed. The comparison focuses on key parameters including stiffness, peak load, and failure modes, providing insight into the effectiveness of the adopted constitutive laws and boundary conditions in replicating the actual behavior of the Glued Solid Timber (GST) beams under four-point bending.

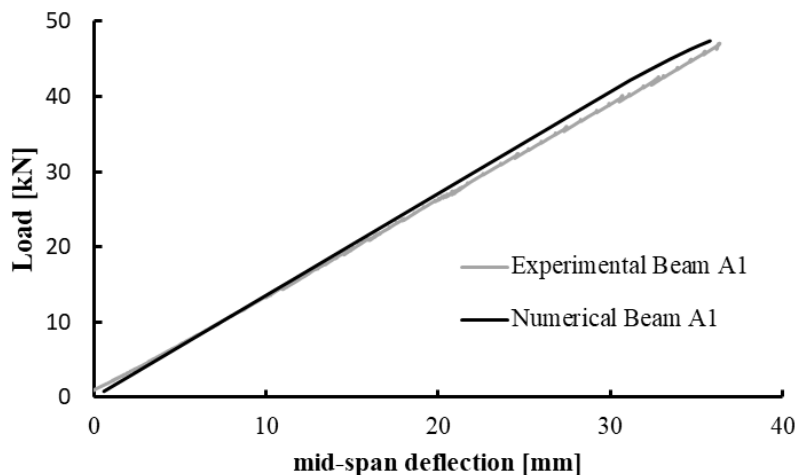


Figure 99. Load – displacement comparison Experiment vs Numerical for beam AI1

A good correlation between the numerical and experimental results was observed in terms of the load–displacement curve for AI1 (Fig. 100) beam, indicating that the numerical model effectively captured the overall response of the beam.

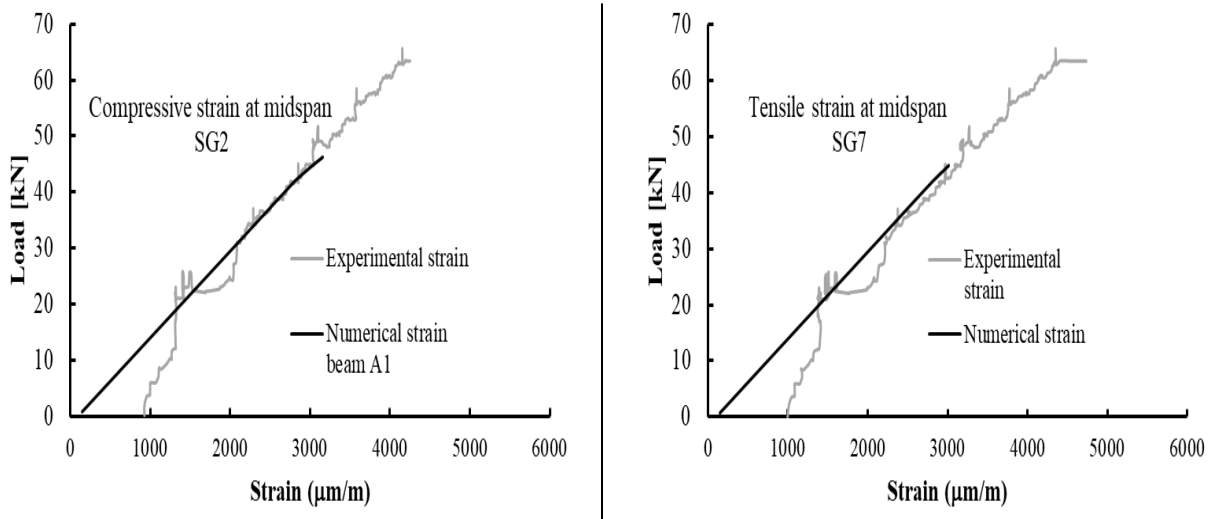


Figure 100. Strain gage comparison in compression and tension for beam AI1

A similarly good correlation was confirmed locally (Fig. 100), with strain gage measurements validating the numerical results in both tension and compression zones, further supporting the accuracy of the model at the material level.

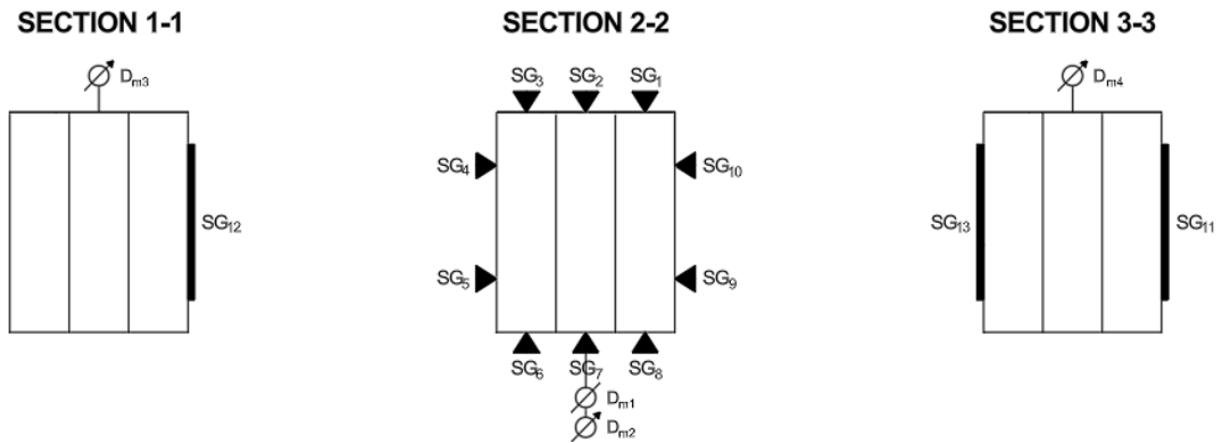


Figure 101. Position of strain gauges: Illustration of the placement of strain gauges along the beam, showing both the tension and compression zones, for beam AI1

Through the figure 103 is illustrated the behavior of the beam cross-section under various loading conditions. Through non-linear analysis, it was observed that at a load of approximately

46.2 kN, the compression zone begins to enter the plastic range, indicating the onset of material yielding. Simultaneously, the neutral axis starts to shift from its original position. By evaluating the results in more detail, it was possible to gain deeper insights into the redistribution of internal stresses and the progression of non-linear behavior across the cross-section, particularly the gradual transition from elastic to plastic states in the compressive region.

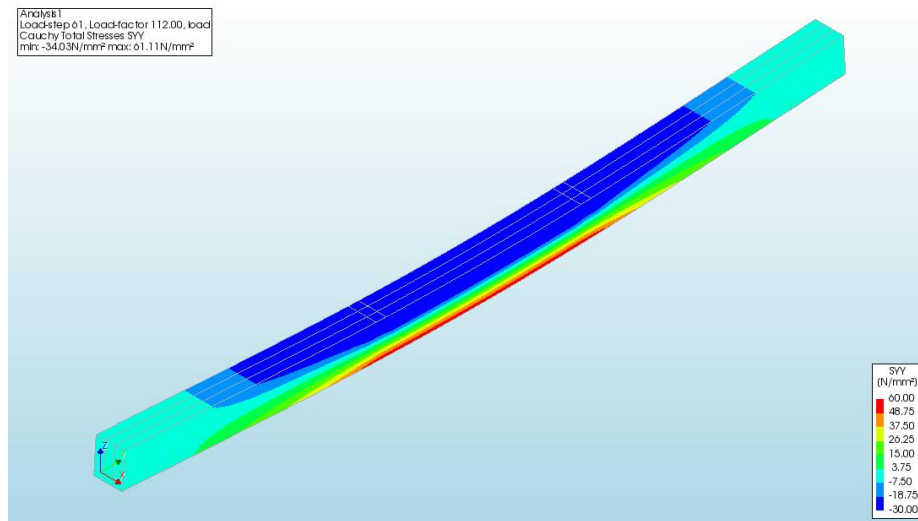


Figure 102. Typical deformed shape of the beam from numerical analysis

Figure 102 shows the typical deformed shape of the beam as obtained from the numerical analysis, along with the corresponding stress field distribution. This visualization helps to identify the critical regions experiencing maximum tensile and compressive stresses,

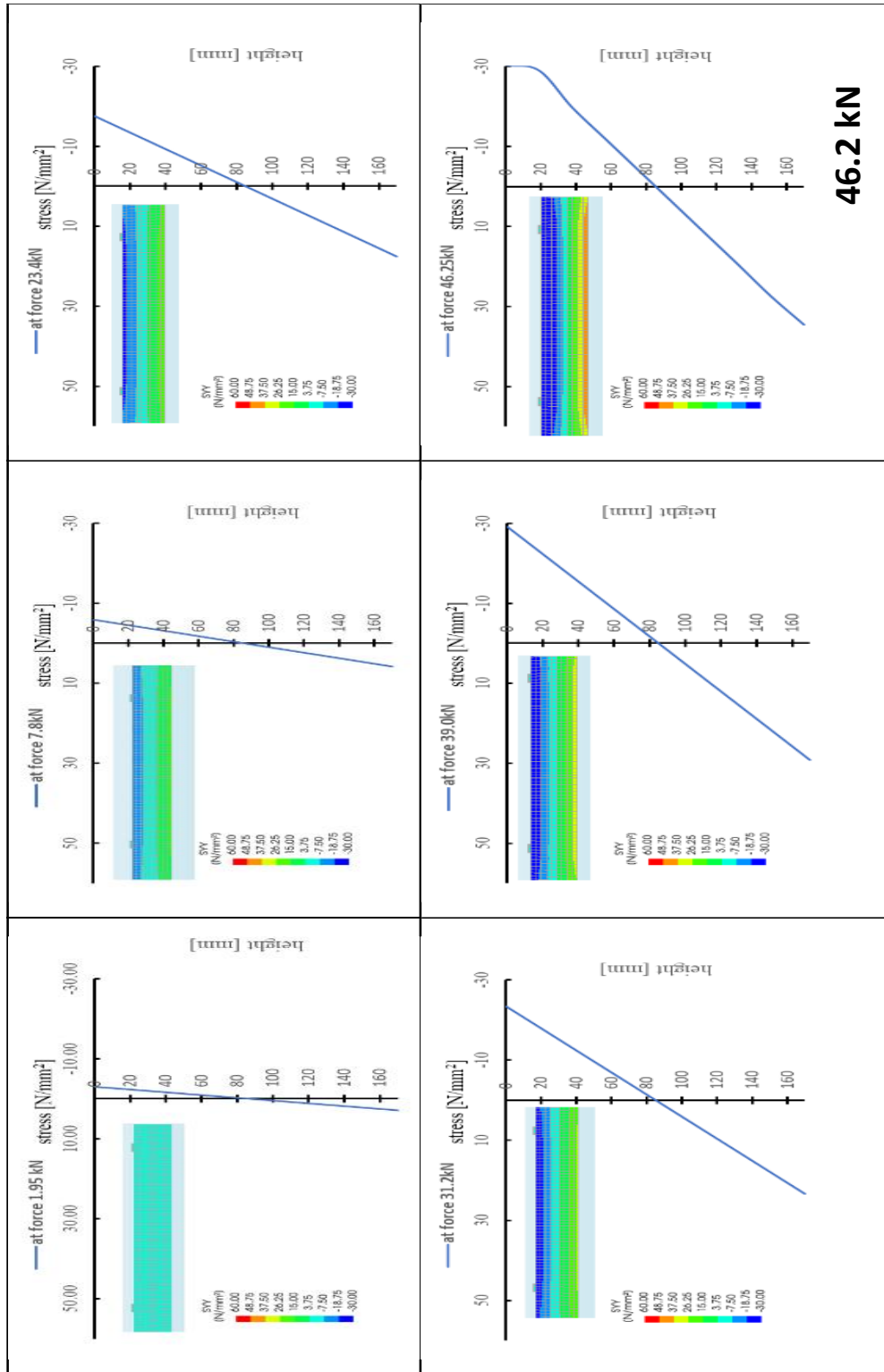


Figure 103. Stress evolution across the beam cross-section under increasing load for beam AI1

The graph above (fig. 103) illustrates the transition from linear elastic behavior to non-linear stress distribution, highlighting the development of plasticity in the compression zone and the increase in tensile stress toward failure. This behavior, specifically observed at a load of 46.2 kN, is captured through non-linear numerical analysis, which enables the observation of stress redistribution and plastic deformation phenomena that cannot be represented under the linear assumption of plane sections.

Bending Tests Results and Discussion

Figures 104 and 105 present the experimental results of sample AI1, the results of which were obtained from Strain Gauge (SG), SG5 to SG9. Where diagram 104 shows the results for SG6, SG7, SG8, while diagram 105 shows the results of SG5 and SG9. The comparisons of the results are made for the exerted force expressed in kN while the strain is expressed in (micrometer/m).

In figure 104 at AI1 from the results obtained from SG6, SG7 and SG8, the results expressed in the diagrams show that the force exerted until the end of the bending tension stress test reaches the value of the maximum force (F_{max}) 69.24 kN. While the maximum strain reaches up to 5137.45 microns/meter.

In figure 105. In AI1 from the results obtained from SG5, and SG9, the results expressed in the diagrams show that the force exerted until the end of the bending tension stress test reaches the value of the maximum force (F_{max}) 69.24 kN, the same as in SG6 SG7, and SG8. While the maximum strain reaches up to 2319.88 microns/meter.

From the obtained results it can be seen that the experimentally obtained curves have a similarity and are in very good agreement with the predicted results (Fpred). The most visible difference between these two graphs is in Strain.

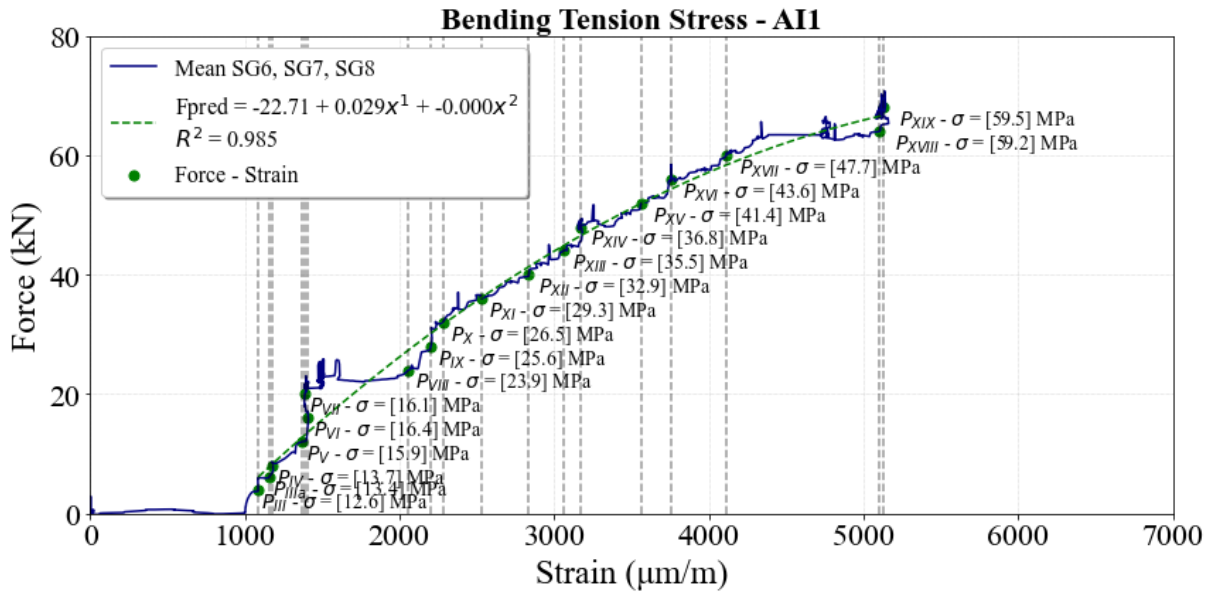


Figure 104. Bending Tension of Mean SG6 SG7, SG8 for beam AI1

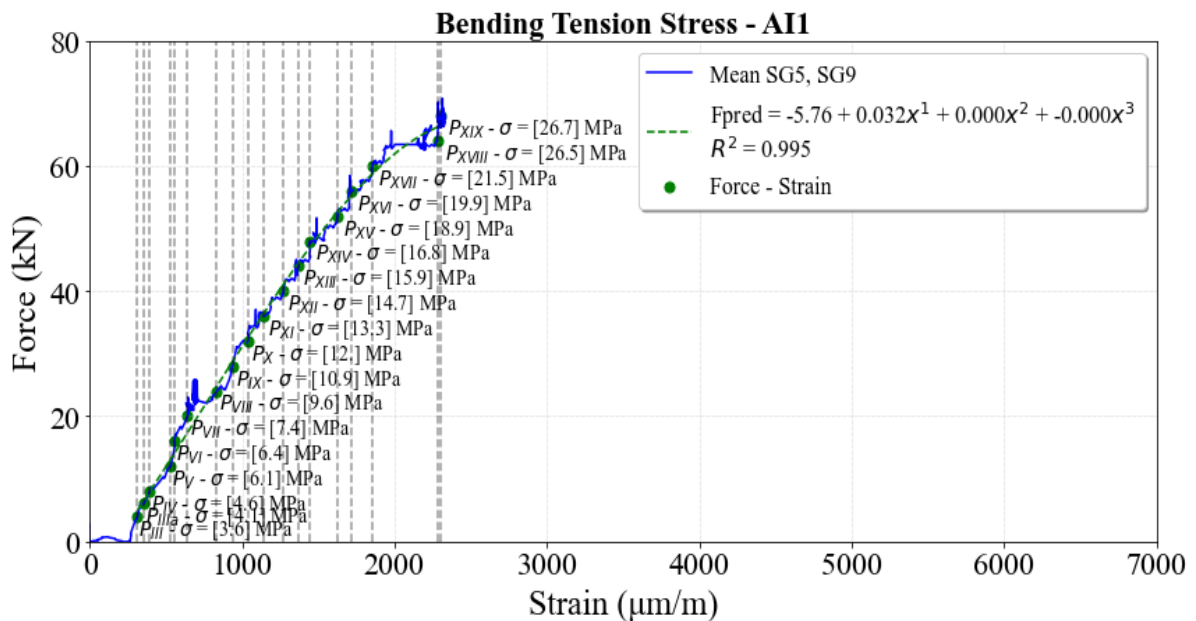


Figure 105. Bending Tension of Mean SG5 and, SG9 for beam AI1

Bending Compression Tests Results and Discussion

Figures 106 and 107 graphically present the experimental results for sample AI1, which were obtained from the Bending Compression experimental test. In these graphs the results are presented for Stress and Strain. Where in figure 106 the results are given for SG1, SG2 and SG3, while in figure 107 the results are given for SG4 and SG10.

In figure 106 for sample AI1, the results expressed graphically for SG1, SG2 and SG3 show that the average maximum force (Fmax) is at the value of 69.24 kN. While the strain for this model (sample) reaches a value of 4426.61 microns/meter.

Figure 1107 shows the experimental results obtained for sample AI2, where the measuring instruments were SG4 and SG10. The average value of the maximum force (Fmax) is 68.08 kN. The strain is indicated at a value of 3372.44 microns/meter.

The studied data show that the experimental results have a linear relationship with the designed results (Fpred). The difference between Figures 106 and 107 lies/stays in the Strain.

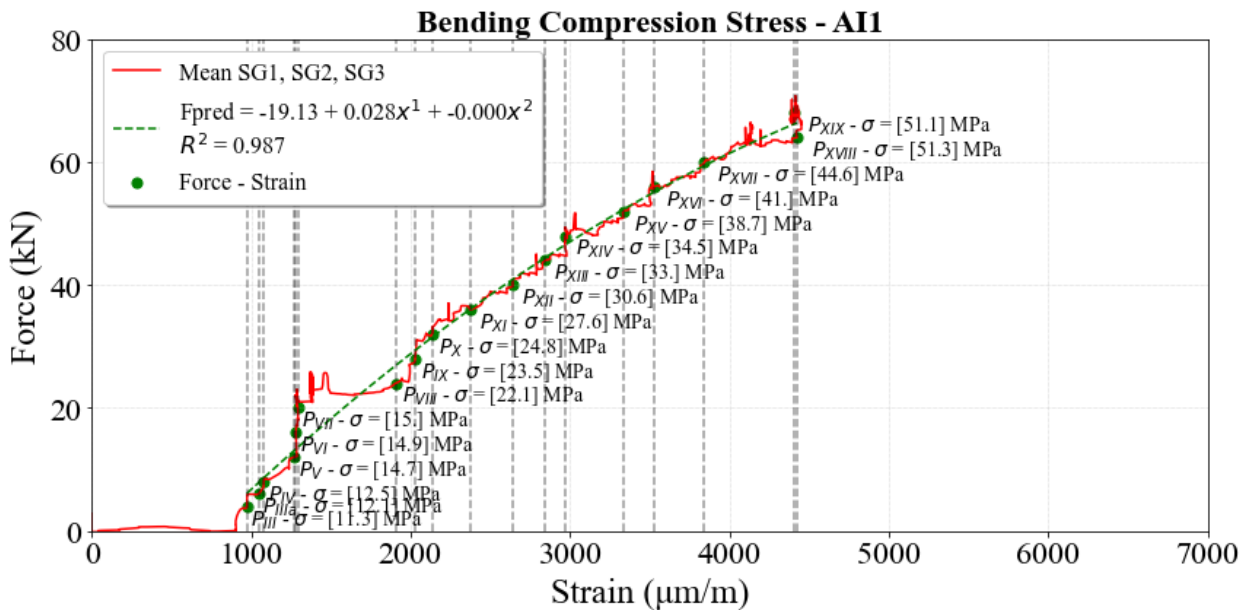


Figure 106. Bending Compression Test of Mean SG5 and, SG9 for beam AI1

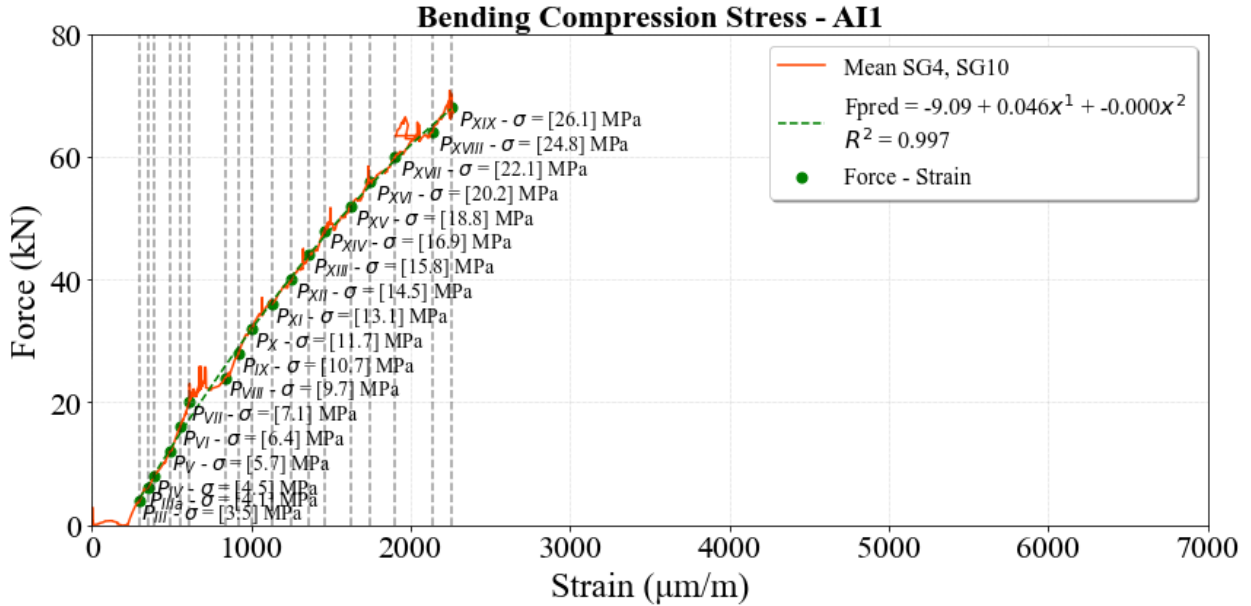


Figure 107. Bending Compression of Mean SG5 and, SG9 for beam AI1

By employing the principle of linear section behavior which assumes that plane sections remain plane and utilizing the strain values measured from the strain gauges, it was possible to generate stress and strain distribution diagrams across the beam cross-section. From the analysis of the linear section behavior, it is assumed that deformation remains proportional to the applied load, in accordance with the principles of linear elasticity. As the load increases, the section deforms uniformly up to the point of failure, while the neutral axis remains stationary, indicating a symmetrical stress distribution between the tension and compression zones.

These diagrams provide a clear visualization of internal behavior under load, supporting both the theoretical assumptions and the experimental observations in the elastic range.

Bending Compression/Tension Strains - AI1

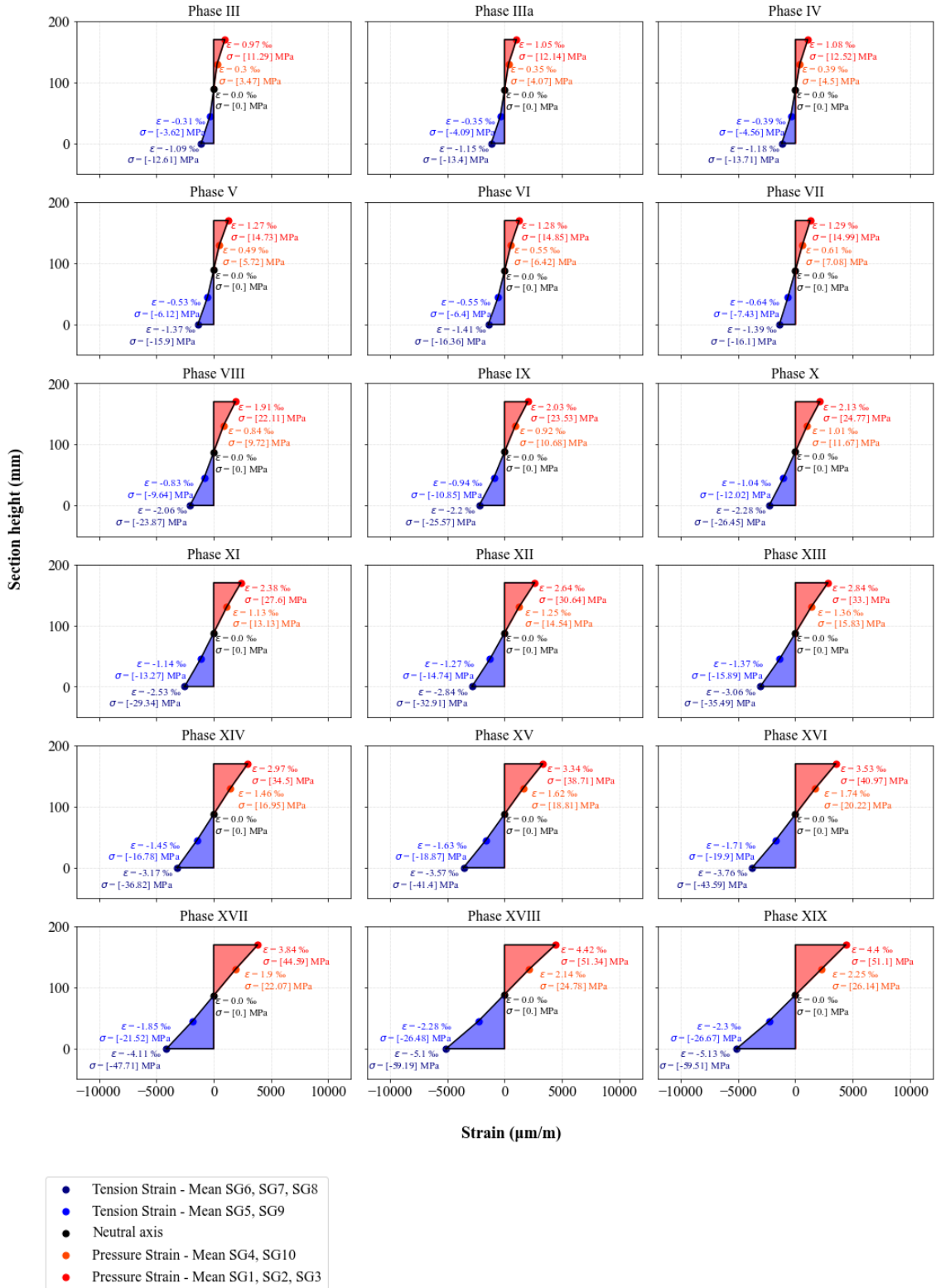


Figure 108. Bending Compression/Tension Strains for beam AI1

5.3.1. AI2 Comparison and discussion

As the AI1 beam, similar trend was observed for the AI2 beam, with a good correlation between the numerical and experimental results in terms of the load–displacement curve, indicating that the numerical model accurately captured the global behavior of the beam.

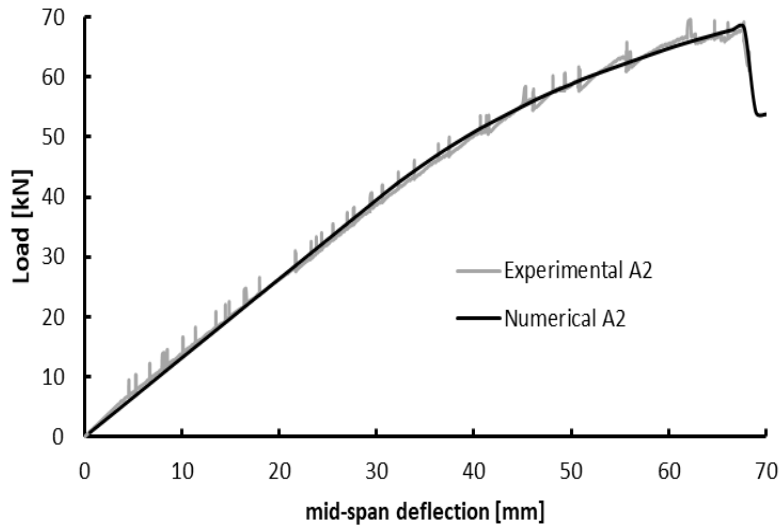


Figure 109. Load – displacement comparison Experiment vs Numerical for beam AI2

Likewise, a strong local agreement was confirmed (Fig. 110), where strain gauge measurements in both the tension and compression zones closely matched the numerical predictions, further verifying the model's effectiveness in representing material-level responses.

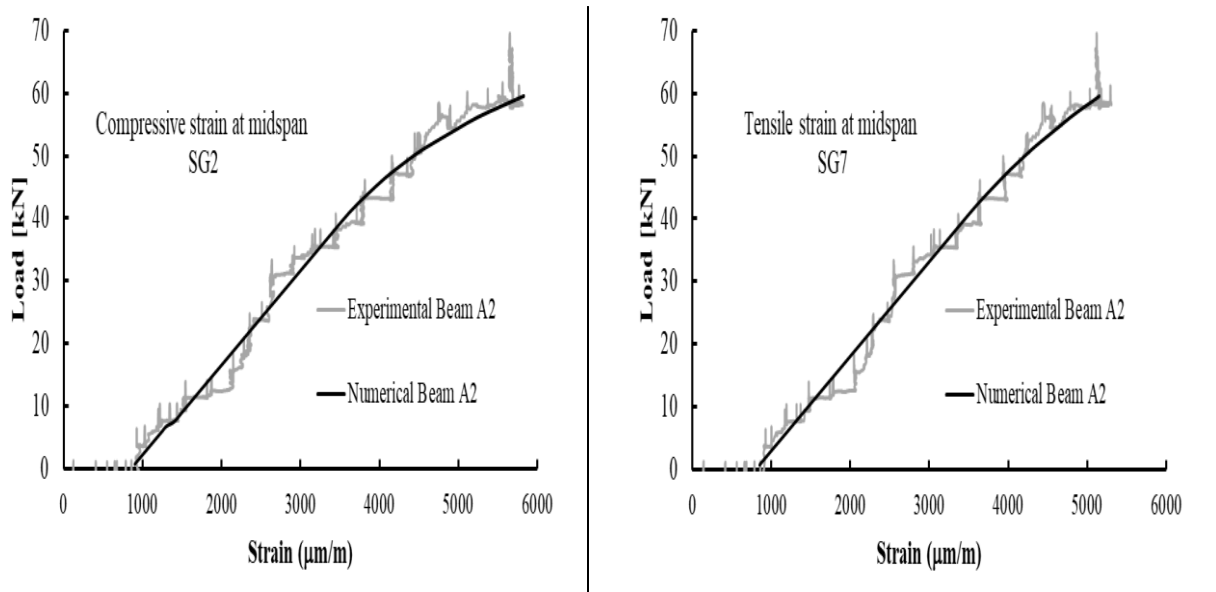


Figure 110. Strain gage comparison in compression and tension for beam AI2

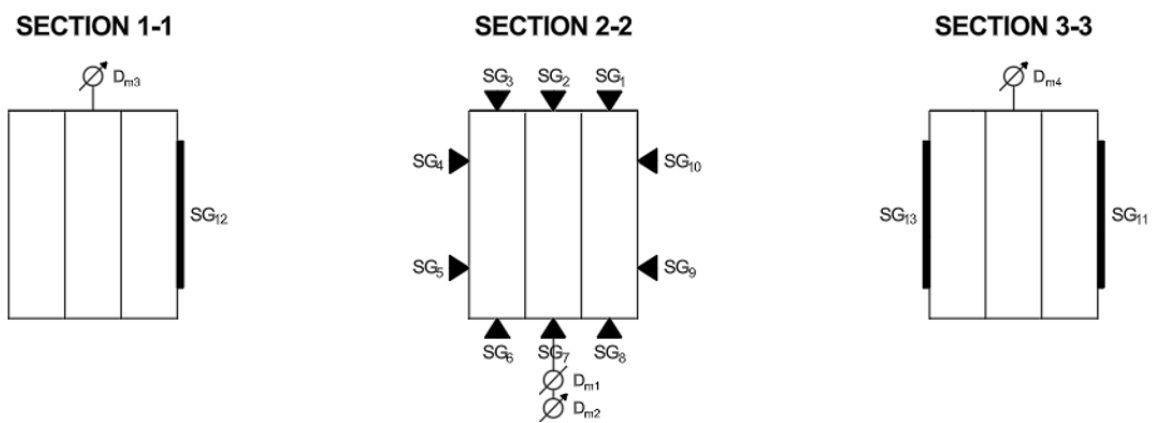


Figure 111. Position of strain gauges: Illustration of the placement of strain gauges along the beam, showing both the tension and compression zones, for beam AI2

The graph below (Fig. 112) illustrates the behavior of the cross-section for AI2 under increasing load. Based on the non-linear analysis, it was noted that at a load of approximately 68.2 kN. Failure occurs in the tensile zone, as the tensile stress reaches the material's ultimate capacity. At the same time, the neutral axis begins to shift, reflecting the redistribution of internal stresses.

A more detailed evaluation of the results provided further insights into the transition from linear to non-linear behavior, particularly highlighting the strain concentration and stress development leading up to brittle tensile failure.

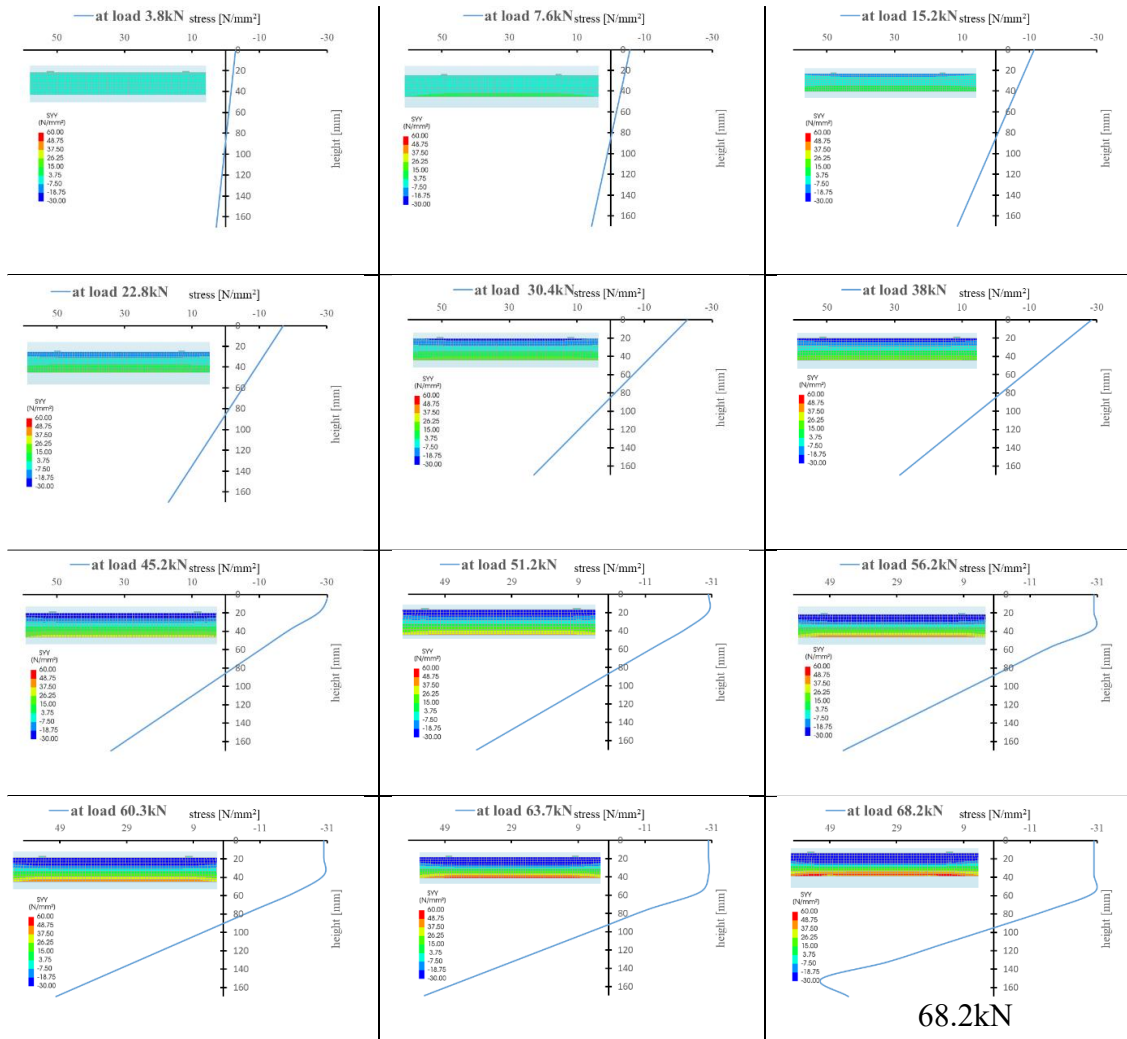


Figure 112. Stress evolution across the beam cross-section under increasing load for beam AI2

Bending tension stress AI2

Figures 113 and 114 show the experimental results of sample AI2. These results are obtained from Strain Gauge (SG), SG5 to SG9. Diagram 26 shows the results for SG6, SG7, SG8, while diagram 114 shows the results of SG5 and SG9. The comparisons of the results were made for the exerted force expressed in kN while the strain was expressed in (micrometer/m).

In Figure 113, In AI2, the data from SG6, SG7 and SG8 show that the force exerted during Bending tension stress reaches the maximum force (Fmax) of 68.08 kN. The maximum strain is up to 5272.56 microns/meter.

In Figure 114, AI2 results from SG5 and SG9 reveal that the applied force until the end of the bending tension test reaches the maximum force (Fmax) of 68.08 kN, which is the same as in SG6, SG7 and SG8. The maximum strain derived from SG5 and SG9 is up to 2468.18 microns/meter.

The obtained results show that the experimentally obtained curves are similar and coincide extremely well with the predicted results (Fpred). The most obvious difference between these two graphs is in the strain.

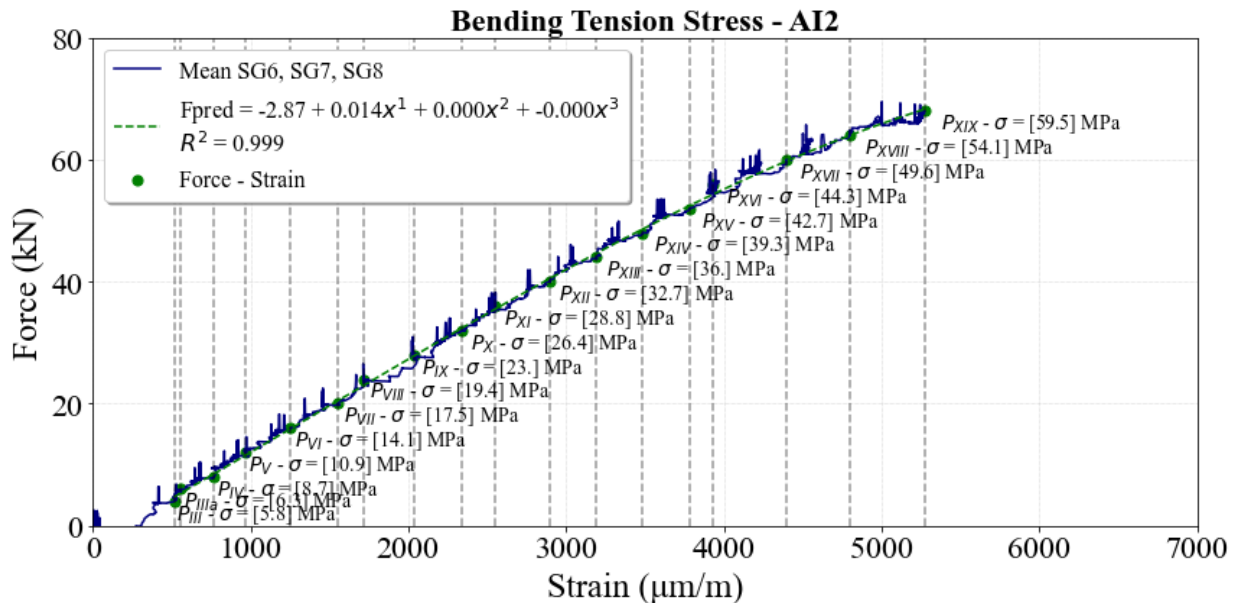


Figure 113. Bending Tension of Mean SG6 SG7, SG8 for beam AI2

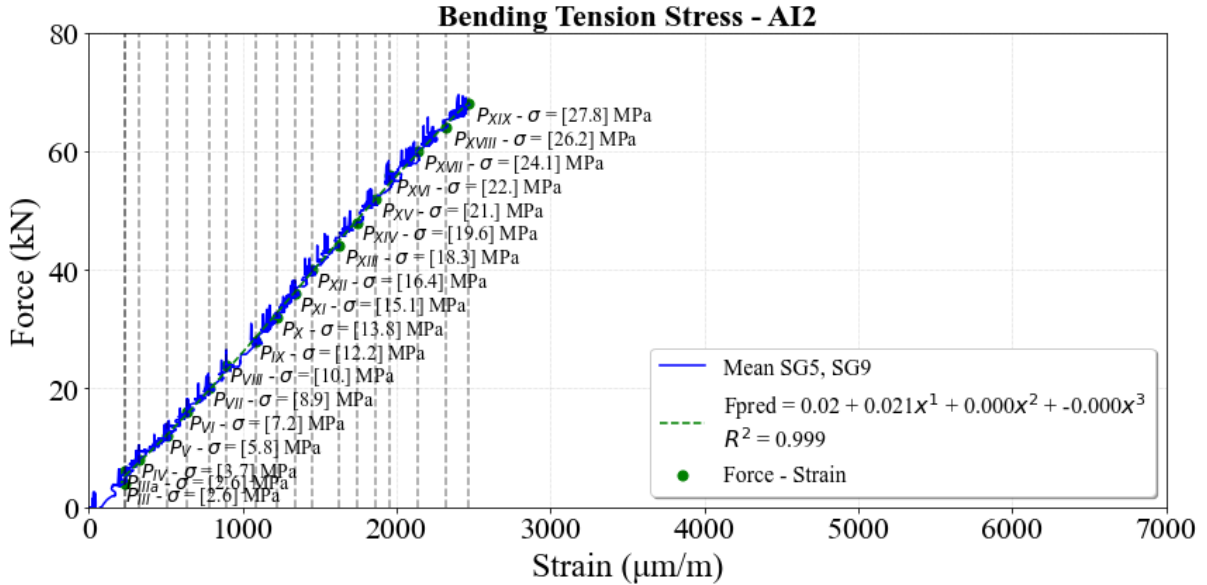


Figure 114. Bending Tension of Mean SG5 and, SG9

Bending Compression Tests Results and Discussion

Figures 115 and 116 present the experimental results for sample AI2 obtained from Bending Compression Tests. These graphs show the results for stress and strain. Figure 115 shows the results for SG1, SG2 and SG3, while Figure 116 shows the results for SG4 and SG10.

The average maximum force (F_{max}) for specimen AI2 is 68.08 kN, as shown in Figure 115, where the data are visually expressed for SG1, SG2 and SG3. While the strain for this model (sample) approaches 5063.51 microns/meter.

Figure 116 shows the experimental results obtained for sample AI2, where the measuring instruments were SG4 and SG10. The average value of the maximum force (F_{max}) is 68.08 kN. Strain is indicated at a value of 3372.44 microns/meter.

The studied data show that the experimental results have a linear relationship with the designed results (F_{pred}). The difference between Figures 115 and 116 is based on Bending Compression Stress.

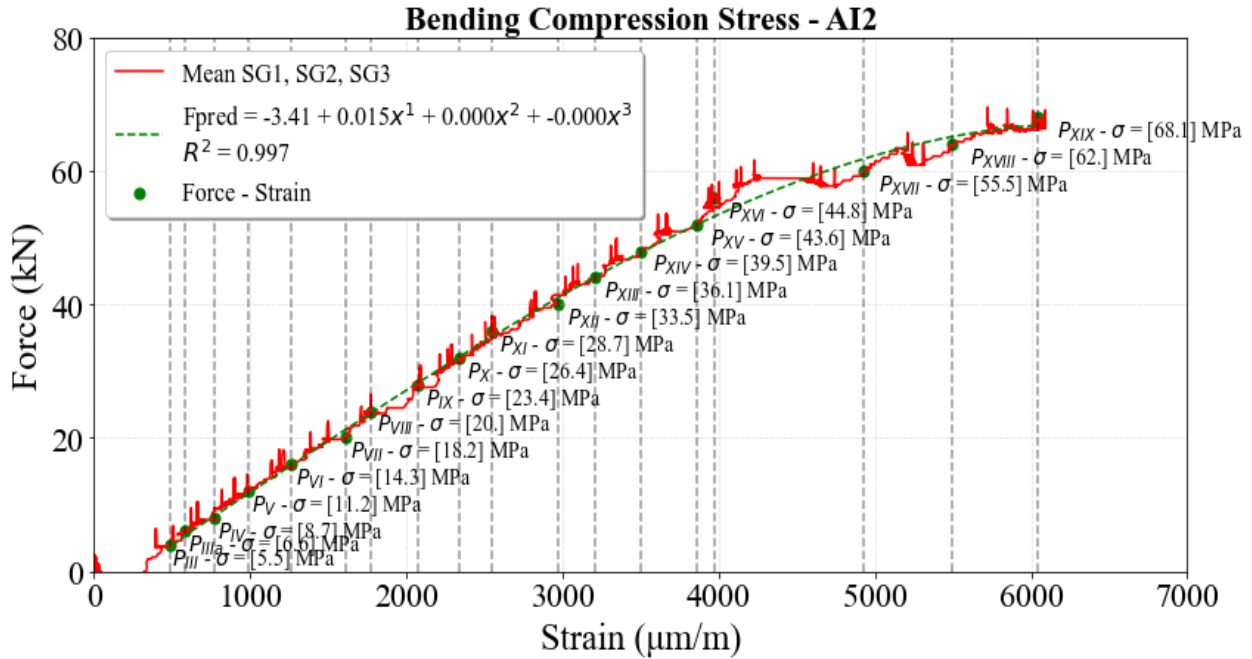


Figure 115. Bending Compression Test of Mean SG1, SG2 and SG9

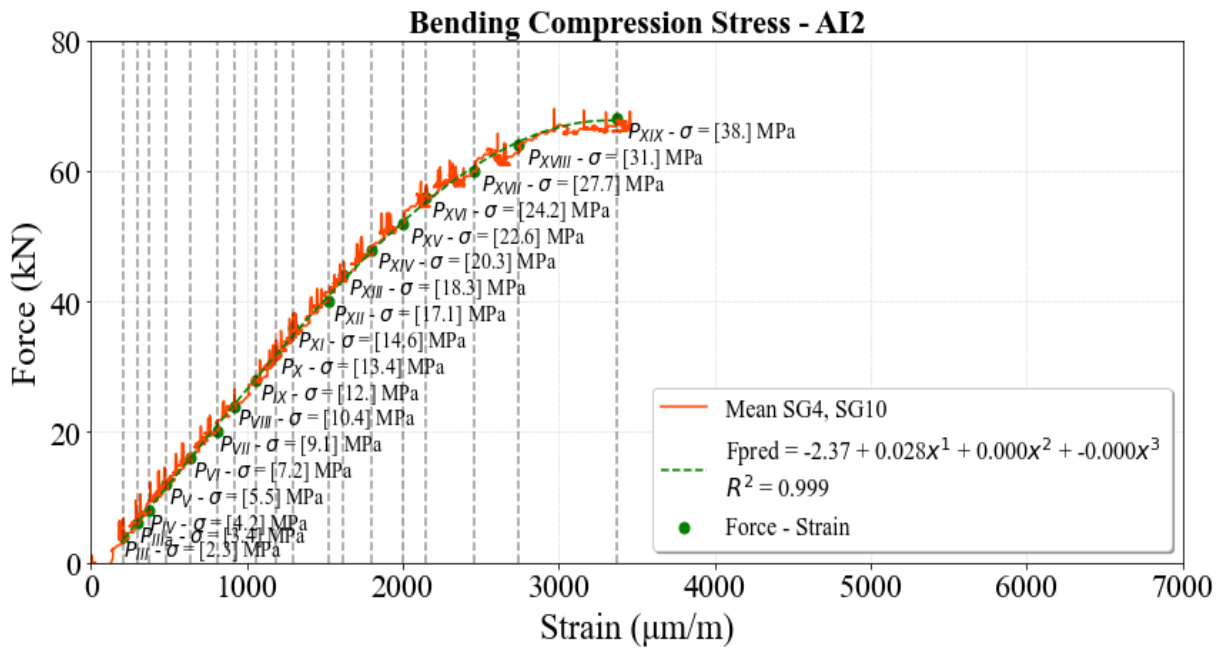


Figure 116. Bending Compression of Mean SG4 and, SG10

Bending Compression/Tension Strains - AI2

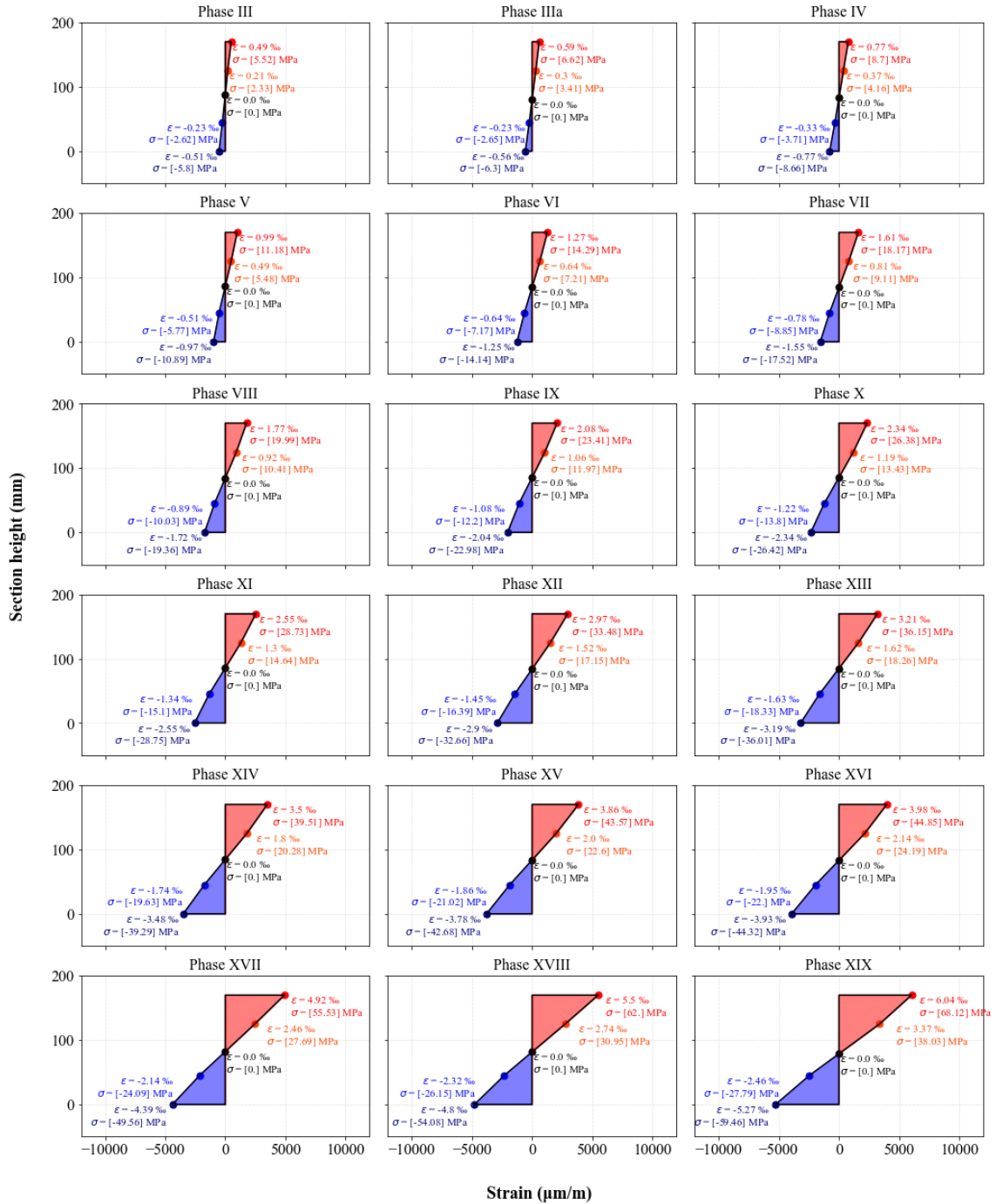


Figure 117. Experimental results bending compression/tension strains AI2

5.3.2. AI3 Comparison and discussion

Similar to the previous cases, AI1 and AI2, a good correlation was observed between the numerical and experimental results for AI3 (Fig. 118). The comparison clearly demonstrates that the structural response of the beam can be distinguished into three distinct phases: the **elastic phase**, characterized by a linear load–displacement relationship; the **plastic phase**, where non-linear behavior begins to develop particularly in the compression zone; and finally, the **failure phase**, marked by a rapid loss of load-bearing capacity. Given the consistency of these observations across all three specimens, it can be reasonably concluded that this three-phase response is characteristic of the typical behavior of Glued Solid Timber (GST) beams under four-point bending conditions.

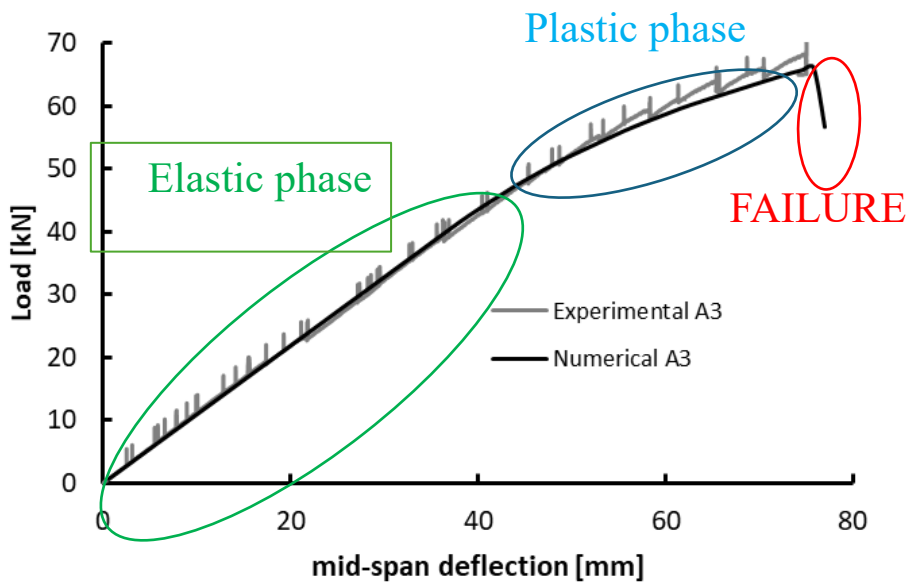


Figure 118. Comparison of experimental and numerical results for beam AI3

Bending Tests Results and Discussion

Figures 119 and 120 present the experimental results of sample AI3, the results of which were obtained from Strain Gauge (SG), SG5 to SG8. Where diagram 119 shows the results for SG6, SG7 and SG8, hile diagram 120 shows the results of SG5. The comparisons of the results were made for the exerted force expressed in kN while the strain was expressed in (micrometer/m).

In figure 119, at AI3 from the results obtained from SG6, SG7 and SG8, the results expressed in the diagrams show that the force exerted until the end of the bending tension stress test reaches the value of the maximum force (Fmax) 67.96 kN. While the maximum strain reaches up to 6111.20 microns/meter.

In figure 120, at AI3 from the results obtained from SG5, the results expressed in the diagrams show that the force exerted until the end of the bending tension stress test reaches the value of the maximum force (Fmax) 67.96 kN. While the maximum strain reaches up to 3663.10 microns/meter.

From the obtained results it can be seen that the experimentally obtained curves have a similarity and are in very good agreement with the predicted results (Fpred). The most visible difference between these two graphs is in Strain.

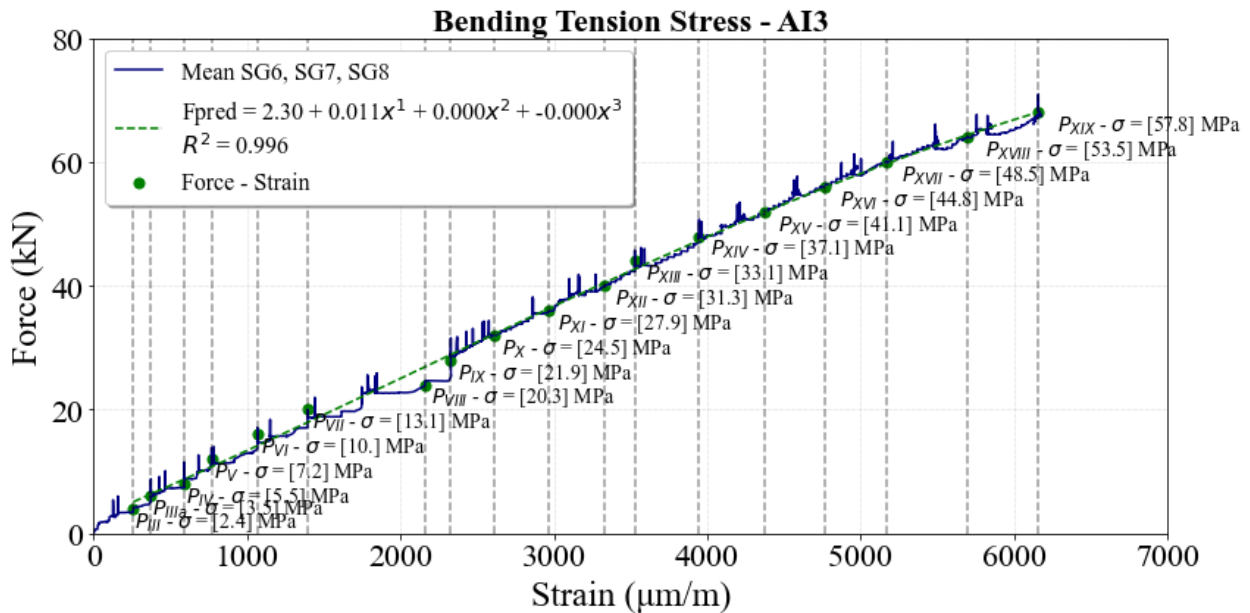


Figure 119. Bending Tension Test of Mean SG6, SG7 and SG8 for beam AI3

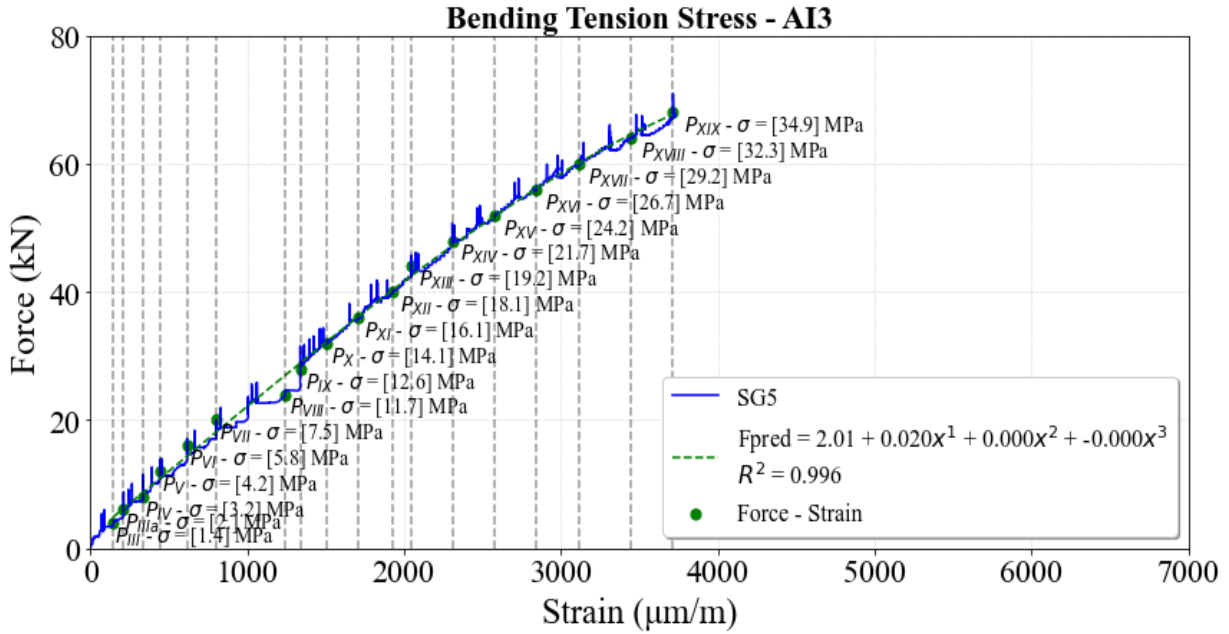


Figure 120. Bending Tension of Mean SG5

Bending Compression Tests Results and Discussion

Figures 121 and 122 graphically show the experimental results for sample AI3, which were obtained from the Bending Compression experimental test. In these graphs the results are presented for Stress and Strain. Where in figure 121 the results for SG2 are given, while in figure 115 the results for SG4 are given.

In figure 121 for sample AI3, the results expressed graphically for SG2 show that the average maximum force (F_{max}) is at the value of 67.96 kN. While the strain for this model (sample) reaches a value of 6657.23 microns/meter.

Figure 122 shows the experimental results obtained for sample AI3, where the measuring instrument was SG4. The average value of the maximum force (F_{max}) is 67.96 kN. The strain is indicated at a value of 2686.45 microns/meter.

The studied data show that the experimental results have a linear relationship with the designed results (Fpred). The difference between Figures 121 and 122 is in the Strain.

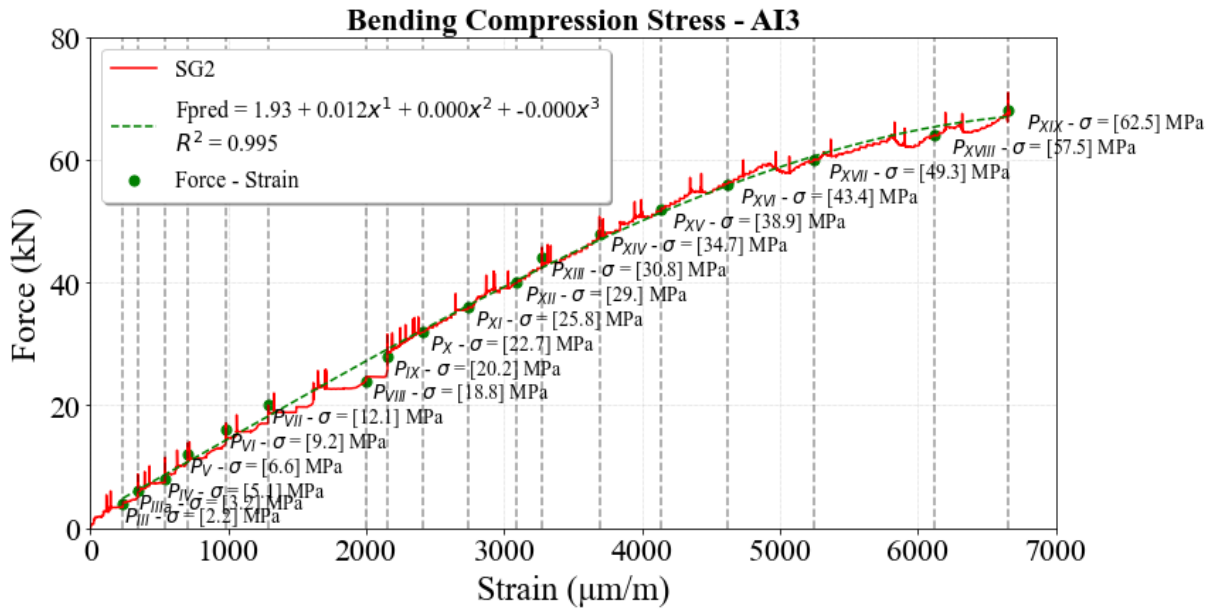


Figure 121. Bending Compression Test of Mean SG2

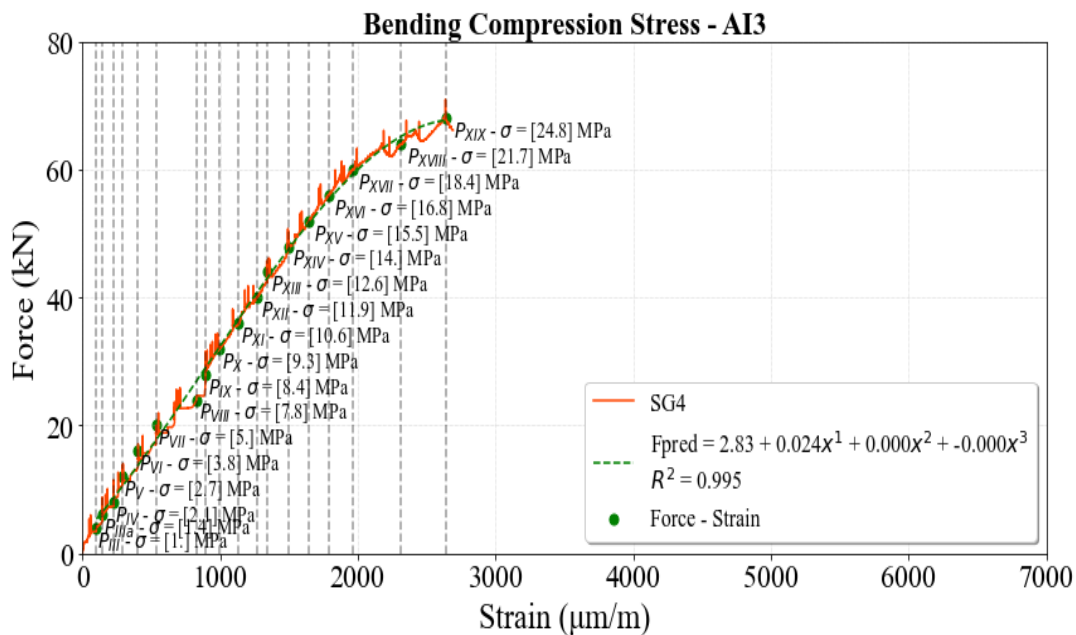


Figure 122. Bending compression test of mean of SG4

Bending Compression/Tension Strains - AI3

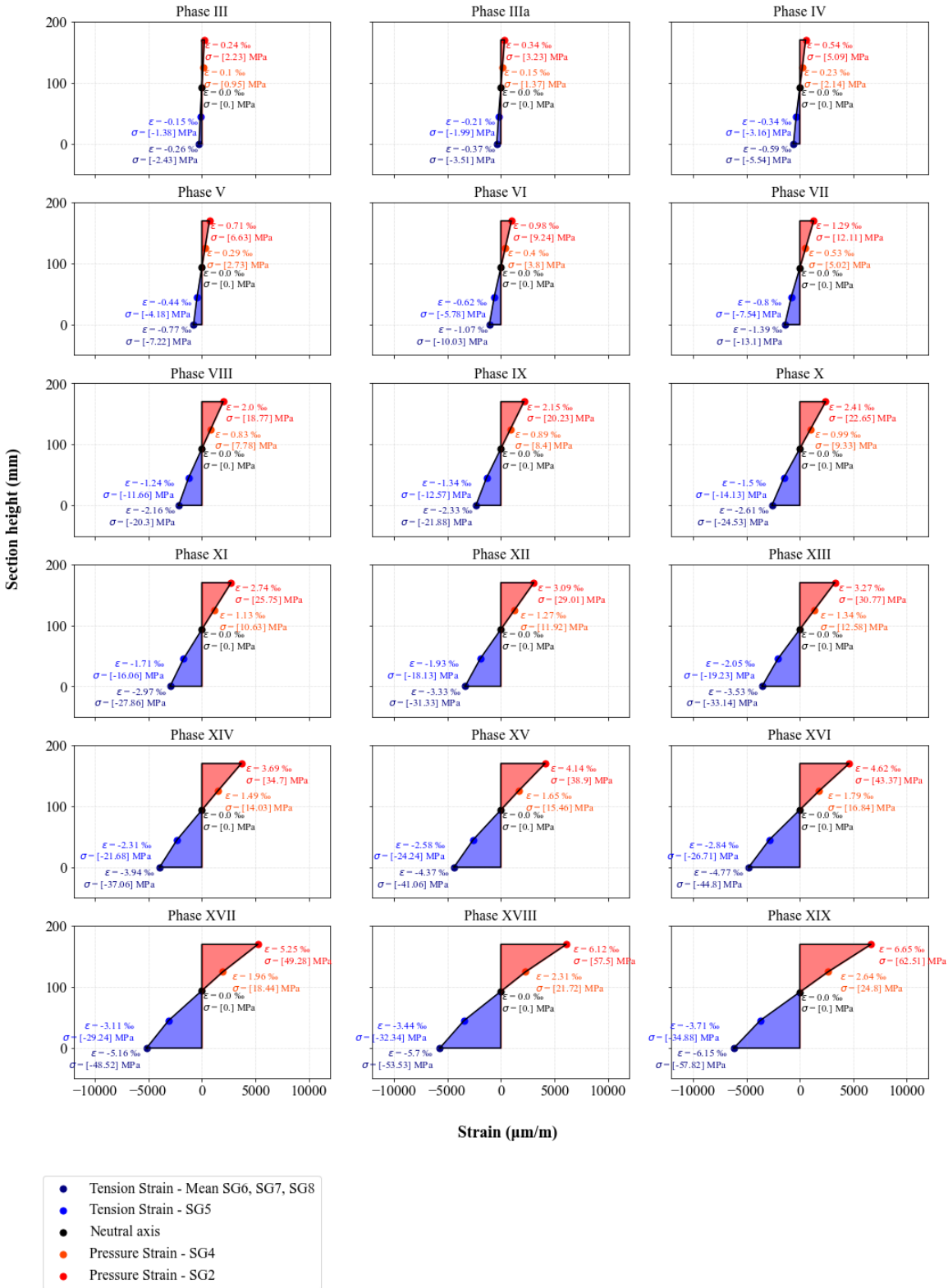


Figure 123. Experimental results bending compression/tension strains AI3

The graph below (fig. 124) presents the load–mid-span deflection behavior for all three beams (A1, A2, and A3), showing both experimental and numerical results.

A comparative analysis reveals several important observations:

- Beam A1 demonstrates excellent agreement between numerical and experimental results throughout the loading process. Both curves follow each other closely in the elastic and early plastic phases. This indicates that the numerical model accurately captures the initial stiffness and the onset of non-linear behavior for this specimen. No significant discrepancies are visible, and the curve progresses smoothly up to the failure stage.
- Beam A2, while generally consistent, shows a slight overestimation in the numerical results, especially in the post-yield (plastic) phase. The red numerical curve lies slightly above the experimental red dotted line, suggesting that the model may predict slightly higher capacity and stiffness than observed in the experiment. Furthermore, the sudden drop in the numerical curve at around 67–68 kN indicates a simulated failure mechanism, which aligns well with the experimental failure point. Despite this, the overall trend remains consistent and the deviation is within acceptable limits.
- Beam A3 also shows good agreement between the numerical (black solid line) and experimental (black dashed line) results. Both curves closely follow each other from the elastic phase into the plastic range. The peak load for both methods is around 68.2 kN, and the failure behavior is captured well. Among all three beams, A3 displays the most stable and consistent match between test and simulation across all loading stages.

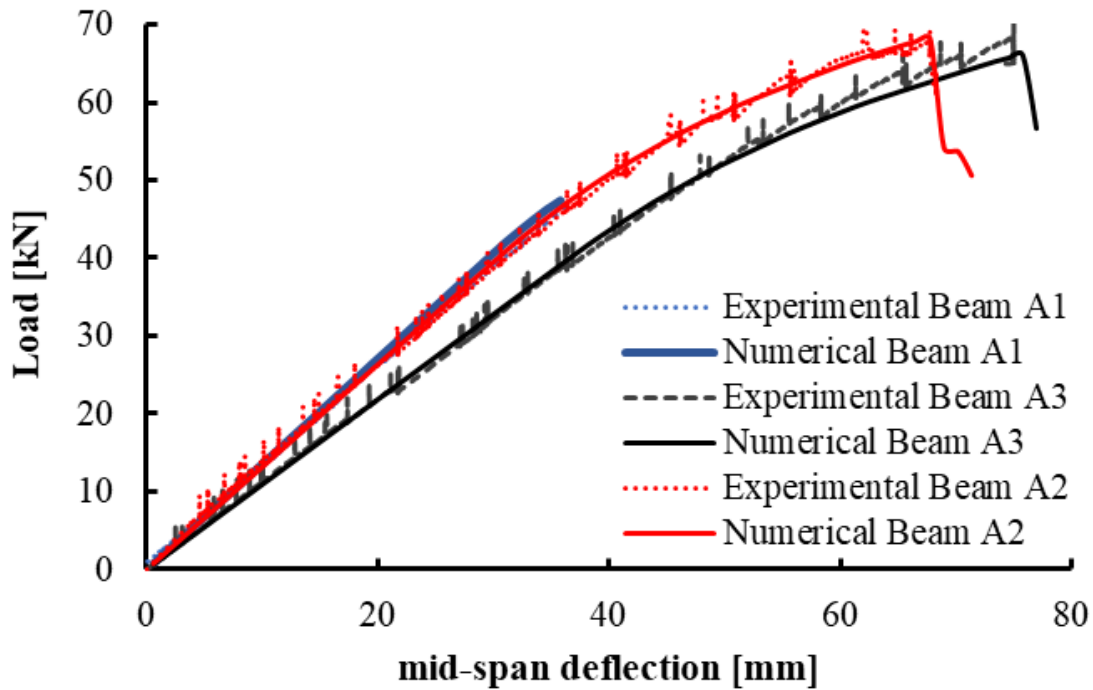


Figure 124. Comparison of experimental vs numerical results for beam A1, A2, A3

All three beams demonstrate comparable structural responses when subjected to loading, with slight differences that may stem from experimental inaccuracies or assumptions made in the model. The numerical models accurately predict the initial stiffness, yield points, and ultimate capacities. The strong alignment between experimental and numerical data in all cases supports the effectiveness and reliability of the modeling technique applied.

Among the three beams, Beam A2 displays the greatest load capacity, achieving up to 68–69 kN. However, it shows a sudden decrease after reaching its peak load, signifying a more brittle failure. In contrast, Beam A1 demonstrates the best overall performance, exhibiting strong strength, stable ductile behavior, and excellent correlation between numerical and experimental outcomes. Beam A3 also performs well with consistent behavior but has a slightly lower capacity compared to A2. In summary, Beam A1 can be regarded as the most well-rounded and dependable option.

5.4. Long term behavior under sustained load (Serie D)

The long-term behavior of the beams was monitored through Test DI1 and Test DI2 over a period of 139 days. Throughout the testing period, the environmental conditions were maintained relatively stable, with an average relative humidity (RH) of 53% and an average temperature of 23.3°C. These controlled conditions help ensure the reliability of the observed time-dependent deformations and provide a consistent basis for evaluating creep and shrinkage effects on the beam specimens.

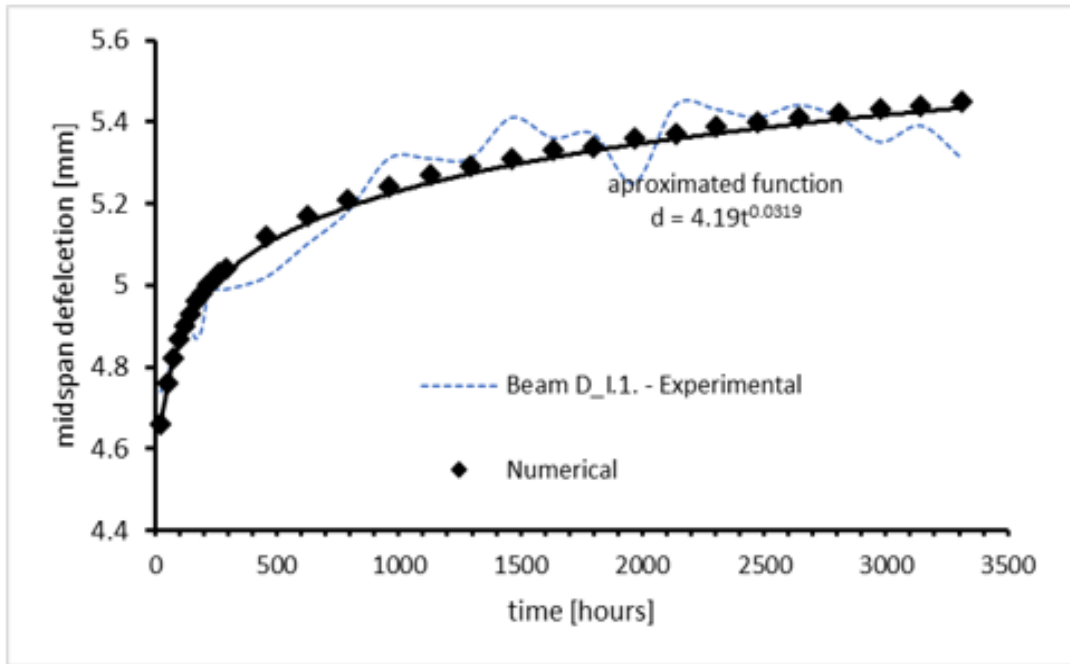


Figure 125. Mid-span deflection depending on hours (DI1)

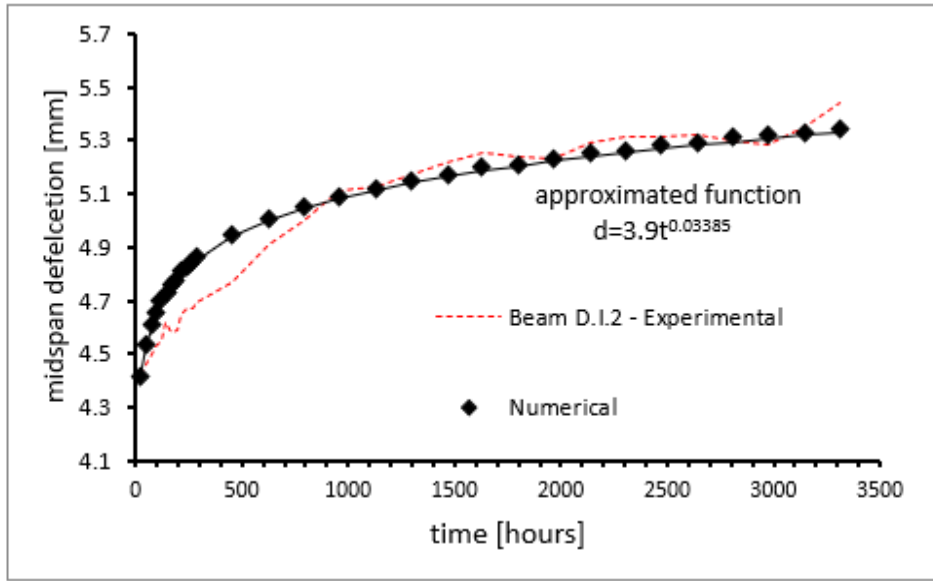


Figure 126. Mid-span deflection depending on hours (DI2)

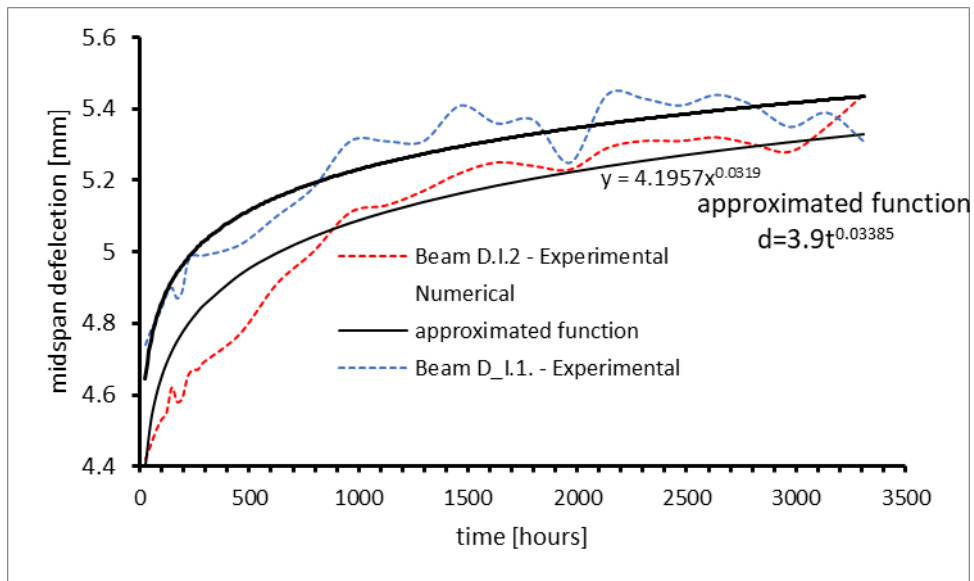


Figure 127. Comparison of experimental results between DI1 and DI2, including approximated function

The initial mid span deflection under sustained load was recorded as 4.4 mm for DI1 and 4.65 mm for DI2, marking the beginning of the long-term loading phase.

This graph above (fig. 126 and 127) presents the midspan deflection of two beams (DI2 and DI1) under sustained load over approximately 3300 hours. It compares experimental results, a numerical model, and an approximated function.

- Deflection increases over time for all curves, indicating time-dependent deformation typical of creep behavior in timber
- The approximated (solid black line) lies between the experimental results, suggesting a good calibration with physical behavior.

This matches the long-term creep trend well, especially after ~500 hours.

The approximated power-law function provides a reasonable prediction of long-term deflection behavior. The numerical model effectively captures the overall creep trend and falls within the experimental range, validating its predictive capacity.

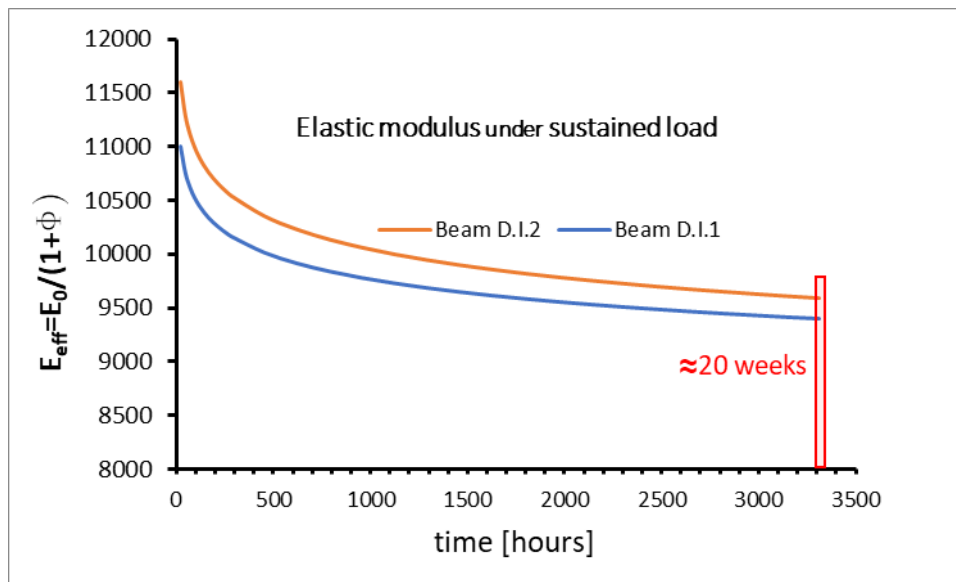


Figure 128. Creep trend and the elastic modulus of DI1 and DI2 under sustained load

The graph above shows how the effective elastic modulus of two beams (DI1 and DI2) decreases over time under sustained load due to creep. Beam DI2 retains a higher modulus than DI1, indicating better resistance to long-term deformation.

Most of the stiffness loss happens early, then levels off, with a noticeable drop over (~15–18%). This highlights the importance of considering creep in long-term structural performance.

This graph shows (fig. 127) how the midspan deflection of Beam DI2 increases over time under sustained loading due to creep. The red dashed line represents experimental measurements, while the black diamonds show numerical results.

The close match between them indicates that the numerical model accurately captures the beam's behavior. Deflection rises more rapidly at the beginning and then slows down, which is typical for creep.

Overall, the graph highlights the importance of accounting for time-dependent deformation in long-term structural analysis.

6. CONCLUSION

Production process

The production process of Glued Solid Timber (GST) beams in this study demonstrated a high degree of robustness and consistency, underpinned by strict adherence to European standards. The selection of defect-free Spruce lamellas, precise machining to uniform dimensions, and control over critical parameters such as moisture content (13.70%) and density (438.33 kg/m³) ensured the reliability of the structural components. Furthermore, the use of structural adhesive, applied with consistent glue line thickness and full curing time, contributed to high-quality bonding across all specimens. These factors collectively confirm that the GST beam production process was not only technically sound but also repeatable and scalable for industrial application.

Experimental Campaign:

The experimental campaign provided a robust dataset across various series. In Serie A, the local modulus of elasticity was measured between 11,840 MPa and 12,600 MPa, while the global values ranged from 10,920 MPa to 11,570 MPa. These results indicate minimal variation (standard deviation ~3.2%) and reflect a high degree of consistency in lamella quality and bonding. The bending strength parallel to the grain (Serie C) yielded values between 37.4 MPa and 41.2 MPa, averaging 39.5 MPa, which is slightly lower than some commercial GLT values but well within the expected performance for GST.

For the compression strength parallel to grain (Serie E), average values reached 33.4 MPa, and for compression perpendicular to the grain (Serie F), values were around 6.9 MPa, aligning well with Eurocode 5 assumptions.

In the long-term tests (Serie D) under sustained load over 3300 hours, most of the stiffness loss occurred in the early stages, followed by a gradual leveling off. A noticeable reduction in stiffness, approximately 15–18% was observed, highlighting the importance of accounting for creep effects in the long-term structural performance of engineered timber elements.

Numerical Modeling

Finite Element Modeling (FEM), conducted using 3D solid elements and material input based on experimental modulus values, produced results in close agreement with physical tests. In the simulation of four-point bending tests (Serie A):

For beam AI1, the numerical load–deflection curve predicted a maximum deflection of 10.3 mm, compared to 10.7 mm experimentally (error < 4%).

The predicted strain values from numerical models at key strain gauge locations (SG5, SG7, SG9) showed differences below $\pm 7\%$ when compared to measured values.

For beam AI3, both experimental and numerical failure initiated at the same section (mid-span tension zone), validating the model's ability to predict crack locations and modes.

All tested specimens (AI1–AI3) exhibited a consistent three-phase response—**elastic**, **plastic**, and **failure**—confirming this behavior as typical for GST beams under four-point bending.

In long-term behavior modeling (Serie D), the simulation results showed good agreement with the experimental deflections, with only minor deviations observed throughout the test duration. The predicted creep trends closely followed the experimental regression curves, confirming the effectiveness of the time-dependent material model in capturing long-term deformation behavior. This consistency between numerical and experimental data supports the reliability of the model for evaluating creep performance in timber structures.

REFERENCES

1. Azzi, Z. *et al.* (2025) 'Review of Nondestructive Testing (NDT) Techniques for Timber Structures', *Infrastructures*, 10(2), p. 28.
2. Chauhan, S. S. (2025) 'Wood Processing', in *Textbook of Forest Science*. Springer, pp. 839–864.
3. Dagher, H. J. *et al.* (1996) 'Effect of FRP reinforcement on low-grade eastern hemlock glulams', in *Proceedings of the National Conference on Wood in Transportation Structures*, pp. 207–214.
4. Dickson, M. and Parker, D. (2014) *Sustainable timber design*. Routledge.
5. Dziurka, D. *et al.* (2022) 'The possibility to use pine timber pieces with small size in the production of glulam beams', *Materials*, 15(9), p. 3154.
6. EN14080:2013. (no date) *EN14080:2013*.
7. Faria, D. L. *et al.* (2024) 'Mechanical characterization of glued laminated timber (glulam) beams produced with rubberwood and green polyurethane adhesive', *Caderno Pedagógico*, 21(7), pp. e5532–e5532.
8. Fiorelli, J. and Dias, A. A. (2003) 'Analysis of the strength and stiffness of timber beams reinforced with carbon fiber and glass fiber', *Materials research*, 6, pp. 193–202.
9. Franke, S., Franke, B. and Harte, A. M. (2015) 'Failure modes and reinforcement techniques for timber beams—State of the art', *Construction and Building Materials*, 97, pp. 2–13.
10. Gentile, C., Svecova, D. and Rizkalla, S. H. (2002) 'Timber beams strengthened with GFRP bars: development and applications', *Journal of Composites for Construction*, 6(1), pp. 11–20.
11. Harrach Muayad Movahedi Rad, Majid, D. H. (2022) 'Reliability-based numerical analysis of glulam beams reinforced by CFRP plate', *Scientific Reports*, 12. doi: 10.1038/s41598-022-17751-6.
12. He, M. *et al.* (2022) 'An Experimental and Analytical Study on the Bending Performance of CFRP-Reinforced Glulam Beams', *Frontiers in Materials*, 8, p. 802249. doi: 10.3389/fmats.2021.802249.
13. Hernandez, R. (1997) *Strength and stiffness of reinforced yellow-poplar glued-*

-
- laminated beams*. US Department of Agriculture, Forest Service, Forest Products Laboratory.
14. Jamnitzky, J. and Deák, A. (2019) ‘TUM-Campus im Olympiapark München: Umsetzung eines Ingenieurholzbaus in seiner gesamten Leistungsstärke’, *Bautechnik*, 96(11), pp. 855–862.
 15. Livas, C., Ekevad, M. and Öhman, M. (2022) ‘Experimental analysis of passively and actively reinforced glued-laminated timber with focus on ductility’, *Wood Material Science & Engineering*, 17(2), pp. 129–137.
 16. Maithani, P. and Mishra, K. (2024) ‘Sustainability in Structure: Innovations in Engineered Wood Products for Green Building’, in *Encyclopedia of Green Materials*. Springer, pp. 1–7.
 17. Masoumi, H., Haghghi, S. T. and Mohammadi, M. (2024) *Building a Strong Foundation: Pioneering Advances in Architecture and Civil Engineering for the Future*. Nobel Sciences.
 18. Mei Nan Li, Ling Zuo, Hongliang Zhao, Yan, L. G. (2021) ‘Study on flexural performance of prestressed glulam continuous beams under control influence’, *Journal of Wood Science*, 67(48). doi: 10.1186/s10086-021-01980-w.
 19. Moody, R. C. and Liu, J. Y. (1999) ‘Glued structural members’, *Wood handbook: wood as an engineering material*. Madison, WI: USDA Forest Service, Forest Products Laboratory, 1999. General technical report FPL; GTR-113: Pages 11.1-11.24, 113.
 20. Patlakas Michele Christovasilis, Ioannis Nocetti, Michela Pizzo, Benedetto, P. B. (2019) ‘Structural performance of a novel Interlocking Glued Solid Timber system’, *Materials and Structures*, 52(27). doi: 10.1617/s11527-019-1324-2.
 21. Plevris, N. and Triantafillou, T. C. (1992) ‘FRP-reinforced wood as structural material’, *Journal of materials in Civil Engineering*, 4(3), pp. 300–317.
 22. Porteous, J. and Kermani, A. (2008) *Structural timber design to Eurocode 5*. John Wiley & Sons.
 23. Romani, M. and Blass, H. J. (2000) ‘Reinforcement of glulam beams with frp reinforcement’. University of Karlsruhe, Alemanha.
 24. Romani, M. and Blaß, H. J. (2001) ‘Design model for FRP reinforced glulam beams’, in *Proceedings of the International Council for Research and Innovation in Building and*
-

Construction (CIB), Working Commission W18 Timber Structures, Meeting.

25. Rosli, M. A. A. *et al.* (2023) ‘Manufacturing study on different glue spread and press pressure for glued laminated timber made from Laran’, *Journal of Advanced Research in Applied Mechanics*.
26. Rug, W. (2006) ‘100 Jahre Hetzer-Patent’, *Bautechnik*, 83(8), pp. 533–540.
27. Shehada, M. (2024) ‘Contribution to the study of mechanical behaviour and the durability of multi-material wood-concrete structures with glued joints’. Université de Toulouse.
28. Simpson, W. T. (1971) ‘Equilibrium moisture content prediction for wood’, *Forest Products Journal*, 21(5), pp. 48–49.
29. Stark, N. and Cai, Z. (2021) ‘Wood-based composite materials: panel products, glued laminated timber, structural composite lumber, and wood–nonwood composites’, *Chapter 11 in FPL-GTR-282*, p. 11.
30. Šuhajdová, E. *et al.* (2023) ‘Experimental Research on Hybrid Hardwood Glue-Laminated Beams’, *Buildings*, 13(4), p. 1055. doi: 10.3390/buildings13041055.
31. Triantafillou, T. C. and Deskovic, N. (1992) ‘Prestressed FRP sheets as external reinforcement of wood members’, *Journal of Structural Engineering*, 118(5), pp. 1270–1284.
32. de Vito Junior William Martins, A. F. V. (2023) ‘Innovative approach for enhancing GLULAM performance with reinforcing steel bars: A BESO-based study’, *Latin American Journal of Solids and Structures*, 20(6). doi: 10.1590/1679-78257558.
33. Wengert, G. and Denig, J. (1995) ‘Lumber drying today and tomorrow’, *Forest Products Journal*, 45(5), p. 22.